Effect of Clay Addition on Mode II Interlaminar Fracture Toughness and Flexural Fatigue Behavior of Glass/Epoxy Composites

Dina Alizadeh

A Thesis

in

The Department

of

Mechanical and Industrial Engineering

Presented in Partial Fulfillment of the Requirements

For the Degree of Master of Applied Science in Mechanical Engineering at

Concordia University

Montreal, Quebec, Canada

May 2016

© Dina Alizadeh, 2016

CONCORDIA UNIVERSITY

School of Graduate Studies

This is to certify that the thesis prepared

By: Dina Alizadeh

Entitled: Effect of Clay Addition on Mode II Interlaminar Fracture Toughness and Flexural Fatigue Behavior of Glass/Epoxy Composites.

And submitted in partial fulfillment of the requirements for the degree of

Master of Applied Science in Mechanical Engineering

Complies with the regulations of the University and meets the accepted standards with respect to originality and quality.

Signed by the final examining committee:

__ Dr. Robin Drew_____ Chair

__ Dr. Martin Pugh_____ Examiner

__ Dr. John Oh_____ Examiner (External to the Program)

__ Dr. Suong V. Hoa_____ Supervisor

__ Dr. Wen F. Xie_____ Supervisor

Approved by:

__Dr. Sivakumar Narayanswamy_____
M.A.Sc. Program Director
Department of Mechanical and Industrial Engineering

__Dr. Amir Asif_____
Dean of Faculty

Date: May 17, 2016

ABSTRACT

Effect of Clay Addition on Mode II Interlaminar Fracture Toughness and Flexural Fatigue Behavior of Glass/Epoxy Composites

Dina Alizadeh

In a few decades, a lot of research have been done to show the effect of nanoparticles in fiber polymer matrix composites. An investigation has been carried out to study the effect of clay addition on Mode II interlaminar fracture toughness and flexural fatigue behavior of glass/epoxy composites. Nanoclay was dispersed in epoxy resin by a high speed homogenizer. Then, hand lay-up and autoclave curing were used to fabricate S-glass/epoxy/nanoclay laminates. Three point end notch flexural specimens were used to determine the interlaminar fracture toughness and flexural fatigue behavior. This study shows that the addition of 2wt% nanoclay into resin improves the Mode II strain energy release rate (G_{IIc}) by 24% and 23% for non-precracked (NPC) and precracked (PC) tests respectively. Fatigue was done in displacement control mode. The results indicated that the crack initiated earlier for regular samples than the modified ones. First, the rate of crack propagation was fast then, it became slow until achieved to the stable condition. At 2wt% nanoclay, 59% and 5% reduction were obtained in the crack growth rate at two regions where the rate of crack propagation changes. SEM indicated the fracture surface of samples after the crack stopped growing. These images were illustrated that fatigue resistance of specimens with nanoclay were enhanced.

ACKNOWLEDGEMENTS

I would like to express my deepest gratitude to my supervisor, Prof. Dr. S.V. Hoa, for his guidance and support throughout the entire MASc. thesis program. It has been a great opportunity for me to work with him. His knowledge, experience and encouragement motivated me to work hard.

I express my sincere to my thesis co-supervisor Dr. W.F. Xie for her kindness and supports during my thesis.

I am grateful to Dr. Rosca for his kind assistance and support, which facilitated the procedure of the project for me.

And last but not least, I am thankful to my husband Mr. Mostapha Marzban for his great suggestions to manage my thesis and his kindness. I thank my parents who always encourage me during my life and their unconditional support. I am also thankful to my brother Dr. Danial Alizadeh who motivated me to continue my education. I dedicate this thesis to my husband and my family.

Table of Contents

List of Figures

List of Tables

List of Equations

Chapter 1

1.1 Introduction

In the past few decades, composites have been used to fabricate many structural parts. It is considered the main competitor for metals due to their superior properties such as; light weight, high strength, high stiffness, good fatigue resistance and good corrosion resistance. Composite materials are applied in industrial structures such as wings of aircrafts, helicopter yoke and blade, robot arms and satellites. The majority of these structures are subjected to cyclic loads. Prediction of fatigue behavior has significant influence on designing practical structures.

One of the main problems in composite materials is delamination. Since the matrix is the weakest part in composites, its strength plays an important role for delamination to occur. In order to increase the strength of matrix, nanoparticles can be added to the resin. Nanotechnology has attracted the attention of researchers due to improved properties of composite materials. Nanoparticles are referred to as the materials which have at least one dimension in the range of nanometer. Nanoclay and carbon nanotubes with high strength and stiffness are the most commonly used nanoparticles. Well-dispersed nanoparticles into the resin at low content (<5wt%) provide superior properties for polymers. These properties are mechanical, thermal, fracture toughness and fatigue behavior.

Several researches have been done to consider the effect of clay addition into resin. Helmy et al. [1] investigated the tensile fatigue behavior of tapered glass/epoxy that contains nanoclay. Two types of samples, filled and unfilled ones were tested under two stress levels at $0.8S_{ult}$ and $0.5S_{ult}$. The crack propagation happened under Mode II failure. The results showed that addition of 2wt% clay enhances the fatigue life of the laminates by 54% and 7% at 0.5 and 0.8 times of the ultimate tensile strength respectively. Kabir et al. [2] investigated the vibration damping property and flexural fatigue behavior of glass/epoxy/nanoclay composites. The cross-ply laminates and quasi-isotropic ones with 1wt% and 2wt% nanoclay were tested. Remarkable improvements were achieved by addition of 2wt% of nanoclay into the resin. 66% and 133% improvement in fatigue life of cross-ply laminates were obtained for 1wt% and 2wt% clay respectively. The quasi-isotropic with 1wt% and 2wt% clay had 62% and 108% improvement in flexural fatigue life. Since little research has been done in Mode II interlaminar fracture and due to the importance of fracture

under shear stresses, this study focuses on considering the effect of clay addition on Mode II interlaminar fracture toughness and flexural fatigue behavior of glass/epoxy composites.

1.2 Thesis motivation

Nanoparticles such as nanoclays, carbon nanotubes and nanocarbons are added in polymers because of various desired effects. Therefore, it is interesting to discover how these particles, even at low concentration, can change the behavior of polymeric materials. The important characteristics of nanoparticles are particle dimensions, aspect ratio and surface area. The length and width of nanoclays are in the order of few microns and the thickness is around 1 nm. They have high aspect ratio and specific surface area (657 m^2/g) [3].

Interlaminar fracture (delamination) is one of the major problems in composite materials. It can lead to failure due to the reduced stiffness of a structure. So it is expected that addition of nanoparticles can improve the interlaminar fracture toughness. There are a lot of research that consider the effect of adding nanoparticles into resin. But most of the works that have been carried out, were in Mode I fracture.

However, sometimes the delamination occurs due to the shear stress, investigation of Mode II interlaminar fracture toughness is really critical. Thus, the incorporation of nanoclay into fiber polymer matrix composite in order to increase the Mode II interlaminar fracture toughness can be useful for structural applications. Also, it is important to consider fatigue life of composite laminates to understand what happens when dynamic load is applied to the structures. One example of these structures is the helicopter main rotor yoke which has a tapered design. It consists of three sublaminates: one internally dropped laminate and two belt sublaminates. Figure 1.1 shows the tapered laminate.

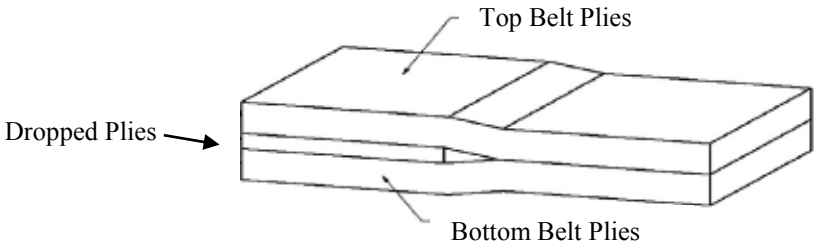

Figure 1.1: The tapered laminate [1].

The main problem of the tapered structure is the existence of material discontinuities inside the laminates. These discontinuities can generate stress concentration that are locations for delamination initiation and propagation. Thus, a reduction of the strength of the laminate can occur due to the tapered design. In order to remove this problem, one solution may be the addition of nanoparticles into the resin.

According to this motivation, several experiments were performed to see the effect of nanoclay on Mode II interlaminar fracture toughness and fatigue behavior in glass/epoxy composites.

1.3 Content of the thesis

In the first chapter of the thesis, an introduction of Mode II interlaminar fracture toughness, fatigue behavior and incorporation of nanoclay into fiber polymer matrix are discussed briefly.

In the second chapter a detailed literature review was done. It consists of nanoclay structure, fabrication of nanocomposites, interlaminar fracture toughness and effect of adding nanoclay on fatigue life.

The materials and experimental procedures are described in chapter 3. The properties of materials are explained in details. Then, the dispersion method, fabrication of samples and test procedures to determine Mode II interlaminar fracture toughness and fatigue behaviors are presented.

Chapter 4 shows the static and dynamic test results. It includes strain energy release rate of Mode II for two types of samples with and without nanoclay. Experimental results from fatigue tests are shown.

The conclusion of the work and contributions are presented in chapter 5. Recommendation for future work is also given in this chapter.

Chapter 2

Literature Review

Most research on nanocomposites started in the nineties. Nanoclays are clay minerals which are added in composites in order to enhance several properties such as increasing Young's modulus and storage modulus, improving stiffness and the toughness of the materials, enhancing resistance to fire and ignition, increasing in thermal properties and reducing cost.

Nanocomposites are a new category of composites, which are particles-filled polymers that at least one dimension of these particles must be in the nanometer range. There are three different types of nanocomposites according to the size of the dispersed particles. When three dimensions are in the order of nanometers, it is called isodimensional nanoparticles such as spherical silica nanoparticles. If two dimensions are in the range of nanometers, it is called nanotubes or whiskers. The carbon nanotubes or cellulose whiskers are the examples of this group. The third group is relating to particles with one dimension in nanometer scale, so the filler is in the form of sheets with one to a few nanometers thick to hundreds to thousands nanometers long. These materials can be obtained by intercalation of the polymer inside the galleries of layered host crystals. Table 2-1 shows the examples of layered host crystals.

Table 2-1: Example of layered host crystals susceptible to intercalation by a polymer [4].

Chemical nature	**Examples**
Element	Graphite
Metal chalcogenides	$(PbS)_{1.18}(TiS_2)_2$, MoS_2
Carbon oxides	Graphite oxide
Metal phosphates	$Zr(HPO_4)$
Clays and layered silicates	Montmorillonite, hectorite, saponite, fluoromica, fluorohectorite, vermiculite, kaolinite, magadiite
Layered double hydroxides	$M_6Al_2(OH)_{16}CO_3nH_2O$; M=Mg, Zn

Among all the layered-host crystals, those based on clay and layered silicates are used more widely because clay materials are easily available and also intercalation chemistry has been studied for a long time.

2.1 Structure of layered silicates

Nano-layered silicates are rock-forming minerals which have constituted approximately 90 percent of the crust of the earth. The silicate group can contain different ratios of silicon and oxygen which leads to several classifications of silicate minerals. One is called phyllosilicates or sheet silicates. They comprise of parallel sheets of silicate tetrahedral with Si_2O_5 or a 2:5 ratio. All phyllosilicates minerals are hydrated, with water or hydroxyl groups attached. Montmorillonite, hectorite and saponite are considered in the group of phyllosilicates that typically form in microscopic crystals, forming a clay. It is a member of smectite group that consists of 2:1 clay, meaning that it has 2 tetrahedral sheets sandwiched around a central octahedral sheet. The thickness of layers is 1 nm and the lateral dimensions vary from 30 nm to several microns or larger, depending on the particular layered silicate. These layers form stacks with a specific Van der Waals gap in between them that is called interlayer or the gallery. Figure 2.1 shows the structure of 2:1 phyllosilicates.

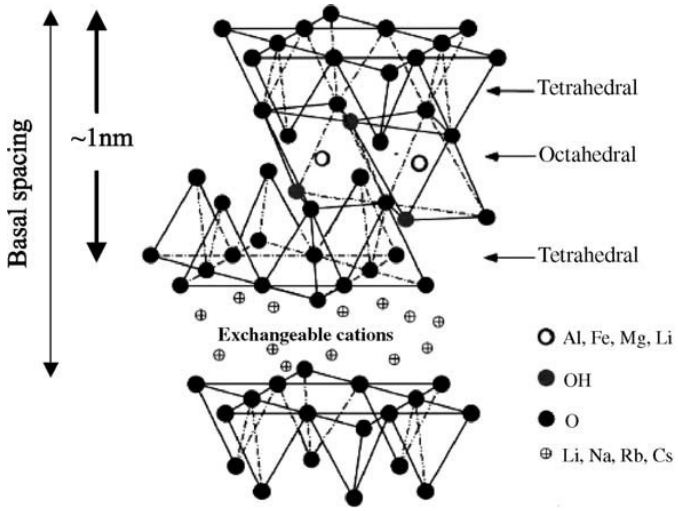

Figure 2.1: Structure of 2:1 phyllosilicates [5].

The negative charges produced by isomorphic substitution within the layers, are counterbalanced by alkali or alkaline earth cations situated in the interlayer. If the forces between the stacks are weak, intercalation will be easy. In this way the structure is more hydrophilic phyllosilicates. In order to have more organophilic, the hydrated cations of the interlayer can be exchanged with

cationic surfactants. The modified clay (organoclay) has special properties such as lower surface energy and more compatibility with organic polymers. Therefore, the intercalation within the galleries under well-defined experimental conditions will be probable.

2.1.1 Types of nanocomposites

Regarding the strength of interfacial interactions, type of layered silicates, type of organic modifier cation, polymer matrix and dispersion method three different types of nanocomposites exist.

- Traditional microcomposites: If the polymer cannot intercalate between the silicate sheets, a phase-separated composite will be produced. For this case, the properties remain the same as traditional microcomposites.
- Intercalated nanocomposites: it occurs when a single or several extended polymer chains are intercalated between the silicate layers.
- Exfoliated nanocomposites: the exfoliation or delamination will happen when the silicate layers are completely and uniformly dispersed in a continuous polymer matrix by an average distance from each other. The clay content in this structure is lower than that in the intercalated one.

Figure 2.2 illustrates different types of nanocomposites.

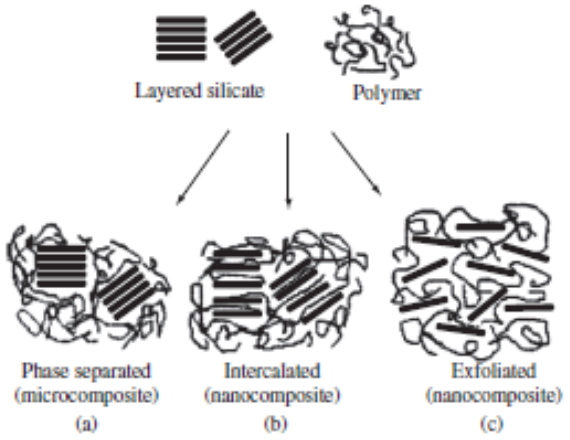

Figure 2.2: Three types of nanocomposites: (a) Phase-separated microcomposite, (b) Intercalated nanocomposite and (c) Exfoliated nanocomposite [6].

There are two complementary techniques to characterize these structures.

- XRD (X-ray diffraction): it is used to identify intercalated structures. By this method the interlayer spacing can be determined.
- TEM (transmission electronic microscopy): it is applied to determine exfoliated structures. Since there is large spacing between the layers and also deficiency of ordering in these nanocomposites, XRD diffractograms cannot show any diffraction peaks. Figure 2.3 illustrates the TEM micrographs for both intercalated and exfoliated nanocomposites.

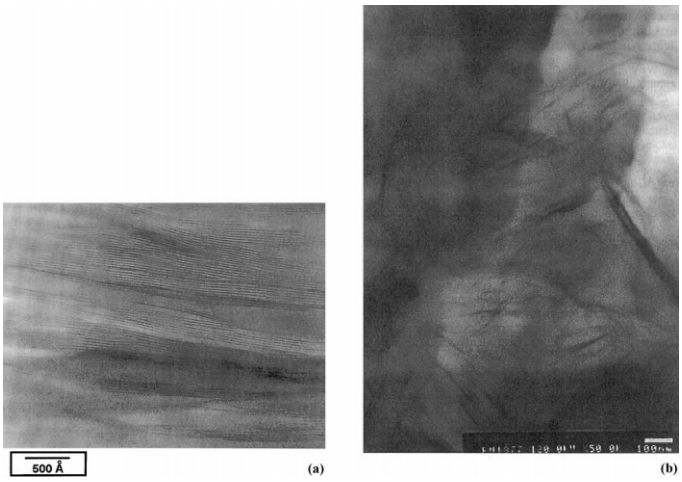

Figure 2.3: TEM micrograph of poly (styrene)-based nanocomposites: (a) intercalated nanocomposite and (b) exfoliated nanocomposites [4].

2.2 Fabrication of nanocomposites

In the fabrication of nanocomposites, the main challenge is dispersion of the clay in the polymer. There are several techniques to prepare polymer-layered silicate nanocomposites. Besides, manufacturing processes for thermoset and thermoplastic are different.

2.2.1 Thermoset nanocomposites fabrication

Two methods have been developed to fabricate thermosetting nanocomposites: In-situ polymerization process and solution process.

2.2.1.1 In-situ polymerization process

It is the popular and conventional method to fabricate thermoset-clay nanocomposites. In this process, the organoclay will be added to monomer and remains there for a certain amount of time to be swelled. The time depends on the polarity of the monomer molecules, the surface treatment of the organoclay and the swelling temperature. Then, the curing agent is added to initiate polymerization. Figure 2.4 shows the flowchart of In-situ polymerization.

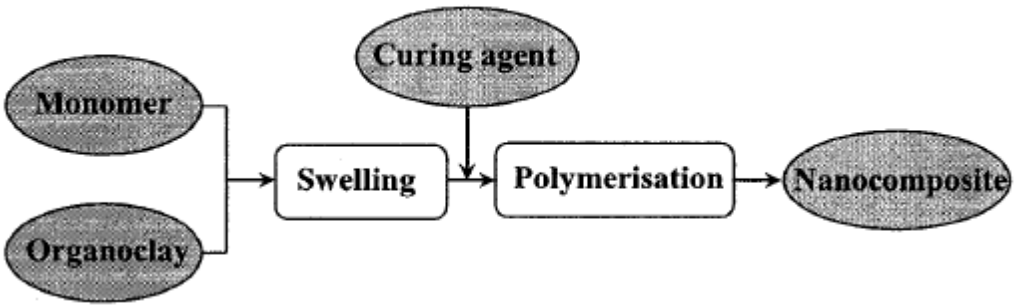

Figure 2.4: Flow chart of In-situ polymerization [6].

Dispersion of clay in monomer does not happen easily. The reason is related to thermodynamic force that keeps silicate layers together and it does not permit the monomer to diffuse into the silicate layers. Several studies have been done to break down the clay aggregates and lead to better dispersion of clay in polymer.

There are a few parameters that influence the dispersion process such as mixing temperature and time, speed of stirring, power of ultrasonic tooling, shearing forces and etc. The first method that is used widely to disperse nanoclay in epoxy, is mixing of organoclay and epoxy directly with mechanical stirring and sonication. However, it is not enough for good dispersion of clay in epoxy. Yasmin et al. [7] applied a three-roll machine to fabricate nanocomposites. The schematic of three-roll machine is indicated in Figure 2.5. First, the feed and apron rolls are set close to the center roll (approximately 10 μm) by screws. The epoxy resin is placed between the feed and the center rolls. The desired wt% of clay will be spread gradually in the resin. Materials are transferred from center roll to apron roll by adhesion and removed by a knife that runs against the roll. When the dispersion is completed, clear and transparent solution will remain. In this method the dispersion is done by shearing forces between the adjacent rolls.

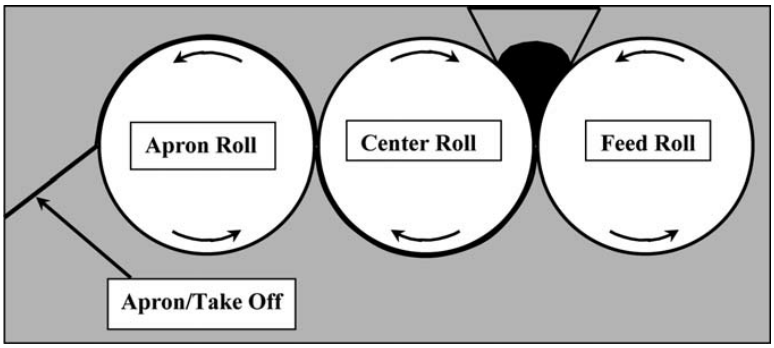

Figure 2.5: Schematic of three-roll mill machine showing the material flow direction [7].

Ngo et al. [8] used a high speed mixing technique to disperse organoclay in epoxies. In this process, the clay and epoxy are dispersed by homogenizer which has been equipped with a cylindrical rotor-stator mixing head of diameter 20 mm. In this method the temperature and speed were controlled during the dispersion. The results are remarkable from this method. The effect of temperature, speed and duration by XRD are illustrated in Figure 2.6, Figure 2.7 and Figure 2.8.

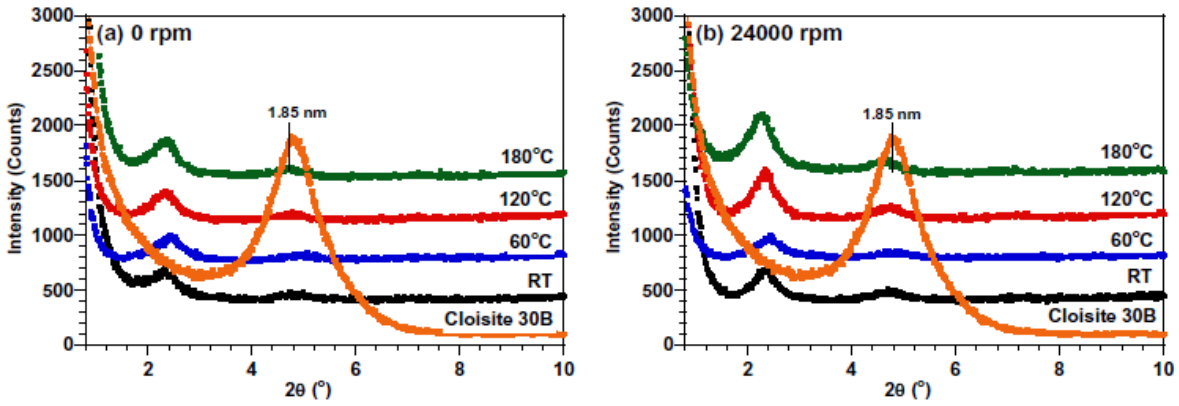

Figure 2.6: XRD curves of EPON828-C30B mixtures after being pre-mixed at different temperature for (a) 0 rpm and (b) 24000 rpm [8].

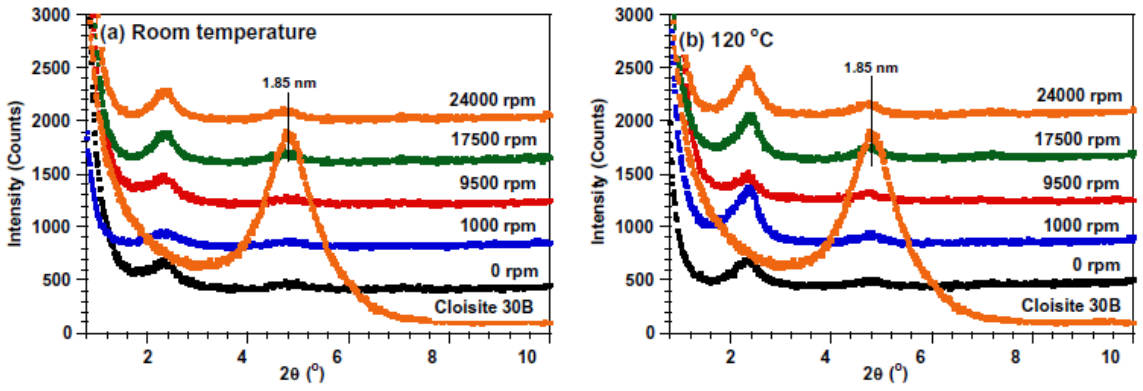

Figure 2.7: XRD curves of EPON828-C30B mixtures after being pre-mixed at different speed (a) room temperature and (b) 120 °C [8].

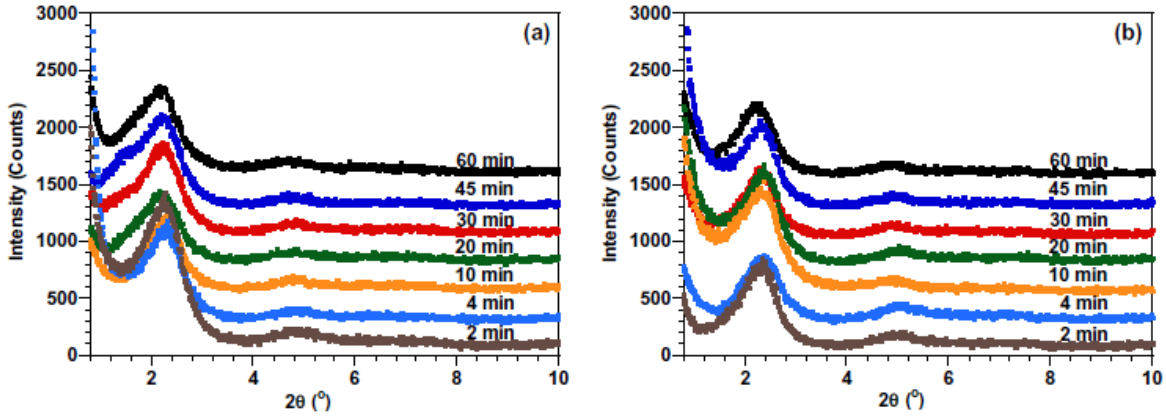

Figure 2.8: XRD curves nanocomposites pre-mixed at room temperature for different durations and cured at (a) room temperature and (b) 120°C [8].

These pictures illustrate that the first peak transfers to the lower angle for the mixture of epoxy-clay compared to the peak of clay C30B. It means that the intercalation has occurred and the degree of intercalation is around 3.72–3.81 nm. This value is higher than original C30B (1.85 nm). The effect of pre-mixing time, temperature and speed on dispersion are shown in Figure 2.9 and Figure 2.10. It is obvious from the pictures that pre-mixing duration and pre-mixing speed along with the temperature have a positive influence on the size reduction of clay aggregates.

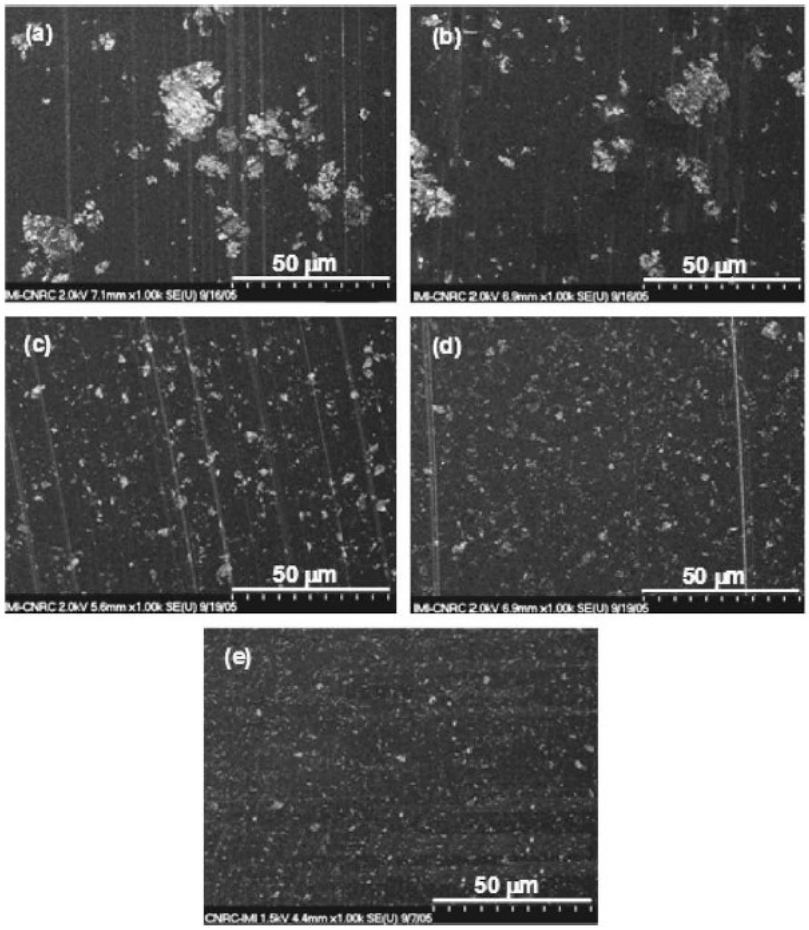

Figure 2.9: SEM image of nanocomposites: (a) pre-mixed at room temperature with 0 rpm, (b) at 120°C for 0 min with 0 rpm, (c) at 120°C for 2 min with 24,000 rpm, (d) at 120°C for 10 min with 24,000 rpm and (e) at 120°C for 60 min with 24,000 rpm [8].

(a) (b)

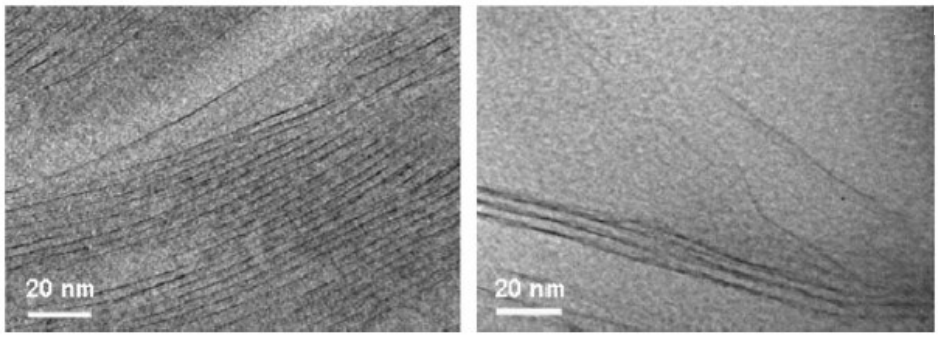

Figure 2.10: TEM image of nanocomposites: pre-mixed at 120°C for (a) 0 min with 0 rpm and (b) 60 min with 24,000 rpm [8].

High speed homogenizer was used to disperse the clay in resin by Kabir [2]. First, the resin is preheated in order to reduce the viscosity then, 2wt% of organoclay is added to resin. Dispersion occurs by high rotational speed of 20,000 rpm for 20 minutes. The temperature was kept below 100 ºC to avoid self-polymerization. Figure 2.11 illustrates the SEM images of fracture surface of epoxy system.

(a) (b)

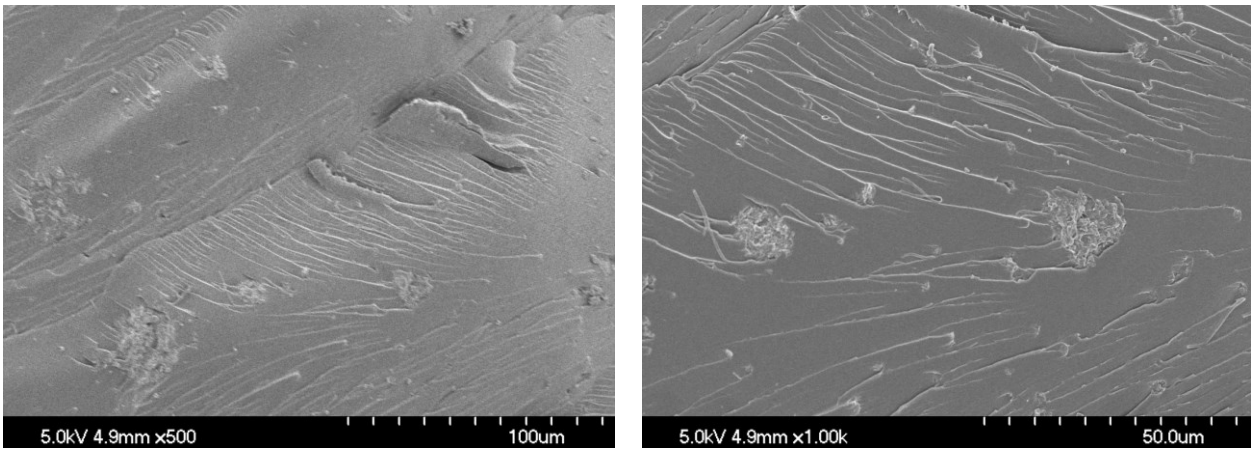

Figure 2.11: SEM images of fracture surface of epoxy system with 2wt% nanoclay: (a) lower magnification and (b) higher magnification [2].

Another technique to have well dispersion of clay and polymer is surface modification of clay. Gianni et al. [9] used an excess of silane as a surface modification to functionalize the clay mineral and also intercalated some monomers or oligomers into galleries at the same time. The result is increasing the interlayer distance. Then, the modified montmorillonite was mixed with a photocurable epoxy matrix in order to prepare nanocomposite coatings. This method shows transparent nanocomposite coatings with better thermal and scratched resistance performance than the regular montmorillonite.

Kornmann et al. [10] used TGDDM resin which was cured with diaminodiphenyl sulfone (DDS). Flurohectorites is layered silicates that modified by means of interlayer cation exchange of sodium cations for protonated dihydro-imidazolines and actadecylamine. The formation of nanocomposites is due to remaining of -OH groups in the molecular structure which has catalytic effect on polymerization occurs between silicate layers. The analytical results obtained from TEM and SEM methods, confirm better dispersion of clay in polymer but show decreasing of Tg.

Muzny et al. [11] prepared a dispersed clay/polymer nanocomposites by joining, via a cationic exchange reaction, surfactant monomers to clay platelets and subsequently polymerizing them with acrylamide. Forming platelet-surfactant micelles prevents clay aggregation. The dynamic light scattering was used to show the homogeneous dispersion of clay platelet into a resin.

Chun-ki et al. [12] developed a method to disperse clay in polymer by using ultrasound sonication. 4wt% of nanoclay is added to resin and stirred by hand. Then, the ultrasound sonication was applied for different sonicating time. This energy can break down the clay agglomeration and form nanoclay clusters. The results of XRD show that sonication time variation would not affect exfoliation of the nanoclay platelets.

2.2.1.2 Solution process

In this process, the organoclay is swollen in a polar solvent such as toluene, N-dimethylformamide or acetone. There is alkylammonium in the clays, so it can swell in polar organic solvents and form gel structures. The polymer which is used in this method, must be dissolved in the solvent and had a very low polarity. Because the clays have been intercalated in the solvent, further intercalation process occurred more easily. Finally, the solvent is evaporated under vacuum. Figure 2.12 shows the flowchart of solution process.

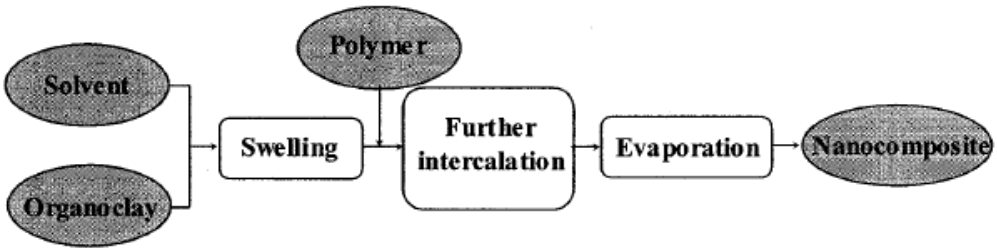

Figure 2.12: Flowchart presenting the different steps of the solution process [6].

Chen et al. [13] fabricated fully exfoliated layered silicate epoxy nanocomposites by applying high-shear-mixing in the presence of acetone and ultrasonication. XRD and TEM show the homogeneous and random dispersion of the clay in the epoxy.

Liu et al. [14], [15] used high pressure mixing (HPM) method to form pastes of nanoclay. First the nanoclay was dispersed in acetone by fluidizer machine at a pressure of 15000 Psi. In order to measure exact concentration of clay, the mixture must be dried for 8 h at 100 °C. Then, the desired

amount of paste is added to epoxy resin and mixed by hand at room temperature. After that mixture is stirred mechanically at 1000 rpm for 30 minutes at room temperature and slow heating is followed up to 120 °C for 1 h. Finally, degassing process is done under vacuum for 30 minutes at 130 °C. The results show that the aggregates of clay are broken to small platelets but the glass transition temperature is decreased with the increase of clay.

The solution process has good results for dispersion of organoclay in epoxy but this method is not applicable in industry, because it requires remarkable amount of solvent and also a cumbersome process of extraction.

2.2.2 Thermoplastic nanocomposite fabrication

There are three different ways to fabricate thermoplastic nanocomposites: In-situ polymerization process, solution process and melt intercalation (compounding) process.

2.2.2.1 In-situ polymerization process

This method was the first one that has been used to combine polymer with clay based on polyamide 6. Messersmith et al. [16] showed that addition of an initiator and increasing the temperature initiate the polymerization process. Ke et al. [17] fabricated poly ethylene terephathalate (PET) by in-situ polymerization technique. The results showed that nanocomposites of PET has 3 times greater crystallization rate than the pure one. In addition, the heat distortion temperature (HDT) for nanocomposites of PET is higher in comparison to pure PET.

Ma et al. [18] manufactured polypropylene/clay by in-situ intercalative polymerization. In order to prepare organoclay, Na-montmorillonite was stirred in distilled water and then intercalative reagent as a hexadecyl-octadecyl trimethylammonium was added. Finally, Ziegler-Natta catalysts ($MgCl_2$, $TiCl_4$) were used to activate the organoclay. The activated montmorillonite plays the role of catalyst for propylene polymerization. During the polymerization, the clay structure is destroyed because of growing PP molecules inside the clay galleries.

Yoonessi et al. [19] prepared highly delaminated clay/poly (dicyclopentadiene) nanocomposites by polymerization of presonicated mixture of the liquid dicyclopentadiene (DCPD) and using modified montmorillonite clays.

2.2.2.2 Solution process

This process is not so common. It happens due to adsorption of polymer onto nanoparticles. The solvent is added to polymer and nanoparticles. When the polymer adsorbs to the delaminated clay sheets, the solvent evaporates. The nanocomposites that were fabricated by this method are as follows: high density polyethylene [20], nematic liquid crystal polymers [21] and polyimide [22]. Vaia et al. [23] manufactured Poly ethylene oxide intercalated in montmorillonite by using deionized water as a solvent. Lee et al. [24] prepared polymethylmethacrylate PMMA-clay hybrid composites by applying emulsion polymerization.

2.2.2.3 Melt intercalation process

In this method, no solvent is required and the polymer matrix combines with the nanoparticles in the molten state. Vaia et al. [25], [26] applied melt intercalation method. In this technique, the layer silicate is mixed with the polymer matrix in the molten state. In order to fabricate nanocomposites, a hydraulic press at pressure of 70 MPa is used to form pellet from mixture of organically modified layered silicates (OLS) and polymer. Then, the pellets are annealed in vacuum above the glass transition temperature of the polymer. If the layer silicates are compatible with the polymer, the polymer can fill the interlayer space and form either an intercalated or an exfoliated nanocomposites.

Liu at al. [27] applied a melt intercalation method to fabricate nylon 6/clay nanocomposites. The mechanical and thermal properties such as heat distortion temperature and strength of the nanocomposites are better than those of nylon 6. This is due to the existence of good bonding between nylon 6 matrix and the clay interface.

Park J. H. et al. [28] applied only melt-blending technique. The ratio of epoxy to clay is 10. XRD and TEM illustrated that the clay particles were exfoliated completely. However, the dispersion of nanoclay to the scale of individual platelets was not achieved [28].

Figure 2.13 shows the flowchart of blending thermoplastic with an organoclay. Schematic illustration of melt intercalation is shown in Figure 2.14.

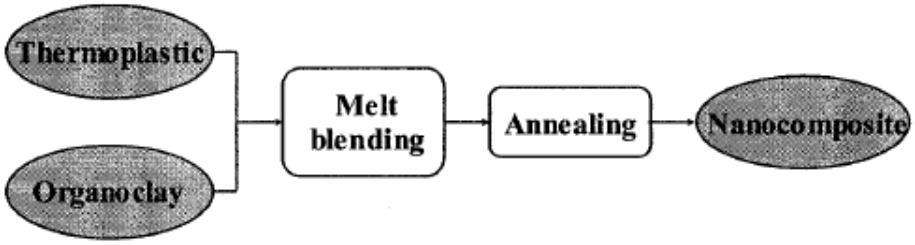

Figure 2.13: Flowchart presenting the different steps of the melt intercalation approach [6].

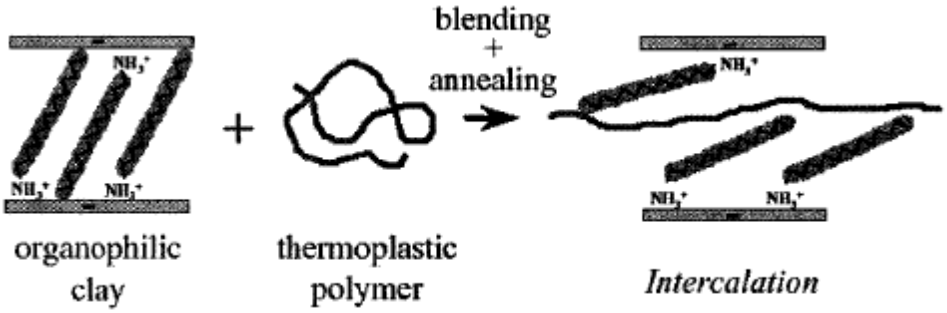

Figure 2.14: Schematic illustration of melt intercalation process [29].

2.3 Interlaminar fracture toughness and measurement methods

Fracture toughness is a property which describes the ability of material containing a crack to resist fracture. In other words, interlaminar fracture toughness is the resistance to delamination growth. The delamination between layers is an important problem in composite laminates since it occurs without any external signs. The results of delamination are loss of stiffness and strength which can lead to safety and reliability problems. There are three basic Modes that are able to make interlaminar cracking or delamination. It can occur also under combinations of them. Figure 2.15 shows these three modes.

- Opening or peel Mode (Mode I)
- Forward sliding shear Mode (Mode II)
- Tearing Mode (Mode III)

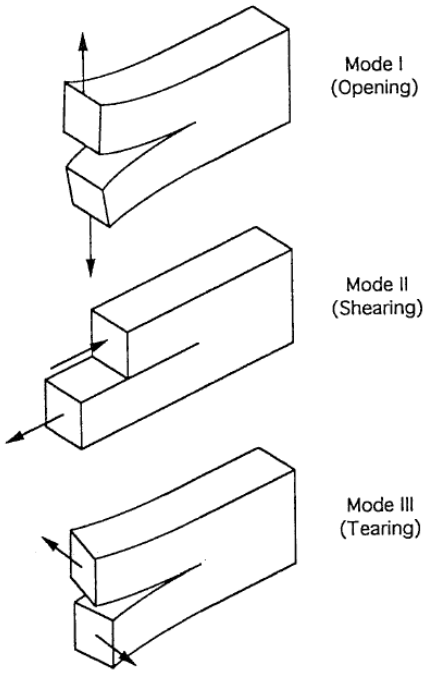

Figure 2.15: Basic delamination Modes in composite material [30].

Strain energy release rates (G_I, G_{II}, or G_{III}) are the indexes to measure the interlaminar fracture toughness. These are the energies released per unit area of crack extension.

2.3.1 Mode I

Interlaminiar tensile stresses make a Mode I fracture. Double cantilever beam (DCB) specimen and the width-tapered double cantilever beam (WTDCB) specimen are the most common configurations for Mode I characterization. Figure 2.16 shows the DCB for measurement of Mode I delamination fracture toughness. Load P is applied at the ends of composite beam and delamination occurs along its midplane over a length a.

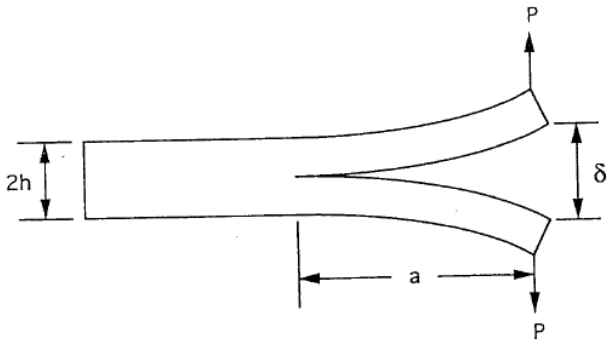

Figure 2.16: Double cantilever beam (DCB) for measurement of Mode I delamination fracture toughness [30].

Gordic et al. [31] obtained Mode I interlaminar fracture toughness of unidirectional carbon fibers/epoxy resin composites. They considered the effects of gamma irradiation at different doses. The interlaminar strain energy release rate is calculated before and after irradiation at various doses. The results showed that G_{Ic} decreases at low doses (5 MGY) and it enhances with increasing dose up to 11.7 MGY. But further increase in amount of gamma irradiation reduces the G_{Ic}.

Mahmood et al. [32] used air-jet texturing to improve the fracture toughness Mode I of laminated glass fabric composites. More surface contacts between the fibers and the resin are produced by using air-jet texturing. The results show that Mode I interlaminar fracture toughness was increased after texturing.

Moura et al. [33] compared interlaminar and intralaminar fracture toughness under Mode I. They considered the effect of bridging on the measured fracture energy which was done by cutting fibers during crack propagation. The results showed that bridging phenomenon has more influence on intralaminar tests.

Siddiqui et al. [34] obtained Mode I interlaminar fracture behavior and mechanical properties of CFRPs for samples with nanoclay and without it. Remarkable improvement in flexural modulus was achieved by addition of nanoclay but the flexural strength decreased. Figure 2.17 shows load versus extension of DCB samples made from CFRP composites with different contents of clay. First the load increases linearly until it reaches the maximum value, then it starts to decrease since the crack occurs. The reduction of the load continued gradually during the propagation of the crack. The results illustrate that the material with higher percentage of nanoclay exhibited much longer

extension at complete fracture as compared to neat epoxy matrix. Figure 2.17 shows that the higher resistance to fracture is obtained by adding nanoclay. As consequence G_{Ic} values of CFRP composites containing clay is enhanced in both initiation and propagation of the crack. For instance, the fracture toughness of composites is doubled with 7wt% nanoclay.

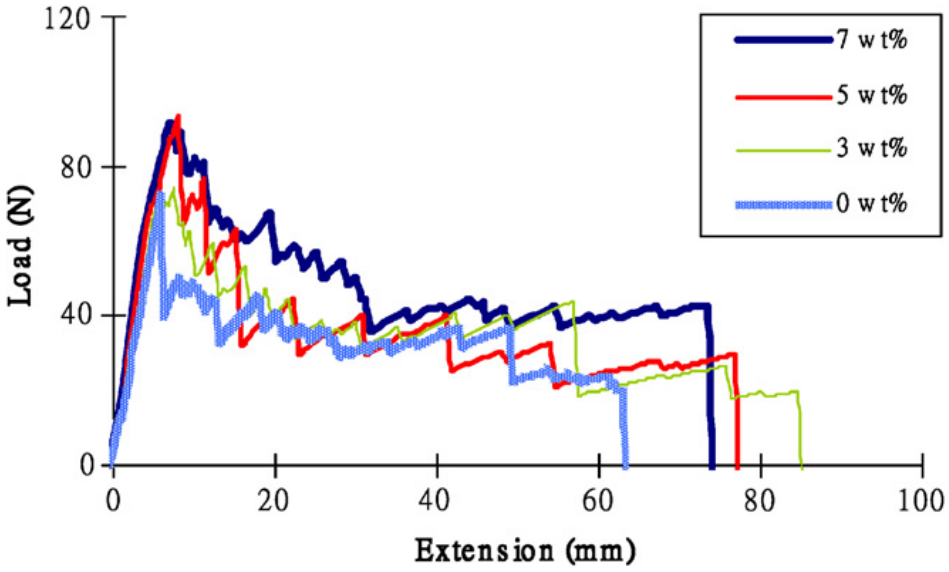

Figure 2.17: Typical load-extension curves of DCB specimens made from CFRP composites with different clay contents [34].

Ramsaroop et al. [35] considered Mode I interlaminar fracture toughness of polypropylene-clay nanocomposites. 1wt%-5wt% nanoclay were added into Polypropylene (PP) matrix. The critical stress intensity factor (K_{Ic}) and strain energy release rate (G_{Ic}) are calculated for all specimens. The results show that magnitude of K_{Ic} and G_{Ic} were enhanced with increasing clay content. At 5wt% nanoclay, the maximum improvement of K_{Ic} and G_{Ic} were 1.75 times and 2.66 times of neat PP. But the rate of increase after 3wt% nanoclay was slow. The reason is, clay starts to agglomerate in the PP matrix. Figure 2.18 shows the crack length versus time. These curves illustrate that time for crack propagation was increased until 3wt% nanoclay but above this value that time was reduced. SEM images showed that structure of nanocomposites was changed by increasing nanoclay content. Neat PP and 5wt% nanoclay show smooth fracture surface but there are extended and elongated deformations before failure at 3wt% nanoclay. These deformations require more time for crack to failure.

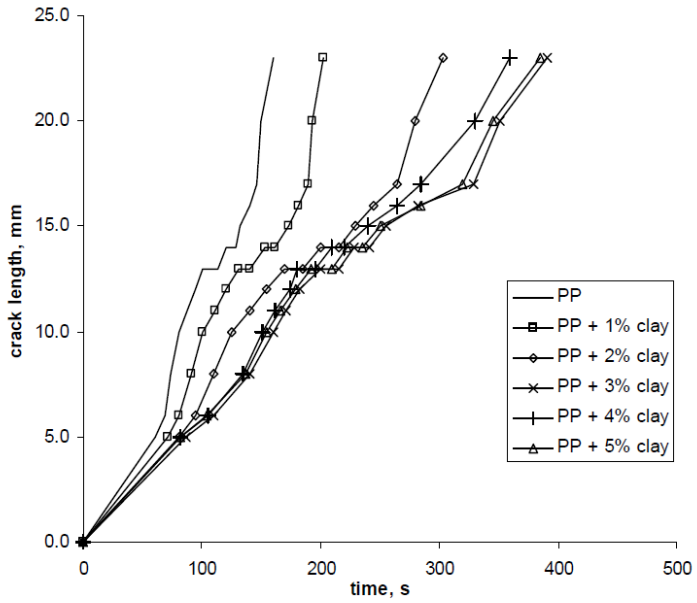

Figure 2.18: Crack length versus time responses for PP and PP-clay composites [35].

Mushtaq et al. [36] considered fracture toughness and toughening mechanisms of unsaturated polyester-based clay nanocomposites. The critical stress intensity factor (K_{Ic}) is a parameter to determine fracture toughness. The compact tension fracture tests were done on samples with different contents of clay. Figure 2.19 shows the fracture toughness values (K_{Ic}) of the neat unsaturated polyester UPE and nanocomposites with various clay loading (1-9wt%).

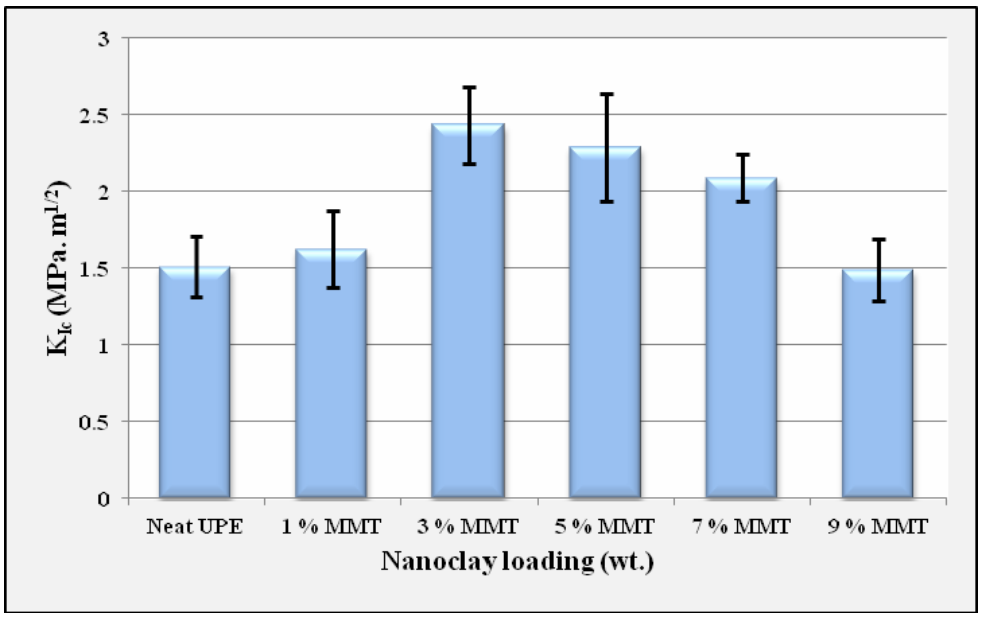

Figure 2.19: Fracture toughness of the neat UPE and the UPE/MMT nanocomposites [36].

According to the results, adding 3wt% nanoclay platelets improved the magnitude of K_{Ic} to 61% higher than the neat UPE. However, due to appearance of clay aggregates and the weak interaction between clay layers and resin, the addition of more clay particles reduced the K_{Ic}. This study manifests adding nanofillers into the resin makes a shift from the highly brittle fracture Mode into the shear yielding deformation mechanism.

Xu et al. [37] evaluated mechanical properties of carbon fiber reinforced epoxy/clay nanocomposites. Montmorillonite (MMT) nanoclay was added to tetraglycidyl diaminodiphenylmethane (TGDDM) epoxy and the samples were prepared through hot melt lay-up plus autoclave process. The opening Mode I interlaminar fracture toughness (G_{Ic}) was calculated for three types of specimens: neat one, 2 phr and 4 phr of clay. According to Figure 2.20 at the first 15-20 mm delamination, G_{Ic} increases faster and then it becomes more stable. The results show that adding 2 phr and 4 phr clay enhance the fracture toughness by 53% and 85% respectively.

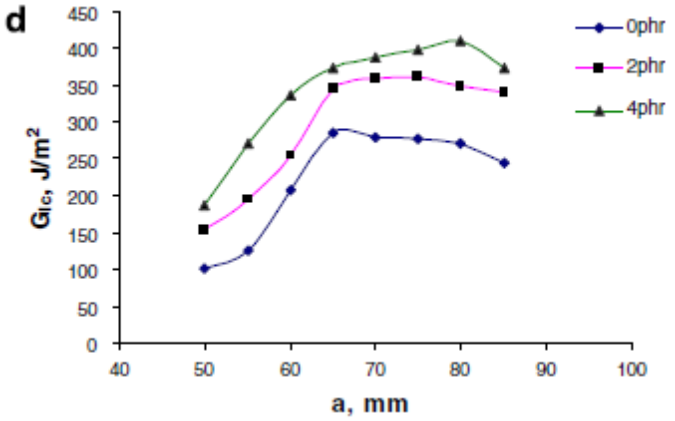

Figure 2.20: Delamination resistance curves (R curves): 0 phr, 2 phr and 4 phr clay [37].

2.3.2 Mode II

Interlaminar shear stresses result in Mode II fractures. The specimen is double cantilever beam (DCB) the same as Mode I. Three-point bending test is done to obtain delamination fracture toughness for Mode II.

2.3.2.1 Testing procedure

There are two methods for obtaining Mode II, the end-notched flexure (ENF) and the end-loaded split beam (ELS). The most popular one is ENF test. The load is applied at the middle of span up to the point of crack initiation. Then, the process is continued until further crack growth happens at the maximum load. Figure 2.21 illustrates the ENF test method.

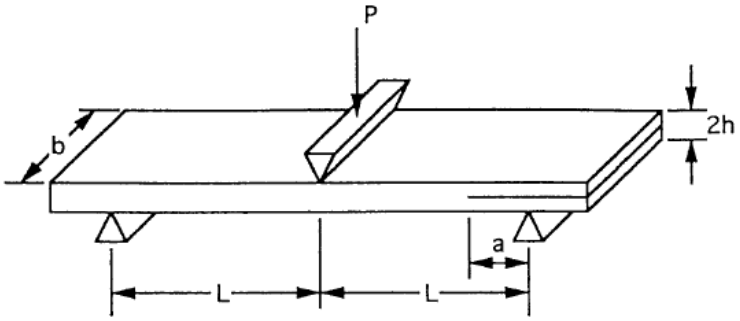

Figure 2.21: End-notched flexure (ENF) specimen for determination of Mode II interlaminar fracture toughness [30].

Davies et al. [38] considered influence of water and accelerated aging on the shear fracture properties of glass epoxy composite. They discovered shear strength and Mode II decreased by prolonged immersion in water. If weight gains are less than 1%, it will not influence on the shear strength. But at higher weight gains, shear strength reduced up to 25%. In addition, the accelerated tests at elevated temperature also reduced the G_{II} but less than long exposure time in water at low temperature.

Gao et al. [39] investigated Mode II delamination and damage resistance of carbon epoxy composite laminates that interleaved with thermoplastic particles. Three types of carbon fiber epoxy in both forms of non-interleaved and interleaved are manufactured. Mode II delamination resistance and damage resistance are remarkably increased.

Pereira et al. [40] obtained Mode II interlaminar fracture toughness of glass epoxy in the form of multidirectional laminates. Two stacking sequences were considered $\Theta/-\Theta$ and $0/\Theta$. The results show that G_{II} increased with Θ for both sequences.

Lee et al. [41] calculated Mode II interlaminar fracture toughness of glass fibers which were filled by carbon beads. The Mode II increased by adding carbon beads as a filler. However, the optimal bead volume fraction was around 15%.

Seyhan et al. [42] evaluated Mode II fracture toughness of E-glass non-crimp fabric/carbon nanotube (CNT) modified polymer based composites. The amount of 0.1wt% of amino functionalized multi walled carbon nanotubes is added to resin. The 3-roll milling technique was applied to disperse carbon nanotubes into the resin. The ENF test is applied to determine the initiation fracture toughness. Figure 2.22 manifests Mode II fracture toughness values of the CNTs is 8% higher than the based ones. Therefore, the nanofillers perform as a rigid fillers and prevent the growing of micro-crack within matrix rich interface area.

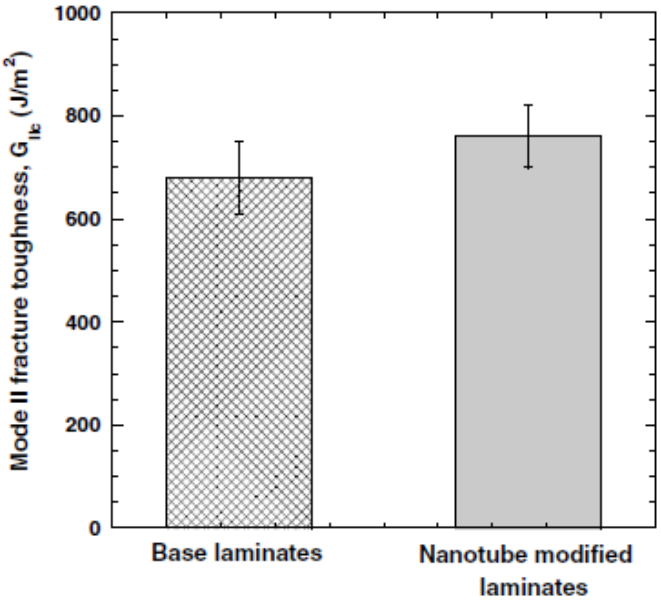

Figure 2.22: Mode II fracture toughness of the base and nanotubes modified composite laminates together [42].

2.3.3 Mode III

In contrast to Mode I and Mode II testing, little amount of data has been reported on Mode III testing. The specimen is a split DCB which is bonded between two aluminum bars. These bars are parallel to the crack plane and perpendicular to the beam axis. Figure 2.23 shows the sample for getting G_{III}. The results of finite element prove that in addition of G_{III} component, there is also G_{II}.

Moreover, the G_{II} component enhances near the free edges. One way to calculate G_{IIIc} is to assume that $G_{IIc} = G_{IIIc}$.

The problem regarding this test is the load drops suddenly as the crack extends, so it will lead to uncertainty in the crack lengths corresponding to the critical load.

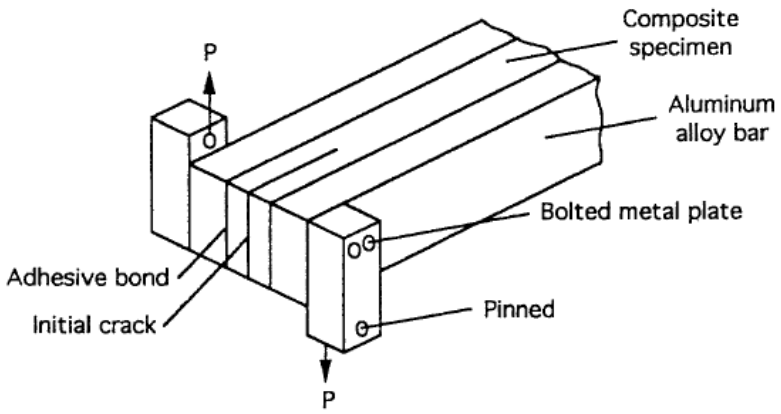

Figure 2.23: Split cantilever beam specimen for determination of Mode III interlaminar fracture toughness [30].

In order to remove this problem a new test was suggested. Figure 2.24 illustrates the configuration of specimen that is a doubly-split DCB. The sample is symmetrical to ensure self-balancing and avoid twisting.

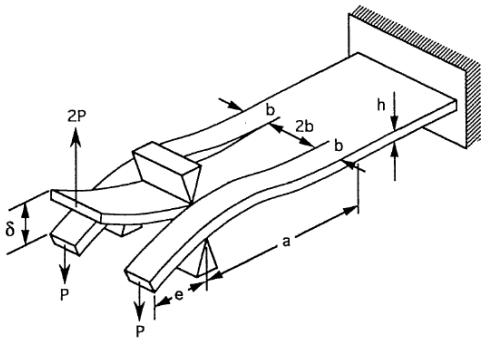

Figure 2.24: Doubly-split double cantilever beam specimen for determination of Mode III fracture toughness [30].

In this test the critical tearing load P remains constant during the propagation of the crack and the fracture toughness is independent of crack length (a+e).

Li et al. [43] considered influence of fiber volume fraction on Mode III interlaminar fracture toughness of glass/epoxy composites. The edge-cracked torsion (ECT) specimens are applied to measure G_{IIIc}. The results show that decreasing fiber volume fraction leads to increase G_{IIIc} corresponding to onset of crack propagation. Moreover, interlaminar matrix cracks in the 90° plies besides to the crack plane occur in both low and high fiber volume fraction. But the number of cracks are numerous in the low fiber volume fraction.

Liao et al. [44] obtained the Mode III fracture toughness in thick composite laminates. Torsion loading was applied on several angle-ply laminates with pre-crack in order to calculate interlaminar fracture toughness (G_{IIIc}). The experimental results indicate that interlaminar fracture toughness changes from 650 to 850 J/m^2 for 0/90, +15/-15 and +45/-45. Since thin material under torsional loading produces large twisting angle, the small deformation theory can not be applied. The limitation of this method is the samples will break at the middle portion for angle larger than 45°.

2.3.4 Mixed mode testing

There are possibilities to have mixed modes. Several test methods exist for mixed mode of I/II such as the cracked-lap shear (CLS), mixed mode bending (MMB), edge delamination tension (EDT) and the Arcan specimen. Figure 2.25 shows the CLS sample. The load P is applied to one arm (strap) of a split unidirectional laminate and then, it is transferred to other arm (lap). The mixed mode shear (Mode II) and peel (Mode I) along the interface between the lap and strap arms is produced.

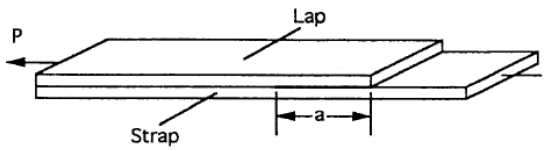

Figure 2.25: Cracked-lap shear specimen [30].

Another specimen is mixed mode bending which is shown in Figure 2.26. The ratio of G_{Ic}/G_{IIc} is only a function of the load position c and half span length L.

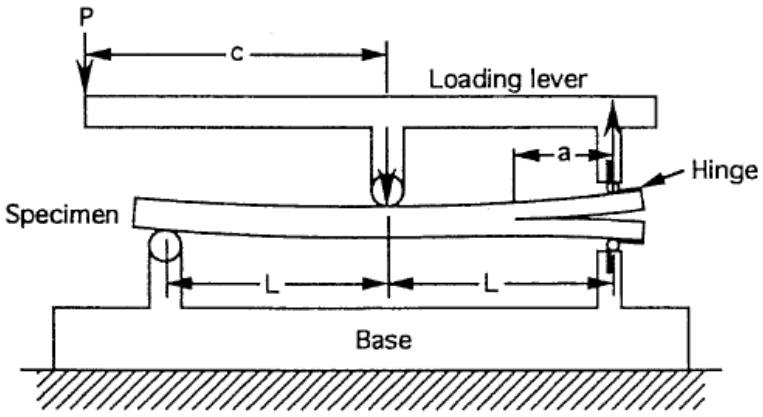

Figure 2.26: Mixed-Mode bending specimen and test apparatus [30].

Mathews et al. [45] determined the interlaminar fracture toughness of a laminate carbon epoxy by using mixed Mode bending test. Analysis of the results in the terms of Mode I and Mode II show that Mode I energy release rate decreased uniformly with increasing Mode II.

Miura et al. [46] characterized fracture toughness of woven glass fiber reinforced polymer composite laminates under mixed mode I/III at cryogenic temperature. They demonstrated that when the temperature is reduced from room temperature to 77 K, fracture toughness of epoxy resins tend to increase. But further reduction of temperature from 77 K to 4 K lead to decrease fracture toughness.

Rys et al. [47] evaluated the effect of stitching on mixed mode fracture toughness. They made samples containing low and high density stitching. The observations show that the delamination resistance improved and propagation suppressed by using stitching method. Also, fracture toughness increased for both low and high density. In addition, they discovered mode I value is enhanced by this method while, it did not significantly influence on value for Mode II.

Zappalorto et al. [48] considered mixed mode I/II fracture toughness of polymer nanoclay nanocomposites. They showed that nanomodification increases the fracture toughness of the epoxy resin.

Ayatollahi et al. [49] investigated mechanical behavior of nanodiamond/epoxy nanocomposites. The amount of 0.1wt% of nanodiamond is added to resin. The results show that the Young modulus and tensile strength were improved but the Mode I fracture toughness was reduced. The reason is the interface between nanodiamond and the epoxy is weak. The nanodiamond particles play a role as a stress concentrator that can reduce the fracture toughness of nanocomposites. Several tests are done on samples to determine mixed mode (I/II) fracture. Figure 2.27 illustrates value of fracture toughness for three different Modes. As mentioned before, Mode I fracture toughness decreases as compared to pure epoxy but Mode II and mixed mode K_I=K_{II} enhance.

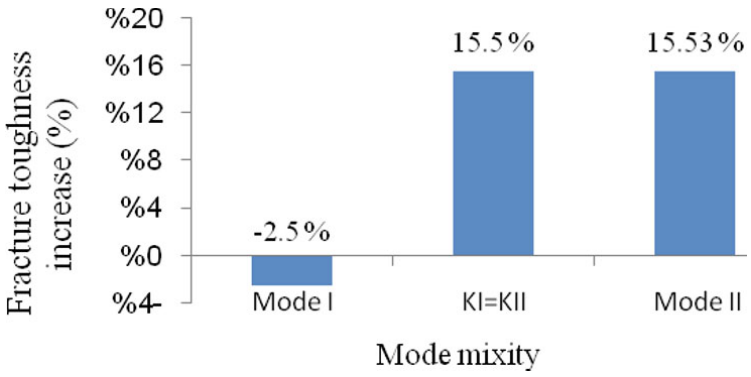

Figure 2.27: Increase in fracture toughness for different Mode [49].

2.4 Effect of nanofillers on fatigue life of composite material

As mentioned before nanoparticles are added in polymer matrix in order to improve strength, stiffness, Young's modulus and storage modulus, thermal and chemical resistance. A lot of research works have been done over last few years to observe the influence of nanofillers on the fatigue life of composite materials. Some of them are explained below.

Shokrieh et al. [50] considered the effect of adding graphene nanoplatelets into epoxy resin and testing flexural bending stress in fatigue conditions. Displacement-controlled method was chosen to run the fatigue test. The results showed that addition of graphene nanoplatelets improved fatigue life of epoxy resin. By adding 0.25wt% of graphene into resin at a stress ratio of 0.43, 27.4 fold improvement was observed.

Reis et al. [51] evaluated the mechanical properties on nanoclayed polymer-based composites. They indicated that the 3wt% nanoclayed composites have higher fatigue strength than the unfilled

ones. Three kinds of specimens have been tested; Polypropylene (PP), Polypropylene and paraffin (PPB) and 3wt% of nanoclay added to polypropylene and paraffin (PPB3). Liquid paraffin consists of small amount of nanoclay. The PPB3 has a fatigue behavior about 10% higher than the PPB and also, 20% higher than the PP.

Song et al. [52] showed that combination of organoclay with polyurethane elastomer can have an influence on fatigue behavior. The most remarkable results were achieved by adding 3wt% organoclay. This nanocomposite can absorb deformation energy. Crack growing occurs that will lead to final failure. Moreover, adding organoclay improved the tensile strengths of these nanocomposites more than 150% compared to unfilled polyurethane.

Wetzel et al. [53] evaluated influences of nanoparticles on mechanical and fracture mechanical properties of epoxy resin. Titanium dioxide (TiO_2) or aluminum dioxide (Al_2O_3) are the nanocomposite used. In order to achieve homogeneous nanoparticle distribution and decrease the size of agglomerates, high shear energy was applied during dispersion. Adding these nanoparticles improved flexural stiffness, flexural strength and fracture toughness of the composite. In addition, the fatigue crack propagation resistance of epoxy is enhanced by adding Al_2O_3. The crack in nanocomposites grows at lower rates than in neat epoxy.

Blackman et al. [54] added 7.8wt% nano-silica (SiO_2) particles into epoxy and considered the effect of them on fracture toughness and fatigue behavior. The results showed both improved in the initial toughness and fatigue behavior.

Chisholm et al. [55] applied nanosized SiC fillers into carbon/epoxy and considered the thermal, mechanical and flexural fatigue behavior of nanocomposites. 1.5wt% to 3wt% nanoparticles were mixed with epoxy by ultrasonic mixing. Vacuum assisted resin transfer molding (VARTM) was a method to fabricate the samples. Flexural fatigue tests were performed at frequency of 3 Hz and stress ratio of 0.1. Figure 2.28 shows S-N diagrams for three systems; neat, 1.5wt% and 3wt%. When the load is above 60% of ultimate flexural strength, the neat system behaves better than the others. But below the 60%, the system with 1.5wt% nanoparticles has better fatigue performance. The reason for this reversal of the fatigue phenomenon has not been understood completely. However, the 3wt% shows very poor fatigue behavior entire for the entire load level.

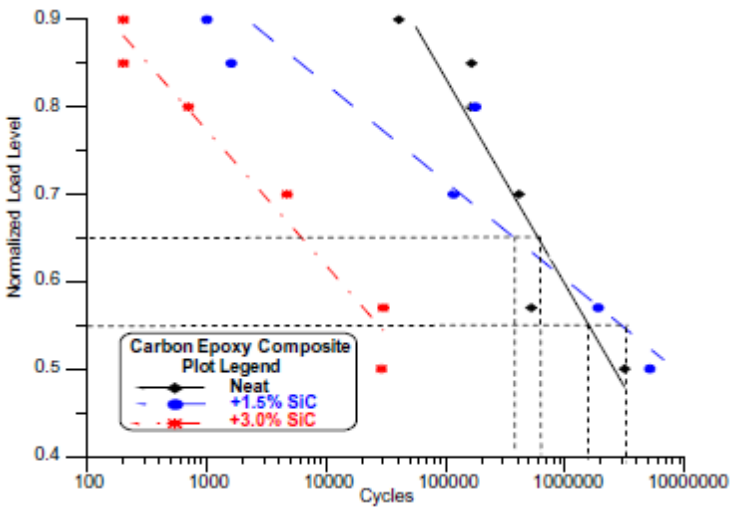

Figure 2.28: S-N diagram (flexural fatigue) [55].

Grimmer et al. [56] investigated the high cycle fatigue behavior in a tension fatigue test by adding 1wt% multi-walled carbon nanotubes into glass/epoxy composites. Two kinds of specimens were made: with CNT and without it. The wet lay-up is the method to fabricate the samples which consist of eight layers of woven glass fabric [0/90] and EPON 826. After curing the specimens under heat and pressure, they were cut in specific dimension in order to do tensile test. Moreover, the center of each sample was drilled to create a stress concentration. In the fatigue test, samples containing 1wt% nanotubes increased the number of load cycles (more than 10^4) to failure. The fatigue life of CNT samples improved for instance, CNT composite samples had fatigue life 2.5 times higher than neat specimens. Figure 2.29 illustrates the applied cyclic stress vs. fatigue life.

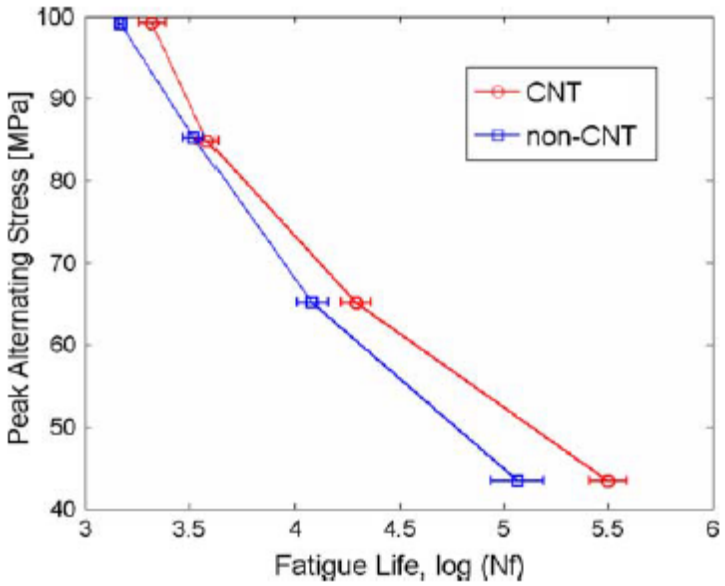

Figure 2.29: Applied cyclic stress vs. fatigue life curve of glass/epoxy laminates with and without 1wt% CNTs [56].

Kabir [2] considered flexural fatigue behavior of glass/epoxy/nanoclay composites. Three types of samples were made; neat glass fiber/epoxy, 1wt% clay/glass fiber/epoxy and 2wt% clay/glass fiber/epoxy. In addition, wet lay-up was the method to fabricate the specimens, that were in both types: cross-ply and quasi-isotropic. The amplitude of displacement was fixed (±6.67mm) lower than ultimate strength of the material. The fracture occurs in the laminate only because of mechanical fatigue rather than thermal failure. Figure 2.30 and Figure 2.31 exhibit strain vs number of cycles of cross-ply and quasi-isotropic laminates. The results show that fatigue damages within cross-ply laminates start accumulating after 100,000-166,000 and 233,000 fatigue cycles but for quasi-isotropic laminates they happen at 108,000-175,000 and 225,000 cycles for neat, 1wt% and 2wt% nanoclay respectively. The maximum strain increases suddenly due to the fact that crack occurs during the fatigue test. As consequence the laminate loses its stiffness and tends to bend more clearly indicating that adding nanoclay has improved the fatigue life of glass-epoxy.

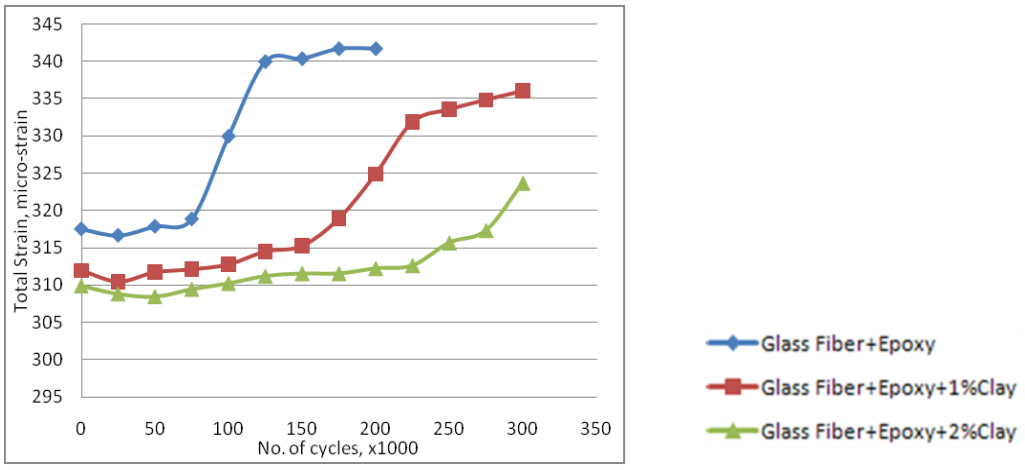

Figure 2.30: Flexural fatigue test results of cross-ply laminates [2].

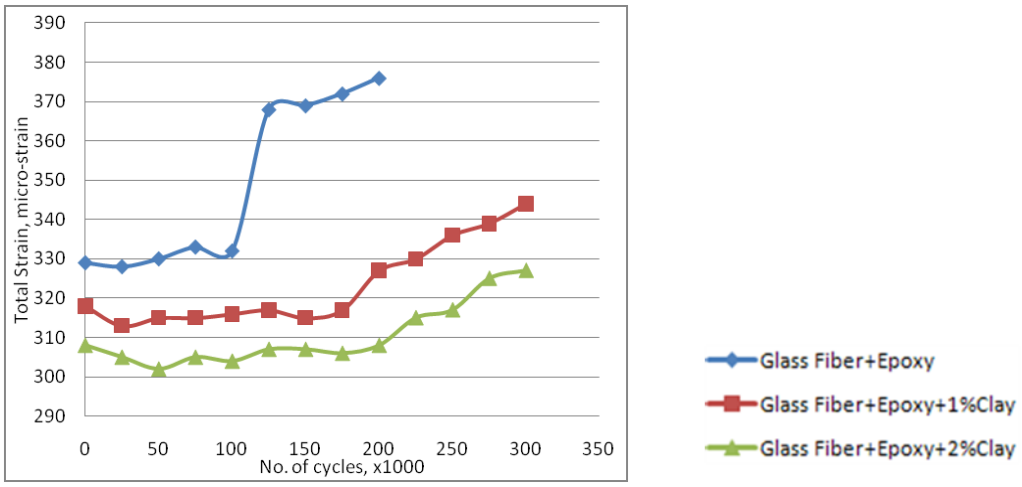

Figure 2.31: Flexural fatigue test results of quasi-isotropic laminates [2].

The cross-ply laminates with 1wt% and 2wt% nanocaly have respectively 66% and 133% improvement in fatigue life in compare to neat glass-epoxy. The quasi-isotropic with 1wt% and 2wt% showed 62% and 108% improvement in flexural fatigue life.

Helmy et al. [1] investigated tensile fatigue behavior of tapered glass fiber reinforced epoxy composites containing nanoclay. The result shows that adding clay prolongs the fatigue life of the laminate. The samples are tested in different stress levels and a load ratio ($\sigma_{min}/\sigma_{max}$) R=0.1 with frequency lower than 10 Hz. The frequency is selected to be low in order to avoid temperature rise particularly at high stress levels. The fatigue crack starts to grow at the resin pocket and propagates along the interface between the belt layer and the core layer in the thicker region of the laminate.

Figure 2.32 illustrates the crack propagation of tapered laminate under tensile fatigue loading. The crack propagation appears in the form of Mode II crack failure.

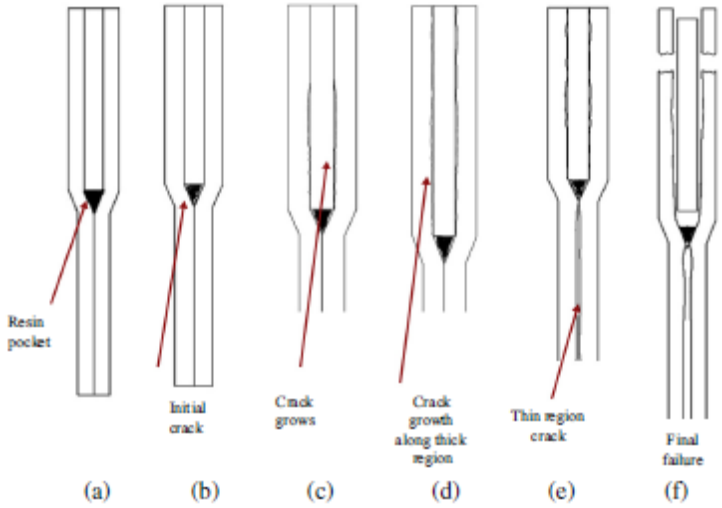

Figure 2.32: Schematic for propagation of failure of tapered beam under fatigue loading [1].

Figure 2.33 shows growing the crack for filled and unfilled laminates at $0.8S_{ult}$ and $0.5S_{ult}$.

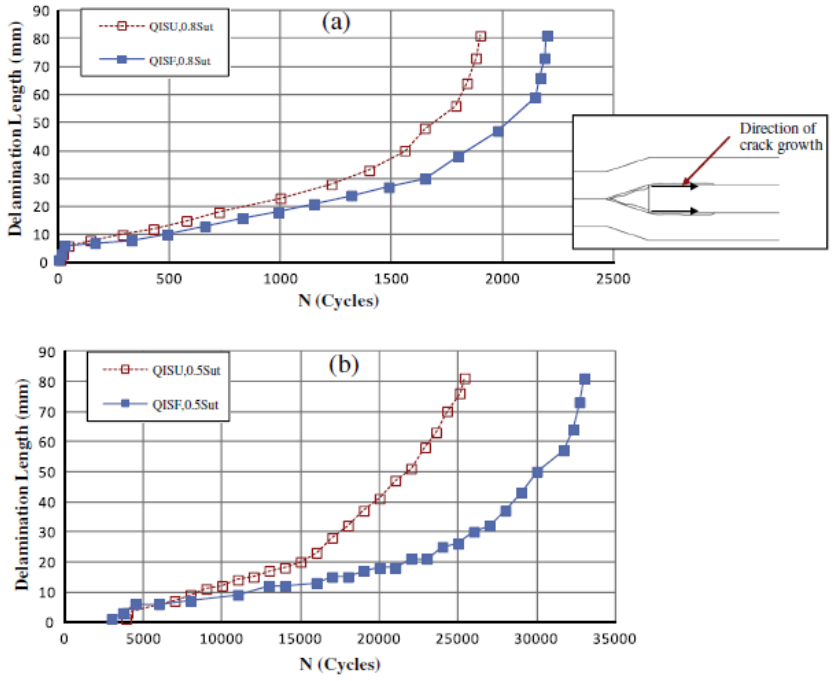

Figure 2.33: Crack growth lengths for QIS of filled and unfilled laminates: (a) at $0.8S_{ult}$ and (b) at $0.5S_{ult}$ [1].

The results illustrate laminates with nanoclay exhibit longer fatigue life than laminates without nanoclay at same stress level. In addition, the nanoclay modification has more effect in tensile fatigue test at low stress level than high one. 54% and 7% improvement are obtained at 0.5 and 0.8 of the ultimate tensile strength.

2.5 Thesis objectives

From above literature review it can be concluded that addition of nanoclay into resin can improve the static and dynamic behavior of composites such as; mechanical, thermal, barrier properties, fracture toughness and fatigue behavior. Achieving these improvements requires several factors such as; compatibility of polymer and clay, proper dispersion of clay into resin, appropriate fabrication method and etc. One example is improving vibration damping property and flexural fatigue behavior of glass/epoxy composites by adding nanoclay.

Investigation of researches showed that there are few works in Mode II interlaminar fracture toughness while, fracture under shear stress is really critical. For instance, the tapered glass/epoxy containing nanoclay was subjected to the tensile test. The delamination growing occurred between the dropped and belt ply. The results showed that the crack propagation is due to Mode II failure. Addition of nanoclay increased the strength and stiffness of laminates and also prolongs the tensile fatigue life. By considering all these points, this thesis has the following objectives;

- To determine the effect of adding clay on Mode II fracture toughness of glass/epoxy laminates.
- To determine the effect of adding clay on flexural fatigue behavior of glass/epoxy composites.

Chapter 3

Materials and Testing Procedure

In the manufacturing of nanocomposites several factors that can affect the quality of samples are considered. The most important factors are dispersion of clay in the resin, compatibility of resin and fiber, processing parameters and curing cycles. The processing parameters influence the dispersion of clay in polymer and physical and mechanical properties of nanocomposites. This chapter explains materials selection, dispersion method of clay in resin, manufacturing of samples and curing cycles. Mode II and Fatigue testing procedures are also presented.

3.1 Materials selection

The materials used are Uni-web S-glass fiber, Organoclay Nanomer 1.30E, EPON 828 as resin and EPICURE 3046 as hardener. The S-glass fiber is manufactured by AGY world Headquarters and supplied by Aerospace Composite Products INC. Also, the Nanomer 1.30E is obtained from Nanocor Inc. which is treated with long chain primary amine intercalant. The resin and hardener are supplied by Hexion Specialty Chemicals.

3.1.1 Uni-web S-glass fiber

S-glass fibers are lighter than other glass fibers such as E-glass and C-glass fiber. They provide 85% more tensile strength and 25% more stiffness than the other glass fibers.

Uni-web S glass fabric is a sheet of unidirectional fibers that are kept in the position by a fine spider web of polymer fibrils. The function of this web is to allow easy cutting of fiber and giving clean edges with no fraying. Some physical and mechanical properties of S-glass are shown in Table 3-1.

Table 3-1: Typical properties of S-glass fiber [57].

Density (g/cc)	2.46
Water absorption (%)	0
Loss on ignition (LOI %)	0.100 – 1.40
Filament diameter (μm)	5 - 25
Tensile strength (MPa)	4890 @ room temperature
Modulus of elasticity (GPa)	86.9
Elongation at break (%)	5.70
Poisson's ratio	0.22

3.1.2 Nanomer 1.30E

Nanomer is a product offerd by Nanocor Inc. It is considered as a montmorillonite clay which has its surface modified by 25-30wt% octadecylamine. This amine is a primary amine intercalant that is more valuable than secondary, ternary or quaternary amine modified nanoclay. Nonomer can be dispersed in resin systems such as polyurethane to produce nanocomposites. Several properties can be improved such as; enhance in chemical resistance, increase in T_g, improved modulus, increased strength and thermal properties.

Nanoclays can be dispersed as very thin particles with high surface area, but addition of nanoclay which cause the viscosity of the resin to increase. In order to reduce this problem sufficient mixing must be applied. Table 3-2 shows several physical and technical details of organoclay Nanomer 1.30E.

Table 3-2: Physical and technical details of organoclay Nanomer I.30E [58].

Appearance	White powder
Organic modifier or intercalant	ODA (octadecyl ammonium)
Modifier concentration (meq/100g Clay)	100
Basal spacing d_{001} (Å)	23.8
Moisture content (%)	3 max
Specific gravity (g/cc)	1.71
Mean dry particle size (µm)	8 to 10
Supplier	Nanocor Inc.

3.1.3 Epoxy (EPON 828)

Epoxy is the most common matrix for advanced composites because of properties such as high strength, good corrosion resistance and excellent adhesion. The chemical structure of epoxy consists of three membered ring with two carbons and an oxygen. One example of epoxies is Shell EPON 828. It is a low temperature cure resin and has low viscosity at room temperature. EPON 828 is undiluted liquid epoxy resin which is based on diglycidyl ether of bisphenol-A (DGEBA). Figure 3.1 and Table 3-3 show structure and typical properties of epoxy EPON 828. Very good mechanical, adhesive, dielectric and chemical resistance properties are obtained when it is cured completely.

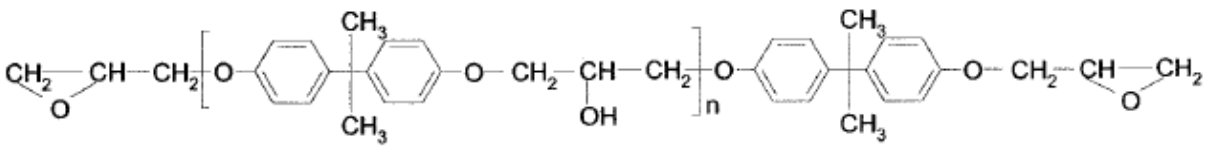

Figure 3.1: Structure of epoxy EPON 828.

Table 3-3: Typical properties of EPON 828 [59].

Visual Appearance	Clear Liquid
Epoxy equivalent weight (g/eq)	185 to 192
Viscosity @ 25 ºC (cPs)	10,000 to 16,000
Density @ 25 ºC (g/cm^3)	1.16
Vapor pressure @ 25°C (mm Hg)	0.03
Refractive index @ 25°C	1.573

3.1.4 Hardener EPICURE 3046

It is an aliphatic amidoamine that consists of triethylene tetramine and tall oil fatty acid polyamide. Tall oil fatty is made by the fractional distillation of tall oil. The chemical structure of EPICURE 3046 contains 18 carbon mono and di-unsaturated fatty acids which is mainly oleic and linoleic acid. It is a very versatile ambient temperature curing agent and provides good compatibility with EPON 828. Some of the advantages of EPICURE 3046 are low viscosity, immediate compatibility, long working life and variable combining ratio. Table 3-4 illustrates characteristics of EPICURE 3046.

Table 3-4: Characteristics of EPICURE 3046 [59].

Amine hydrogen equivalent weight (AHEW) (g/eq)	90
Viscosity @ 25 °C (cPs)	120 to 280
phr (parts per hundred)	35

3.2 Dispersion method

In order to disperse the clay into resin, a high speed homogenizer was used. The main parts of the high speed homogenizer are an internal rotor and external stator that is called rotor-stator generator. It is shielded in a 316 stainless steel shaft. The function of the rotor is to act as a centrifugal pump, so the liquid is recirculated and solids are suspended through the generator. The rotor can provide speed of 6500 rpm to 24000 rpm via a variable speed electric motor. High rotational speed generates a centrifugal force which axially draws the mixture of the liquid resin and the suspended solids into the dispersion head. Then, it is forced radially through the slots of the rotor-stator arrangements. Due to differential speed between rotor and stator, high shear force is produced that can generate very high turbulent energy in the shear gap. Therefore, dispersion of clay into the resin occurs because of this energy. In addition, the high turbulent energy enhances the temperature of the mixture and the viscosity will be reduced. As a result, the dispersion happens much easier. Figure 3.2 shows a high speed homogenizer, rotor-stator assembly and its working principle.

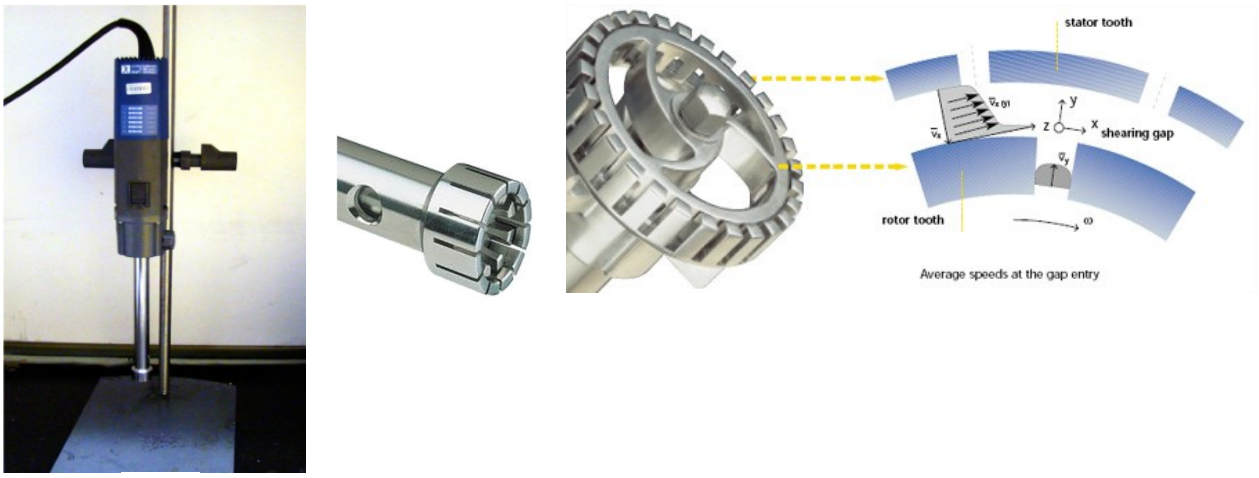

(a) (b) (c)

Figure 3.2: Photograph of (a) High speed homogenizer (b) Rotor-stator assembly (c) Rotor-stator working principle [60].

In this thesis, first resin EPON 828 was preheated to 45 ºC in order to reduce the viscosity. Then, 2wt% of organoclay Nanomer 1.30E was added to the resin. The mixture was blended by a spatula. Afterward, the high speed homogenizer was applied to disperse the clay into the resin. It was mixed

at speed of 20,000 rpm for 20 minutes. The important point during the mixing process is to keep the temperature below the 100 ºC to avoid self-polymerization. Cold water bath was used to keep the temperature below 100 ºC. It was only warm by the touch of a hand. An amount of 35 phr hardener was added to the mixture after dispersion of clay and resin. It was stirred by spatula slowly. In order to remove entrapment air the vacuum mixer was used.

3.3 Sample preparation

The technique which is used in this thesis is wet lay-up and auto clave molding process. A steel plate with proper dimensions was used to fabricate flat plate laminates. First the surface of the mold was cleaned by acetone and covered by a small amount of release agent. The required size glass fibers were cut in 0º direction. Here, 30 layers of fibers were used in order to get a suitable thickness. Then, a layer of fiber was placed on a mold and sufficient amount of mixture resin/clay/hardener was added on the fiber layer. It is important to distribute the mixture of resin uniformly on each fiber. During the distribution compact pressure was applied to adhere the fiber plies. This action was repeated until all layers are deposited. During the lay-up a non-adhesive film is inserted at midplane of the laminate. The function of this film is to serve as the initiation site for the delamination. The thickness of the film is 13 μm. The polymer film is used because it prevents folding or crimping at the cut end of the insert. Before inserting the film in the laminate, both sides of the film was coated with a mold release agent (Frekote 700-NC). After finishing the lay-up, a caul plate was used to apply uniform pressure, a porous release film, the bleeder and the breather to absorb excess resin and to remove entrapped air were placed on top of the laminate respectively. Finally, the sealant tape was placed around the mold and a vacuum bag with a vacuum valve are placed on the lay-up and sealed properly. Figure 3.3 shows a vacuum bagging sequence.

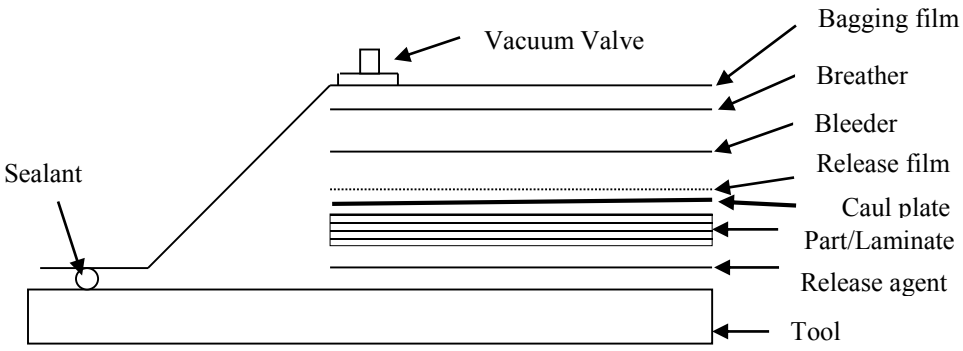

Figure 3.3: Typical cross-section of a vacuum bag [2].

At the end, the entire vacuum bag assembly was placed inside the autoclave and a pressure of 50 psi was applied during the curing process to help the further compaction of the laminate. Figure 3.4 illustrates the whole procedure of making the specimens.

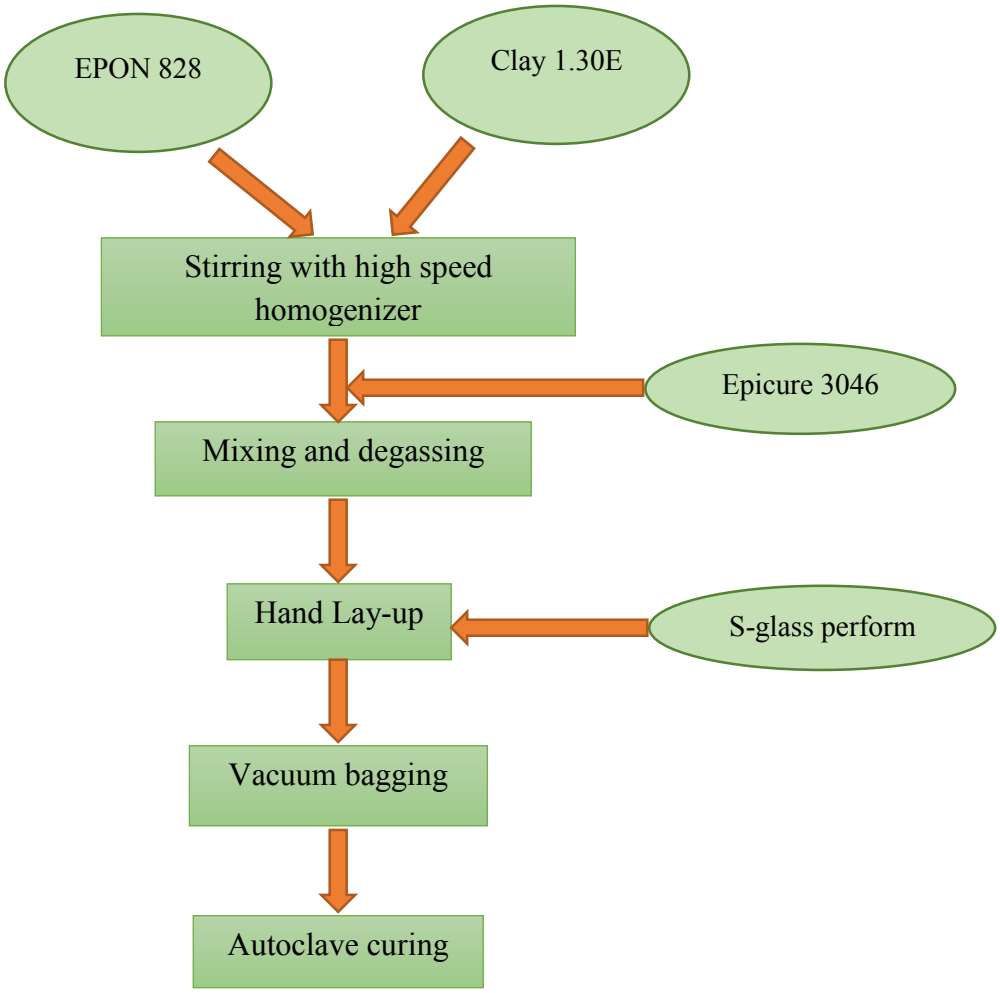

Figure 3.4: Flowchart for sample manufacturing.

3.4 Autoclave curing

The autoclave is a cylindrical vessel that can apply temperature and pressure during the curing process. Figure 3.5 shows the curing cycle. The laminate is heated from room temperature to 120 °C in 60 min then it is remained at this temperature for 120 min. Then, the temperature is increased to 140 °C in 15 min and is held at this temperature for 120 min.

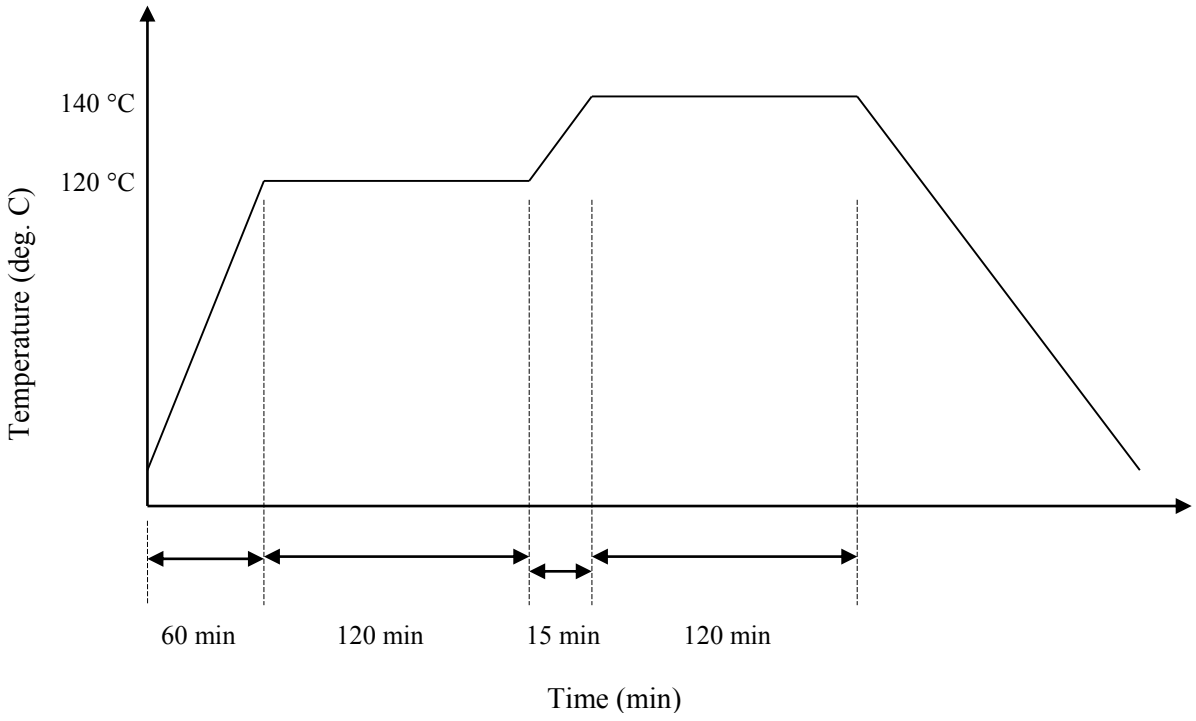

Figure 3.5: Cure cycle for S-glass/epoxy composite laminates [2].

Figure 3.6 shows differential scanning calorimeters (DSC) and T_g results for both laminates without nanoclay and with nanoclay. The DSC test is a method to check the degree of cure for samples. The amount of heat that is generated during curing is calculated from the area under the peak in the DSC curve. When there is no peak, it implies that laminates have been cured completely. In other words, all crosslinks between resin molecules and curing agent have taken place. In this study 100% cure has occurred inside the composite laminates. Table 3-5 shows glass transition temperature (T_g) for both samples without clay and with clay.

(a)

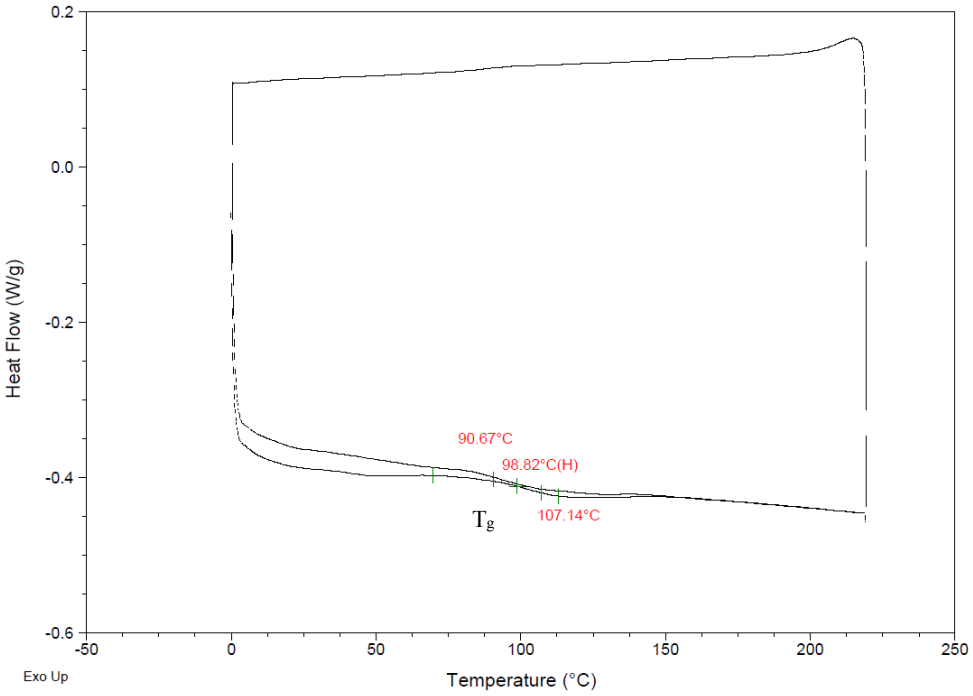

(b)

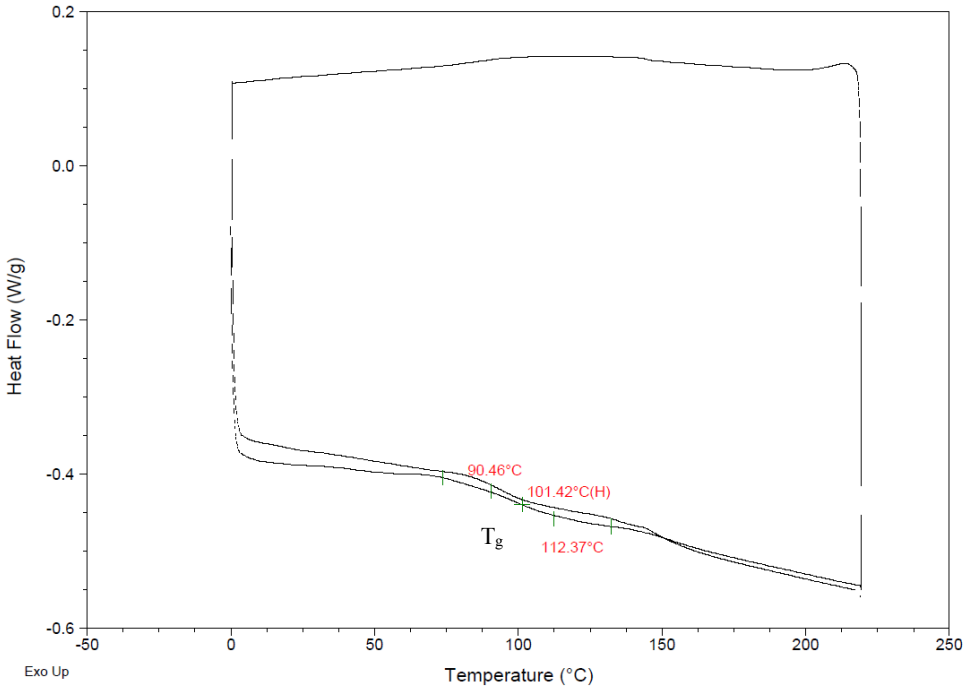

Figure 3.6: DSC graphs of laminates (a) without nanoclay (b) with nanoclay.

Table 3-5: Glass transition temperature (Tg) for both samples without clay and with clay.

Samples	**T_g (°C)**
Without clay	99
With clay	101

Optical microscope images of cross section of laminates without nanoclay and with nanoclay are shown in Figure 3.7 and Figure 3.8. The percentage of void volume fractions are 0.8% and 0.9% for regular samples and modified ones respectively.

(a) (b)

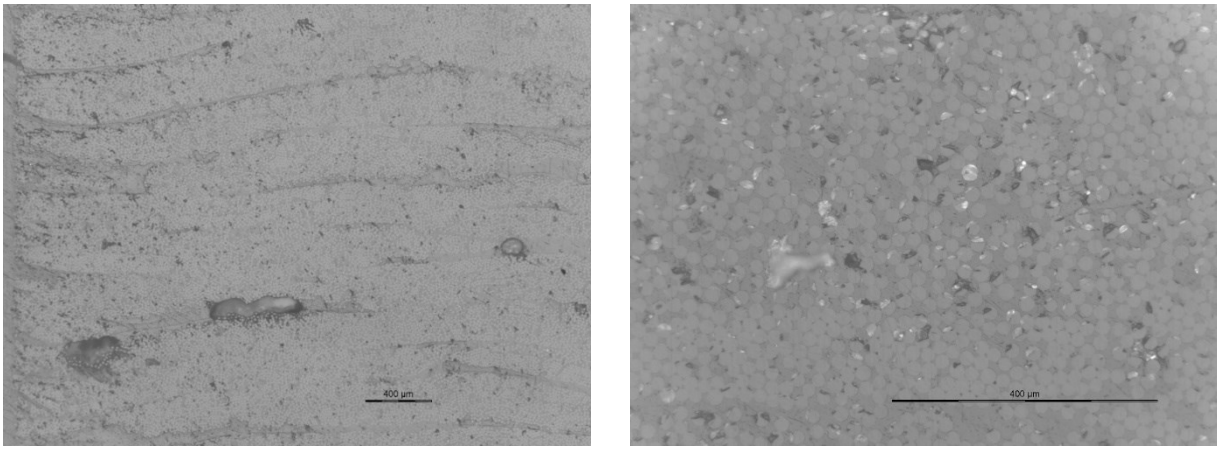

Figure 3.7: Optical microscopic image of cross section of laminate without nanoclay (a) lower magnification (b) higher magnification.

(a) (b)

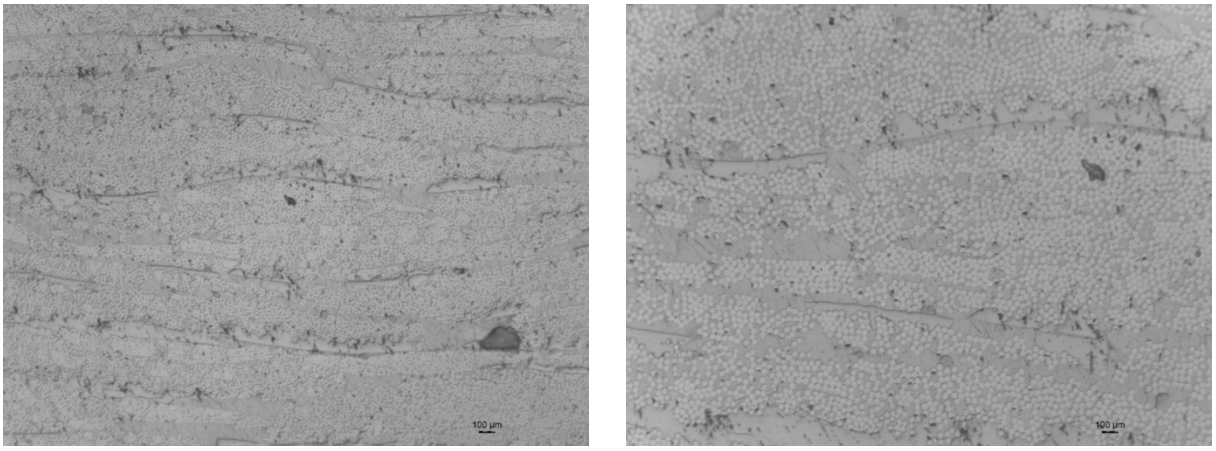

Figure 3.8: Optical microscopic image of cross section of laminate with nanoclay (a) lower magnification (b) higher magnification.

3.5 Problems regarding to sample fabrication

- Addition of the nanoclay increases the viscosity of the resin. Removing voids from the resin system and removing extra resin from the laminates are difficult during the curing process. In addition, generation of voids in samples can reduce the quality of the final laminate.
- During the dispersion of clay into resin the temperature goes up fast. Besides, Nanomer 1.30E can react with amine intercalant above 100 °C. The temperature needs to be maintained under 100 °C. In order to keep the temperature under 100 °C, a cold water bath was used and the temperature was monitored by touching the bath with hand.
- The thickness of laminates with nanoclay is higher than the neat one, even though the number of the fiber layers, the fabrication process and curing procedure were the same for both types of laminates. A caul plate was placed on top of the samples before the vacuuming in order to insert the same pressure on all laminates. The average thickness was 3.79 ± 0.16 mm and 4.08 ± 0.42 mm for samples without clay and with clay respectively.

3.6 Microstructure of nanocomposites

A scanning electron microscope (SEM) was used to show the dispersion of nanoparticles within epoxy before doing the test. Figure 3.9 indicates the SEM images of fracture surface of fiber/epoxy/nanoclay. The bright spots are clay aggregates which are visible in the images. A uniform distribution of clay into resin is shown in the images.

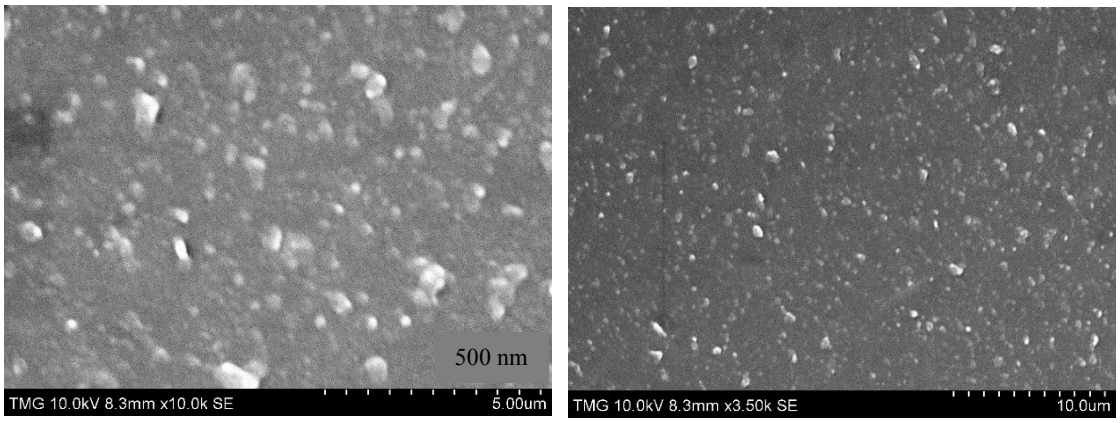

Figure 3.9: SEM images of fracture of glass/fiber/epoxy system with 2wt% nanoclay at different magnification.

3.7 Testing procedure

3.7.1 Mode II interlaminar fracture toughness

Fracture test was done according to ASTM D7905. This test was conducted using end-notched flexure (ENF) specimen to determine the Mode II interlaminar fracture toughness (G_{IIc}) of unidirectional glass fiber polymer matrix composite laminates. This method is limited to unidirectional fiber reinforced laminates. In ENF test, a sample is loaded with a mid-plane starter crack at one end in three point bending. Figure 3.10 and Figure 3.11 show the schematic and photo of specimen for interlaminar facture test. Crack length (a_0) is measured from the support roller to the crack tip. The half span length (L) is distance between the support roller and the center of loading roller. Compliance calibration (CC) method was performed on each specimen prior to testing in order to determine the relationship between specimen compliance and crack length. It is the only acceptable data reduction method for this test to calculate strain energy release rate (G_{IIc}). Non-precracked (NPC) and precracked (PC) fracture toughness were determined. The NPC fracture toughness was determined from the samples containing a thin Teflon film insert. It acts as a crack starter. The PC toughness was determined after the crack propagation occurred from the preimplanted insert during the NPC fracture test.

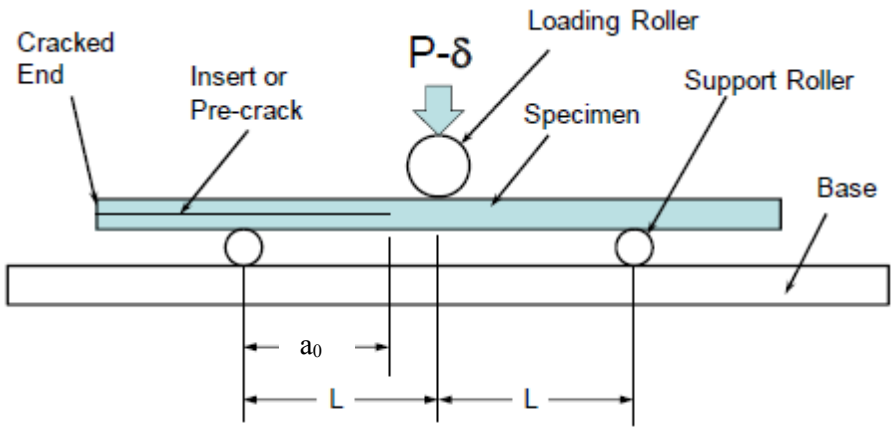

Figure 3.10: Schematic of the ENF test for experimental samples [61].

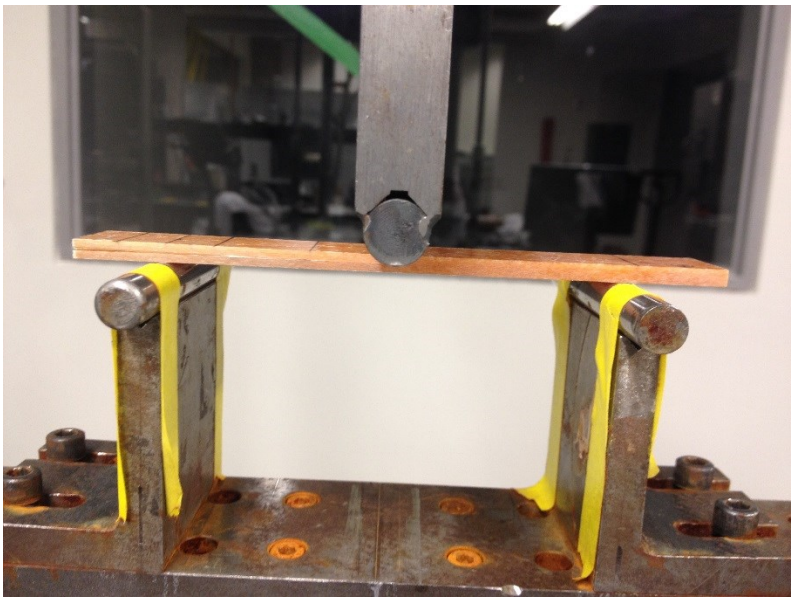

Figure 3.11: Photograph of experimental set-up for Mode II fracture toughness.

3.7.1.1 Test set up

After manufacturing the laminate, it was cut to desired size by a diamond saw. According to ASTM D7905, sample configurations are shown in Table 3-6 and Figure 3.12.

Table 3-6: Dimensions of sample according to ASTM D7905 [61].

Width	Span Length	Thickness
19-26 mm [0.75-1 in]	86-102 mm [3.39-4 in]	3.4-4.7 mm [0.133-0.185 in]

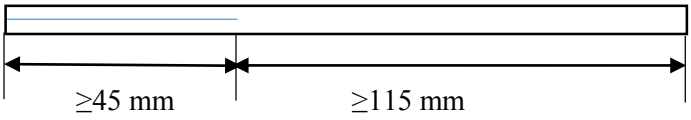

Figure 3.12: Specimen-ENF test [61].

The ratio between crack length and half-length of span is shown in Equation (3-1).

$$\frac{a_0}{L} = 0.6 \qquad (3\text{-}1)$$

Where;

a_0 = Crack length

L = Half-length of span

The actual dimensions of the samples are shown in Table 3-7.

Table 3-7: Dimensions of the actual samples.

Samples		**Width B (mm)**	**Span Length L (mm)**	**Thickness 2h (mm)**	**Crack length a_0 (mm)**
Without clay	1	20.81 ± 0.13	99.83	3.66 ± 0.04	29.77
	2	20.90 ± 0.03	100.43	4 ± 0.01	29.81
	3	20.84 ± 0.05	99.66	3.66 ± 0.03	29.94
	4	20.95 ± 0.02	100.18	3.85 ± 0.07	29.95
	Average	20.88 ± 0.06	100.03 ± 0.35	3.79 ± 0.16	29.87 ± 0.09
With clay	1	19.78 ± 0.06	100.19	4.7 ± 0.09	29.36
	2	19.87 ± 0.1	99.43	3.9 ± 0.09	29.65
	3	19.90 ± 0.09	99.84	3.9 ± 0.1	29.41
	4	19.80 ± 0.006	99.85	3.82 ± 0.07	29.13
	Average	19.84 ± 0.06	99.82 ± 0.31	4.08 ± 0.42	29.39 ± 0.2

The width (B) was measured at three points of the laminates that were at the locations of the three rollers. Thickness of each specimen was measured at six different points where the width was measured. The thickness is calculated as an average of these values.

There are three different fixtures for applying the force. They can be fixed, rotatable or rolling. The rolling fixture was used at this study. The loading noses have to contact uniformly the sample across its width. The load is applied in the middle of span length under displacement controlled loading. The displacement is recorded using center roller displacement.

According to ASTM D7905 the radius of the loading roller should be in the range of 4.7 to 9.6 mm [0.185 to 0.378 in] and the support rollers have the same radius in the range of 3.0 to 6.4 mm [0.118 to 0.25 in]. In this test the radius of the loading roller and support rollers are equal to 6.08 mm and 4.9 mm respectively. The alignment features are installed to the test fixture to ensure that the loading and support rollers are parallel and also the roller direction is perpendicular to the longitudinal direction of the sample.

3.7.1.2 Non-precracked (NPC) fracture toughness test from samples containing Teflon insert

In this method, crack propagation during NPC test is used to create the precrack for PC test. Three tests were performed. They are two compliance calibration tests and a fracture test. Figure 3.13 shows a schematic of the specimen and the compliance calibration markings on a specimen for NPC test. The end of Teflon film was located at a_i=75mm from the cracked end. It is also at a_0=30 mm from the left support roller. The two compliance calibration tests are done before fracture testing.

- First compliance calibration test: The support roller is placed at distance of a_1=20 mm from the crack tip. It is loaded up to half of the expected value of the critical load (P_c). The critical load causes the crack to propagate at that particular crack length. A graph of displacement versus load is plotted to obtain the 1st compliance.
- Second compliance calibration test: The support roller is located at distance of a_2=40 mm from the crack tip and it was reloaded to determine the 2nd compliance. These loads during the CC tests do not cause the crack propagation.
- Fracture test: The sample is repositioned in the fixture, so that the crack length is equal to a_0=30 mm and it was loaded until the crack started to grow or the force dropped. Then the sample was unloaded at rate of 0.5 mm/min [0.02 in/min]. The loading data versus displacement produced the 3rd compliance value.

Nominal rate for loading all CC and fracture tests in displacement control method must be at the range of 0.1 to 0.8 mm/min [0.004 to 0.031 in/min]. The rate of 0.5 mm/min was used in this test.

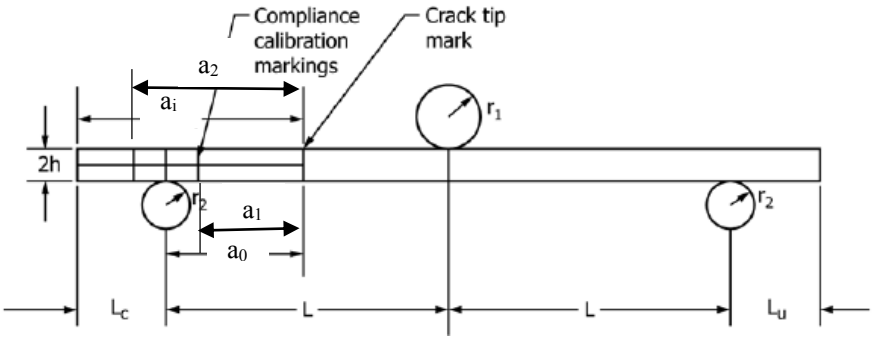

Figure 3.13: ENF specimen, fixture and dimensions *[61]*.

Three typical curves of displacement versus load are shown in Figure 3.14. Their slopes are the compliances ($C = \frac{\delta}{P}$).

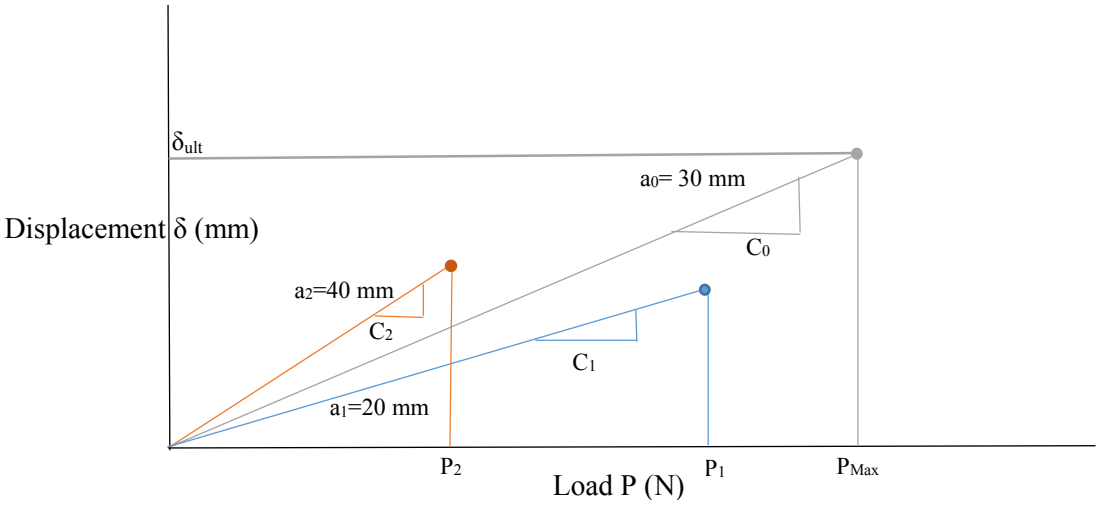

Figure 3.14: Displacement versus load.

These three compliances (C_0, C_1 and C_2) are plotted against a^3. Figure 3.15 shows compliance versus crack length cubed. The CC coefficients are determined by using a linear least squares linear regression analysis of the compliance.

$$C = A + ma^3 \qquad (3\text{-}2)$$

Where;

A = Intercept from the regression analysis (CC coefficient)

m = Slope from the regression analysis (CC coefficient)

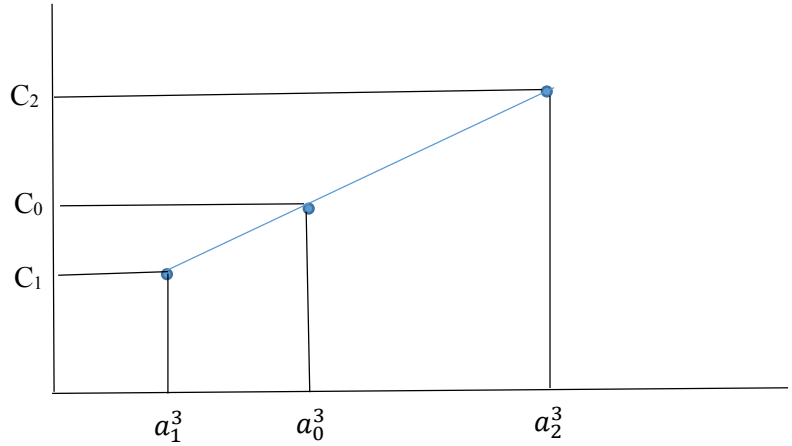

Figure 3.15: Compliance versus crack length cubed.

3.7.1.3 Critical force and force determination for compliance calibration

Equation (3-3) expresses the critical force at crack length of a_1=20 mm and a_2=40 mm that is derived by using classical beam theory (CBT) [61]. Equation (3-4) shows peak forces (P_1 and P_2) during CC at each crack length.

$$P_c = \frac{4B}{3a_j}\sqrt{G_{IIc}E_{1f}h^3} \quad , j = 1, 2 \qquad (3\text{-}3)$$

$$P_j = \frac{2B}{3a_j}\sqrt{G_{IIc}E_{1f}h^3} \quad , j = 1, 2 \qquad (3\text{-}4)$$

Where;

B = Width of sample

E_{1f} = Flexural modulus

h = Half-thickness of sample

a_j = The j^{th} crack length

Flexural modulus is obtained from equation (3-5).

$$E_{1f} = \frac{L^3}{4ABh^3} \qquad (3\text{-}5)$$

Where;

A = CC coefficient

L = Half-length of span

3.7.1.4 Exploratory test

In order to determine the peak forces during the CC tests, values of G_{IIc} and E_{1f} are required. But for the first sample, these values do not exist. Therefore, in the first test of a new material that is called exploratory test, the values for peak forces during CC are selected randomly. Proper choice of P_1 and P_2 will influence on candidate toughness G_Q that whether or not it is acceptable. In certain examples, a value of G_Q is not acceptable from the first test but it is used as an improved approximation for G_{IIc}. The values of G_Q and E_{1f} which are obtained from the first test are placed in equation (3-4) to determine new values for the peak forces during CC. Then the test is repeated.

3.7.1.5 Determination of candidate toughness

The candidate toughness is calculated as follows:

$$G_Q = \frac{3mP_{Max}^2 a_0^2}{2B} \qquad (3\text{-}6)$$

Where;

m = CC coefficient

P_{Max} = Maximum force from the fracture test

Figure 3.16 shows a typical load versus displacement curve from the fracture test. First, the displacement increases by increasing the load until the fracture happens and the crack starts to grow. The maximum force at the fracture and the ultimate displacement are depicted by P_{Max} and δ_{ult} respectively. After the crack propagation, the amount of load reduces.

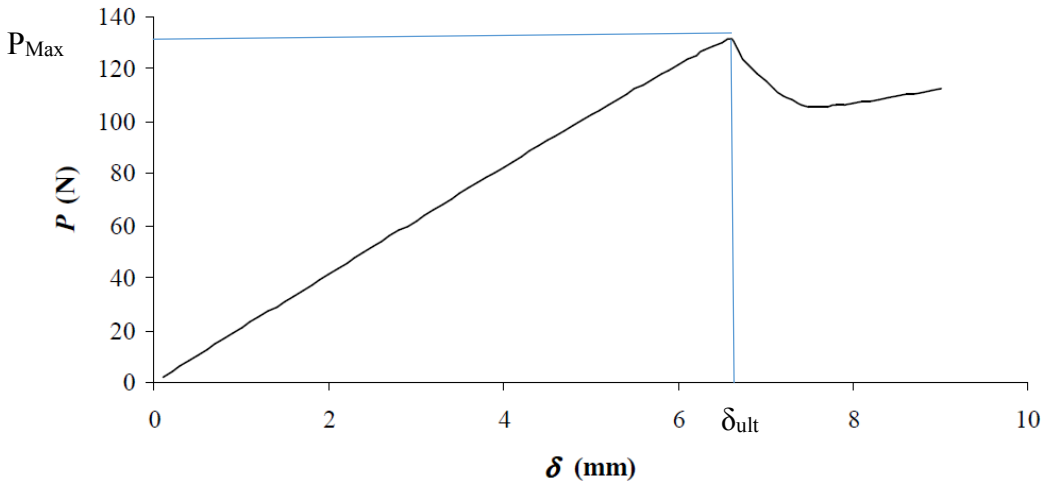

Figure 3.16: P-δ curve of the ENF test.

3.7.1.6 Candidate toughness evaluation

After determining the candidate toughness, the results must be checked for validity by calculation of percentage of candidate toughness ($\%G_Q$) which is determined by equation (3-7).

$$\%\, G_{Qj} = \left[\frac{100(P_j a_j)^2}{(P_{Max} a_0)^2}\right] ; j = 1, 2 \qquad (3\text{-}7)$$

Where;

G_{Qj} = Two values of G_Q associated with the two compliance tests

P_j = Peak value of the force during CC at a_j

a_j = j^{th} crack length used during CC

If the results are in the range of $15 \leq \%G_Q \leq 35$, then the candidate toughness will be acceptable. Otherwise, the results from this test (G_Q and E_{1f}) are used to choose the appropriate peak forces (P_1 and P_2) during subsequent CC tests.

3.7.1.7 Toughness determination

The value of G_Q that is obtained can be used as a good approximation for G_{IIc}. If the candidate toughness is accepted by candidate toughness evaluation, then $G_{IIc} = G_Q$. Otherwise, the test is repeated until confirming by candidate toughness evaluation.

3.7.1.8 Precracked (PC) fracture toughness test

After precracking the specimen during the NPC test, the sample is ready for the PC fracture testing. The location of the crack tip can be determined from the unloading data of NPC test. The compliance of the unloading data at the end of NPC test (after crack propagation) is calculated by the curve of displacement versus force. Thus, the location of the crack tip is as follows:

$$a_{calc} = \left(\frac{C_u - A}{m}\right)^{1/3} \qquad (3\text{-}8)$$

Where;

a_{calc} = Crack length

C_u = Specimen compliance from unloading after the NPC test

A and m = CC coefficients from the NPC test

The distance of a_{calc} is from the center of roller support of NPC fracture test to the crack tip as shown in Figure 3.17 where a_0 is an artificial crack length for NPC test.

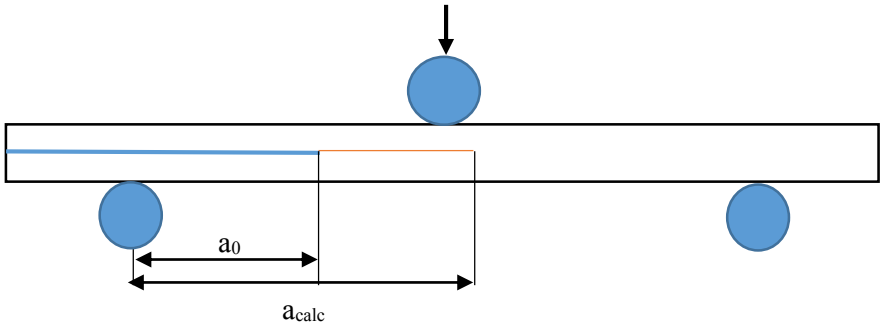

Figure 3.17: The location of crack tip (a_{calc}) for PC test.

The location of the crack tip can also be determined visually. It is an average of locations at two sides of width. If the visually determined crack tip (a_{vis}) is longer than the a_{calc}, the a_{vis} will be used for the placement of PC crack tip mark. In this thesis a_{vis} was used since it was longer than a_{calc}. This new PC crack tip was marked on sample. Three PC CC markings at 20, 30 and 40 mm from the new crack tip are shown in Figure 3.18. The distance of 30 mm is for PC fracture test and the other two distances are used for CC testing. The procedure of the test is the same as NPC test, two CC and one fracture tests.

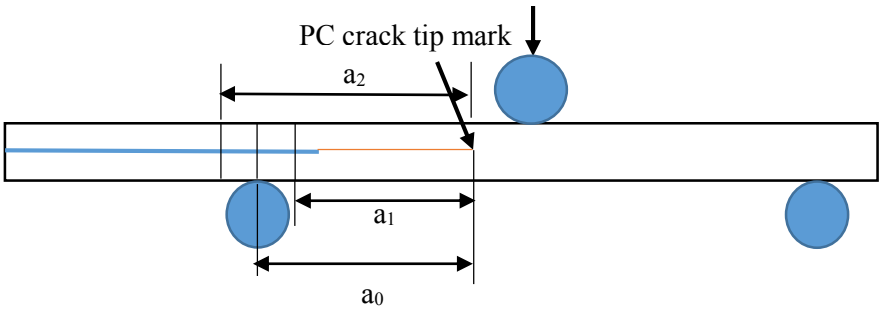

Figure 3.18: Configuration of specimen for precracked (PC) test.

3.7.2 Flexural fatigue test

Fatigue is the situation when a material cracks or fails under the repeated load is applied. The failure consists of three steps: crack initiation, crack propagation and fracture. In this thesis the flexural fatigue under displacement control was considered. Sample manufacturing and dimensions are the same as Mode II interlaminar fracture toughness test samples. The edges of the samples were colored by white paint to facilitate observation of crack propagation. They were scaled at every 5 mm in order to measure the delamination length. In addition, a camera was used to take a picture at every 5 seconds. A light source (lamp) was placed beside the sample for better observation. Figure 3.19 and Figure 3.20 illustrate the sample and fatigue test set-up.

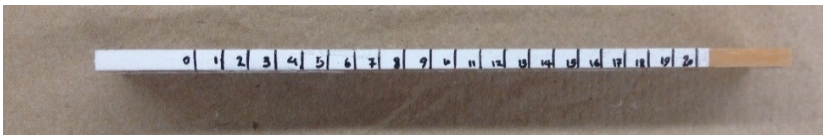

Figure 3.19: Typical fatigue sample with scale.

Figure 3.20: Experimental set-up for flexural fatigue test.

A loading arm was attached to the surface of samples by a double sided tape to avoid the lateral movement of the specimen during the test. All fatigue tests were performed under a displacement ratio ($\delta_{min}/\delta_{max}$) of 0.1 and frequency of 4 Hz. The specimens were tested at maximum displacement level of 0.8 δ_{ult}. Ultimate displacement (δ_{ult}) as shown in Figure 3.16 means the displacement when the failure happened during the interlaminar fracture test. According to experimental data, it is equal to 4.06 ± 0.53 mm.

3.7.2.1 (a-N) curve

The fatigue test was done under constant displacement amplitude.

$\delta_{max} = 0.8\ \delta_{ult}$

$\delta_{min} = 0.08\ \delta_{ult}$

The data obtained by MTS machine are time, number of cycles, load and displacement. At each time, the number of cycles was determined. The length of delamination was measured from the images of camera at that specific time. As a result, the length of delamination versus the number

of cycles (N) to failure is plotted. A typical curve of delamination length versus number of cycles can be seen in Figure 3.21. The slope of this curve shows the crack propagation rate.

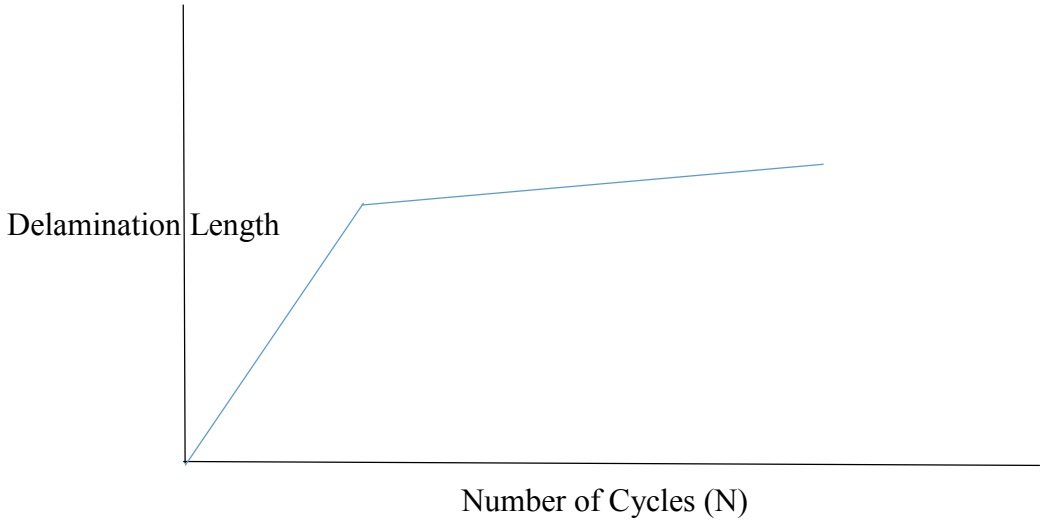

Figure 3.21: Delamination length versus number of cycles.

Chapter 4

Fracture Toughness and Flexural Fatigue Test Results

4.1 Fracture toughness test

4.1.1 NPC exploratory test

Figure 4.1 shows the compliance of NPC exploratory test for specimen without clay. The P_1 and P_2 for CC tests are selected randomly. Figure 4.2 illustrates three compliances versus crack length cubed (a^3).

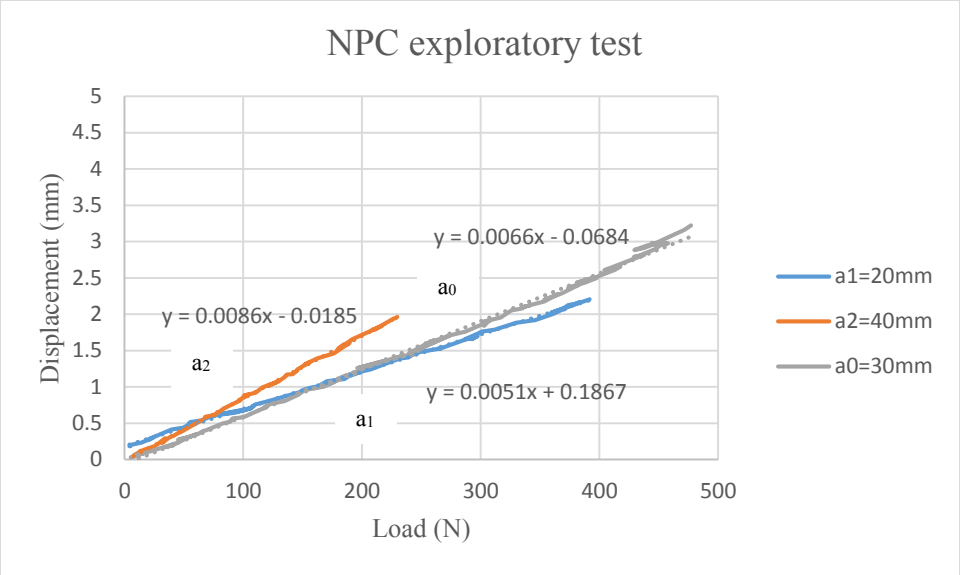

Figure 4.1: Compliance of specimens without clay for NPC exploratory test.

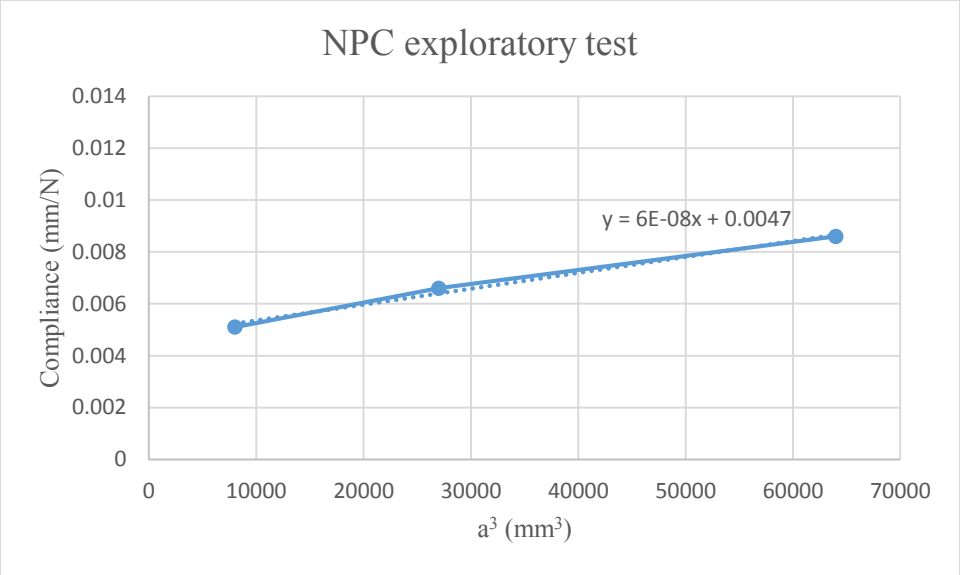

Figure 4.2: Compliance versus crack length cubed of samples without clay for NPC exploratory test.

Candidate toughness and flexural modulus were calculated by using data in Table 4-1. The percentage of candidates toughness (%G_Q) were equal to 30% and 41% at a_1=20 mm and a_2=40 mm respectively. The value of 41% was not in the range of $15 \leq {}_{\%}G_Q \leq 35$. Therefore, the candidate toughness was not acceptable. But, it was placed in equation (3-4) in order to determine the new values for peak forces during CC tests. These values are shown in Table 4-2.

Table 4-1: Candidate toughness of NPC exploratory test for regular sample.

P_1 (N) at a_1 = 20 mm	**P_2 (N) at a_1 = 40 mm**	**P_{max} (N) at a_1 = 30 mm**	**m 1/(Nmm²)**	**A (mm/N)**	**Half-Thickness h (mm)**	**E_{1f} (N/mm²)**	**G_Q (KJ/m²)**
392	230	477	$6 * 10^{-8}$	0.0047	1.83	55425	0.92

The NPC exploratory test was also done for modified sample. The peak forces during the CC tests were estimated higher than the regular samples. The candidate toughness of first test was acceptable by selecting theses values (P_1=406 N and P_2=200 N) as shown in Table 4-2. The other peak forces during CC tests for modified specimens were selected in this range.

4.1.2 Compliance of NPC test

Figure 4.3 and Figure 4.4 illustrate the compliance of NPC test for both specimens without clay and with clay. At each crack length the compliance is the slope of displacement versus force.

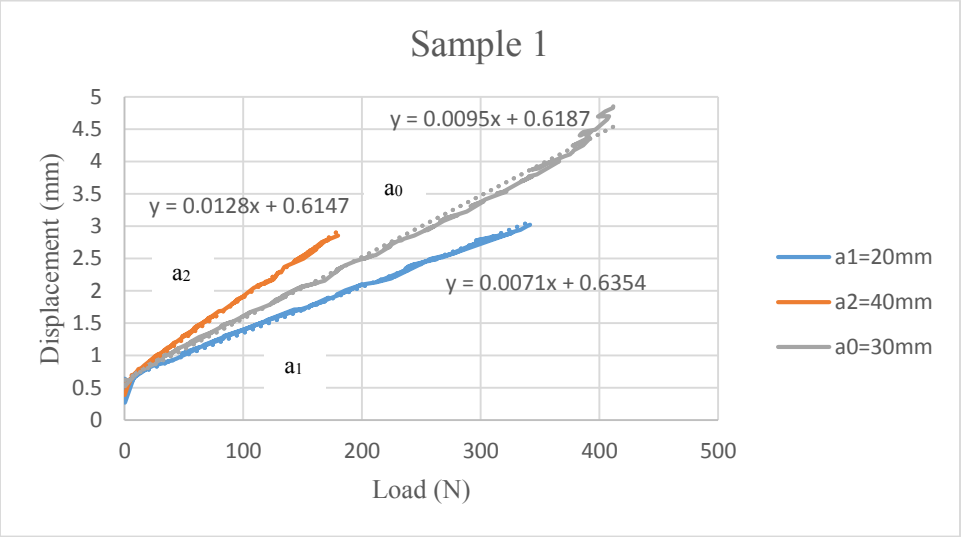

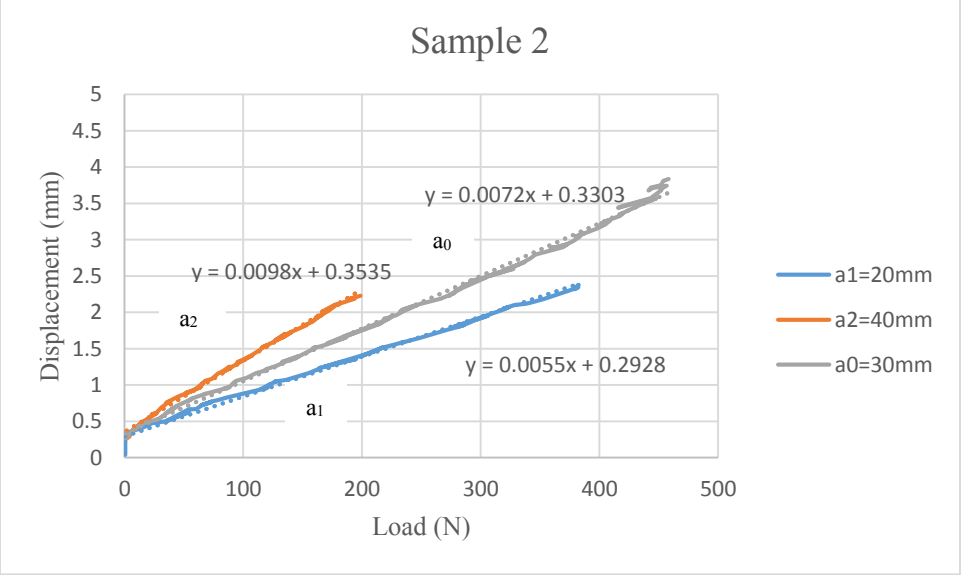

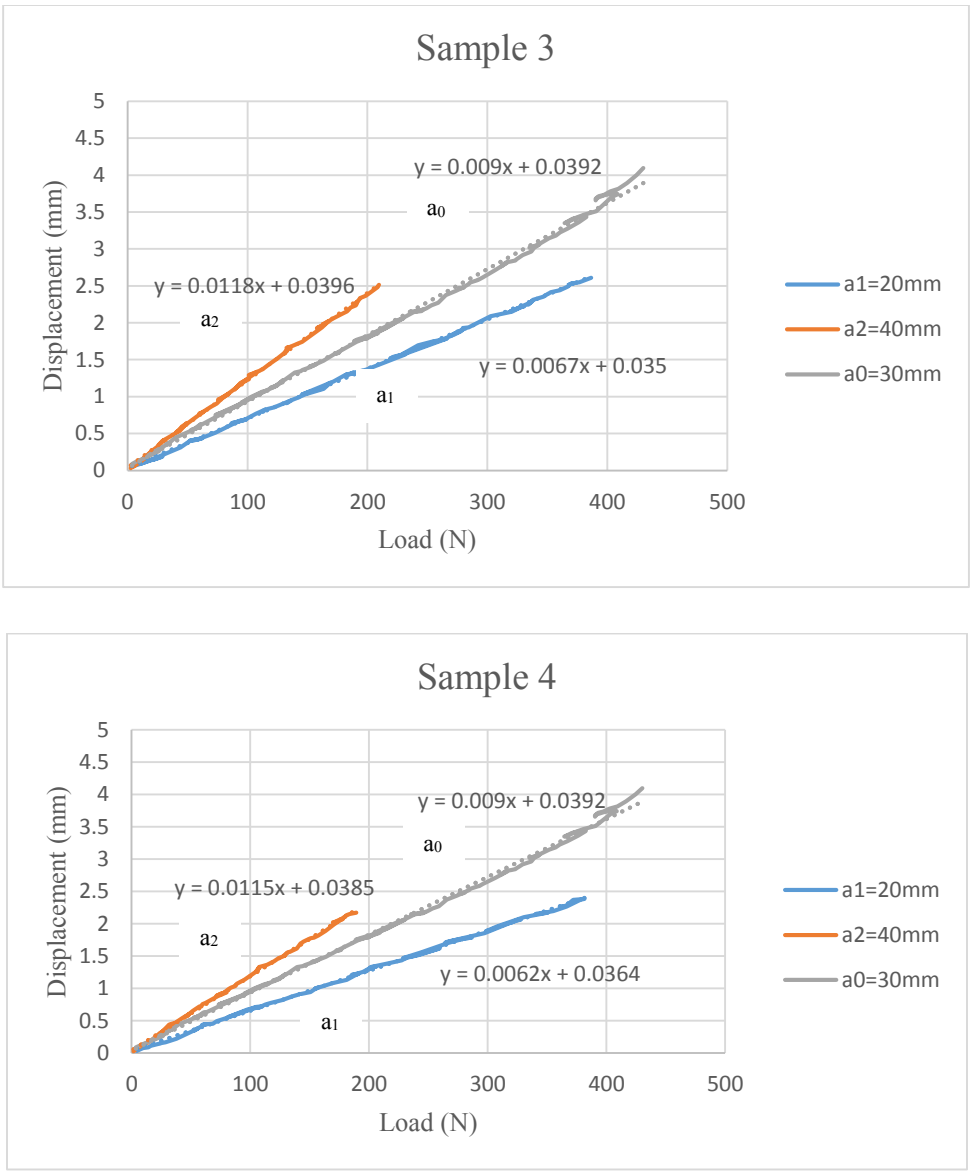

Figure 4.3: Compliance of specimens without clay for NPC test.

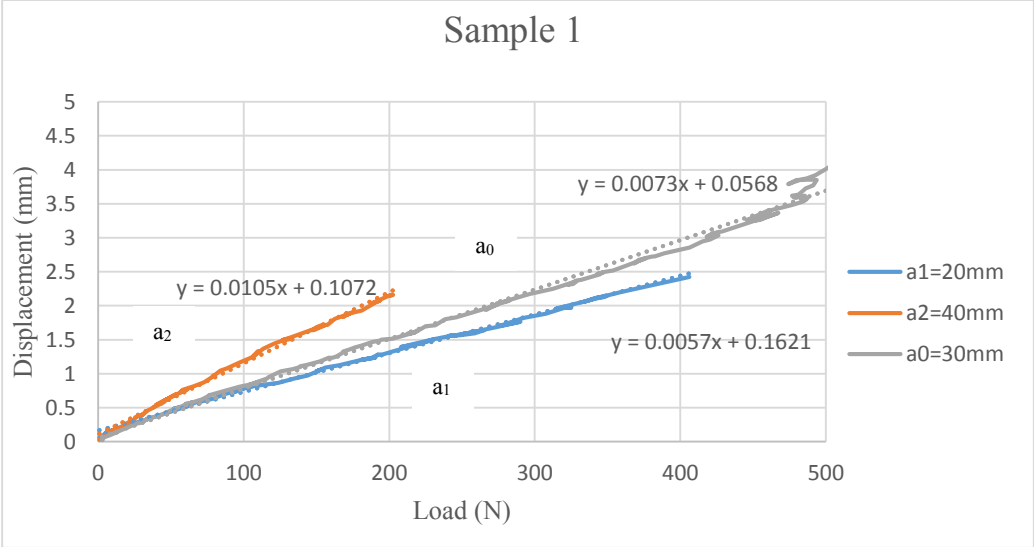
Sample 1
Displacement (mm)
Load (N)
y = 0.0073x + 0.0568
y = 0.0105x + 0.1072
y = 0.0057x + 0.1621
a0
a1
a2
a1=20mm
a2=40mm
a0=30mm

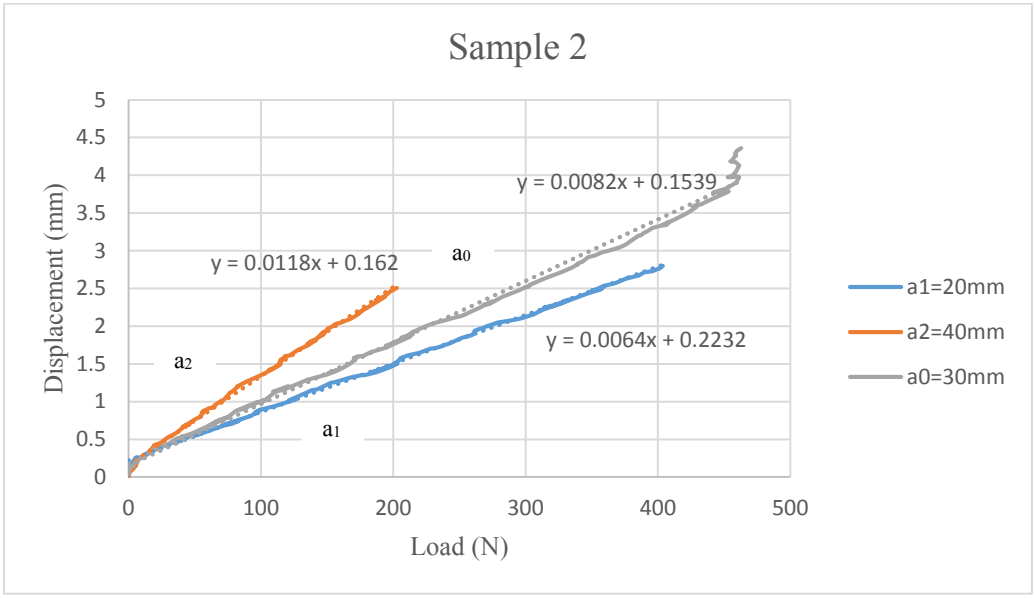
Sample 2
Displacement (mm)
Load (N)
y = 0.0082x + 0.1539
y = 0.0118x + 0.162
y = 0.0064x + 0.2232
a0
a1
a2
a1=20mm
a2=40mm
a0=30mm

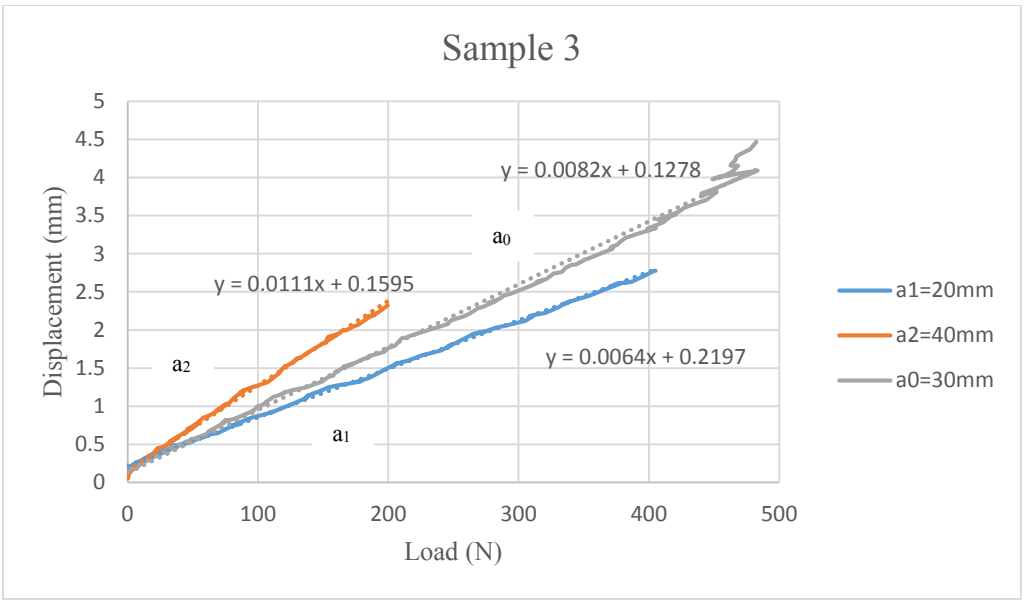

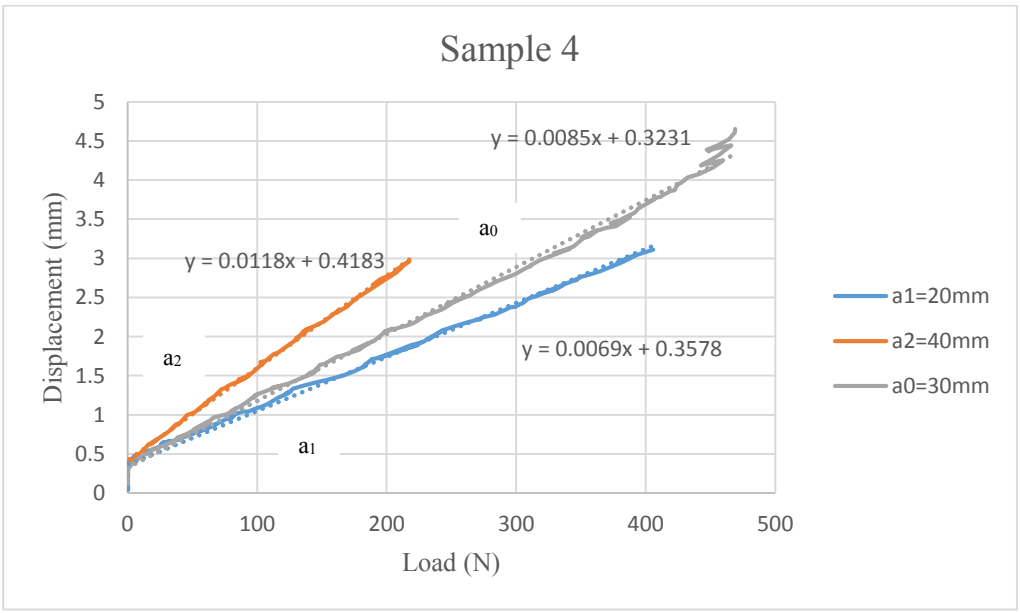

Figure 4.4: Compliance of specimens with clay for NPC test.

As explained in chapter 3, peak forces during CC method are estimated by equation (3-4). Table 4-2 shows the applied forces during the CC tests and maximum force to fracture of samples without clay and with clay from NPC test.

Table 4-2: Applied peak load of NPC test during CC method and maximum force to fracture.

Samples		P_1 (N) at a_1=20 mm	P_2 (N) at a_2=40 mm	P_{max} (N) at a_0=30 mm
Glass/epoxy	1	341	180	412
	2	382	199	458
	3	377	161	430
	4	364	189	430
	Average	366 ± 18.31	189 ± 16.15	432.5 ± 19
Nanoclay/glass/epoxy	1	406	200	505
	2	404	203	463
	3	405	200	482
	4	406	208	469
	Average	405.25 ± 0.96	202.75 ± 3.77	479.75 ± 18.61

It is obvious that the P_1 and P_2 of NPC test are increased by 10.7% and 7.3% with addition of 2wt% nanoclay 1.30E compared to neat epoxy. In addition, the maximum fracture load that is required to propagate the crack is improved by 10.9% at 2wt% of nanoclay.

Compliance values of NPC test are shown in Table 4-3 and Table 4-4.

Table 4-3: Compliances of samples without clay for NPC test.

Samples	**C_1 at a_1**	**C_2 at a_2**	**C_0 at a_0**
1	0.0071	0.0128	0.0095
2	0.0055	0.0098	0.0072
3	0.0067	0.0118	0.0090
4	0.0062	0.0115	0.0090
Average	0.0064 ± 0.0007	0.0114 ± 0.0012	0.0087 ± 0.0010

Table 4-4: Compliance amounts of samples with clay for NPC test.

Samples	**C_1 at a_1**	**C_2 at a_2**	**C_0 at a_0**
1	0.0057	0.0105	0.0073
2	0.0064	0.0118	0.0082
3	0.0064	0.0111	0.0082
4	0.0069	0.0118	0.0085
Average	0.0064 ± 0.0005	0.0113 ± 0.0006	0.0081 ± 0.0005

4.1.3 PC exploratory test

The peak forces of regular sample during CC tests were selected randomly. At first test, the candidate toughness was acceptable by using these values (P_1=235 N and P_2=122 N). In addition, P_1=300 N and P_2=160 N were chosen for modified sample as an exploratory test. The result of G_Q was also allowable. Then the other forces were selected in these ranges for regular and modified specimens as shown in Table 4-5.

4.1.4 Compliance of PC test

Figure 4.5 and Figure 4.6 illustrate the compliance of PC test for both specimens without clay and with clay.

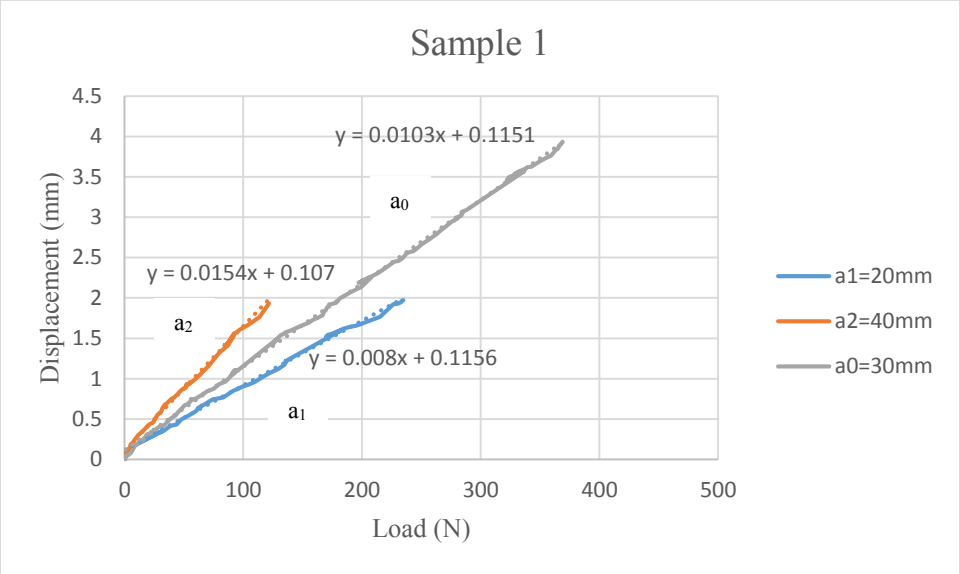

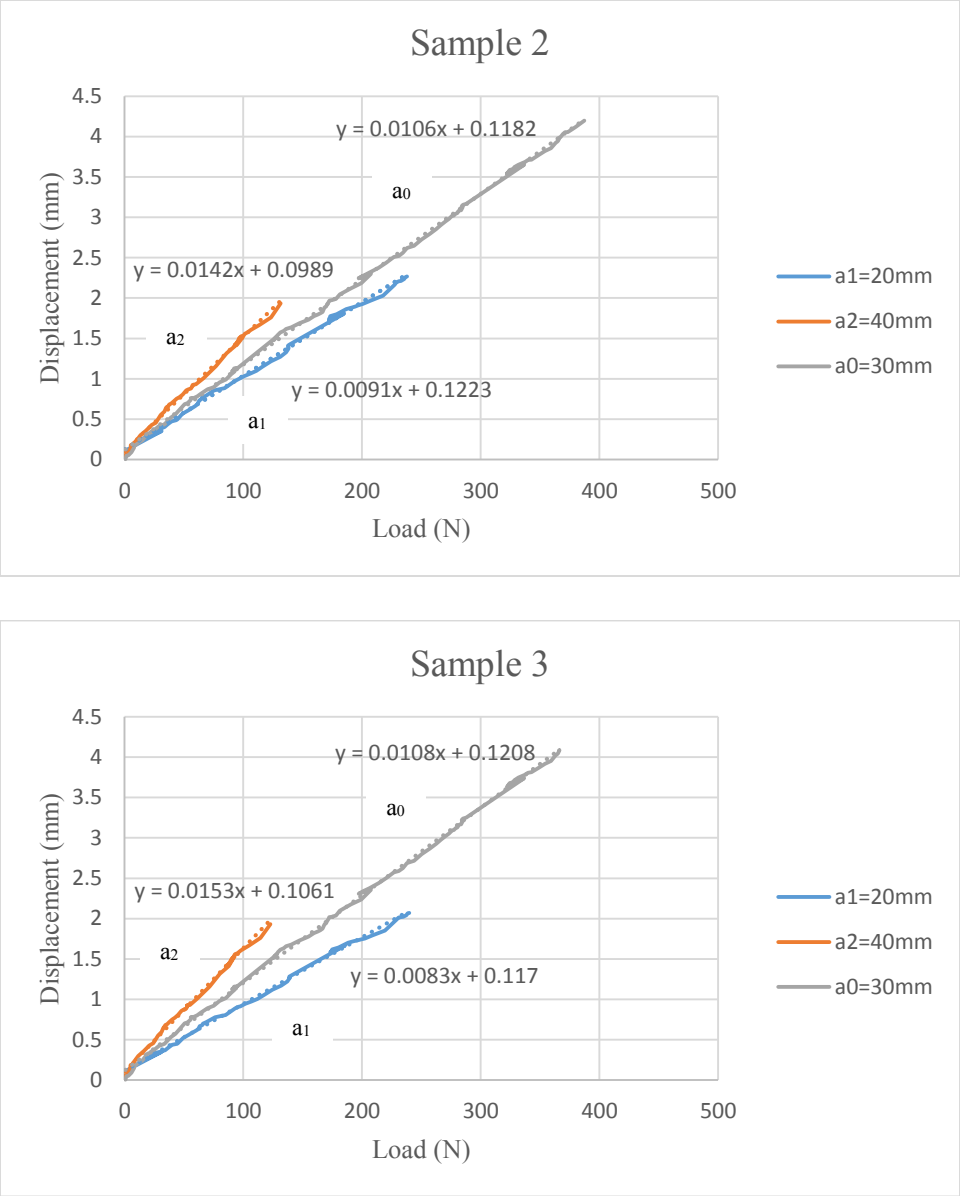

Figure 4.5: Compliance of specimens without clay for PC test.

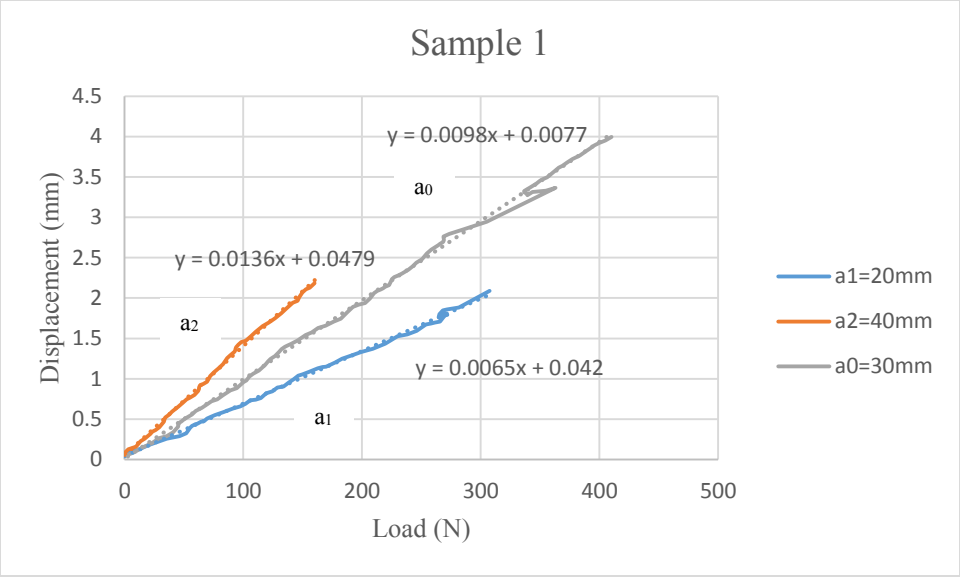
Sample 1
Displacement (mm)
Load (N)
y = 0.0098x + 0.0077
a0
y = 0.0136x + 0.0479
a2
y = 0.0065x + 0.042
a1
a1=20mm
a2=40mm
a0=30mm

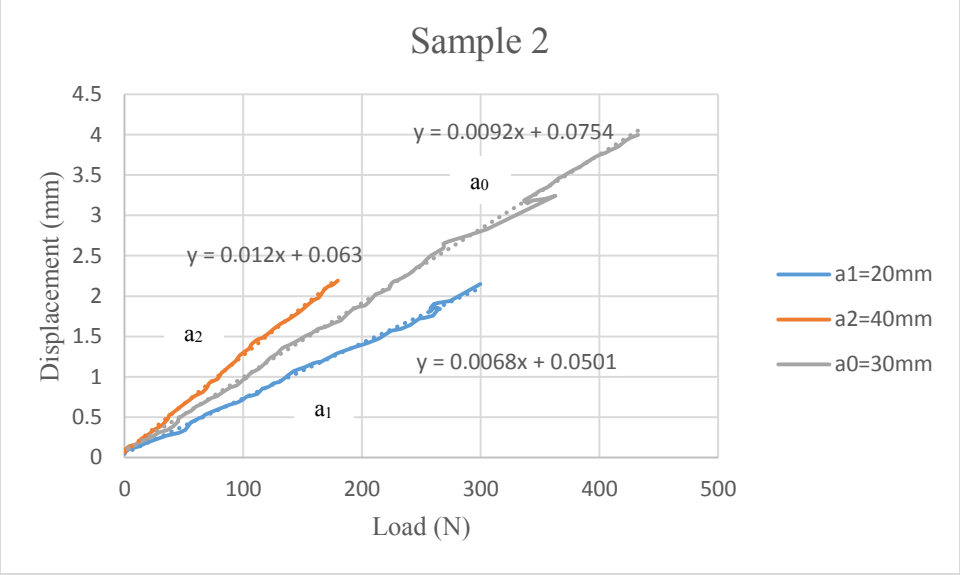
Sample 2
Displacement (mm)
Load (N)
y = 0.0092x + 0.0754
a0
y = 0.012x + 0.063
a2
y = 0.0068x + 0.0501
a1
a1=20mm
a2=40mm
a0=30mm

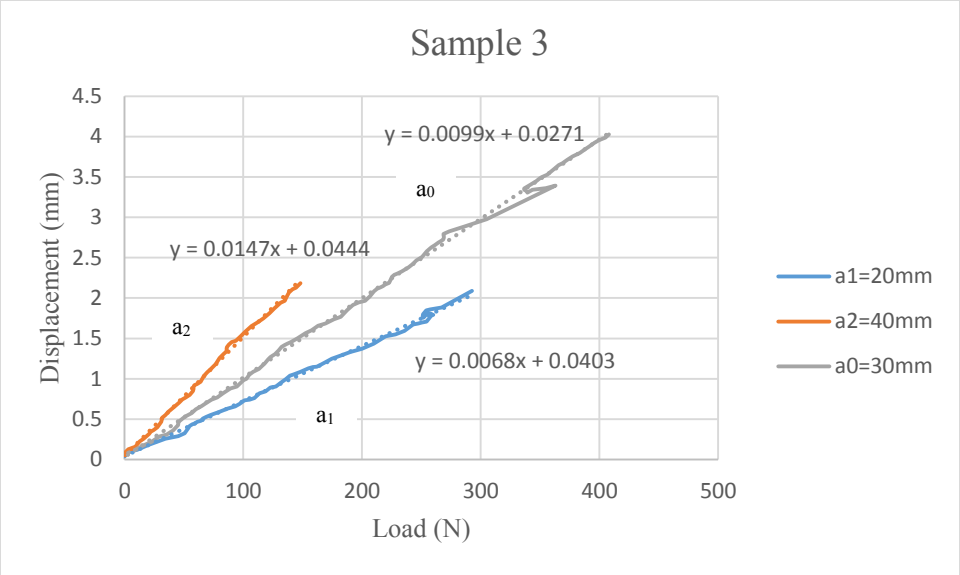

Figure 4.6: Compliance of specimens with clay for PC test.

Table 4-5 shows the applied forces during the CC tests and maximum force to fracture of samples without clay and with clay from PC test.

Table 4-5: Applied peak load of PC test during the CC method and maximum force to fracture.

Samples		**P_1 (N) at a_1=20 mm**	**P_2 (N) at a_2=40 mm**	**P_{max} (N) at a_0=30 mm**
Glass/epoxy	1	235	122	369
	2	238	132	387
	3	240	123	366
	Average	237.67 ± 2.52	125.67 ± 5.51	374 ± 11.36
Nanoclay/glass/epoxy	1	300	160	410
	2	299	177	432
	3	293	148	408
	Average	297.33 ± 3.79	161.67 ± 14.58	416.67 ± 13.32

At 2wt% nanoclay, P_1 and P_2 of PC test are increased by 25% and 28.6% in comparison to regular samples. Moreover, the P_{max} has improvement of 11.4% for specimens with 2wt%nanoclay.

Compliance values of PC test are shown in Table 4-6 and Table 4-7.

Table 4-6: Compliances of samples without clay for PC test.

Samples	**C_1 at a_1**	**C_2 at a_2**	**C_0 at a_0**
1	0.008	0.0154	0.0103
2	0.0091	0.0142	0.0106
3	0.0083	0.0153	0.0108
Average	0.0085 ± 0.0007	0.0150 ± 0.007	0.0106 ± 0.0003

Table 4-7: Compliances of samples with clay for PC test.

Samples	**C_1 at a_1**	**C_2 at a_2**	**C_0 at a_0**
1	0.0065	0.0136	0.0098
2	0.0068	0.0120	0.0092
3	0.0068	0.0147	0.0099
Average	0.0067 ± 0.0002	0.0134 ± 0.0014	0.0096 ± 0.0004

4.1.5 CC coefficients of NPC test

Figure 4.7 and Figure 4.8 show the three compliances versus crack length cubed (a^3). The slope of these graphs are m and the intercepts are A according to equation (3-2). The CC coefficients are indicated in Table 4-8 and Table 4-9.

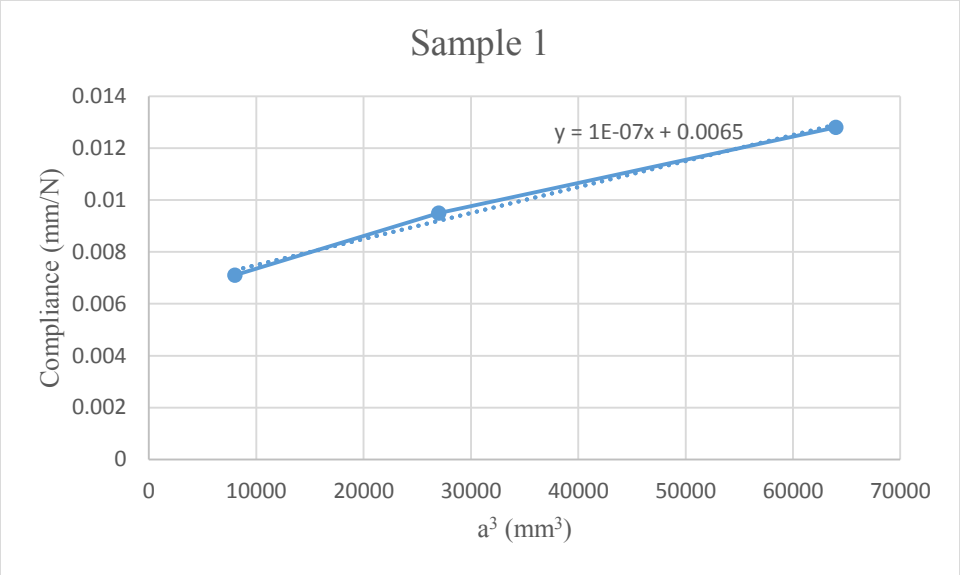
Sample 1
y = 1E-07x + 0.0065
Compliance (mm/N)
0.014
0.012
0.01
0.008
0.006
0.004
0.002
0
0
10000
20000
30000
40000
50000
60000
70000
a3 (mm3)

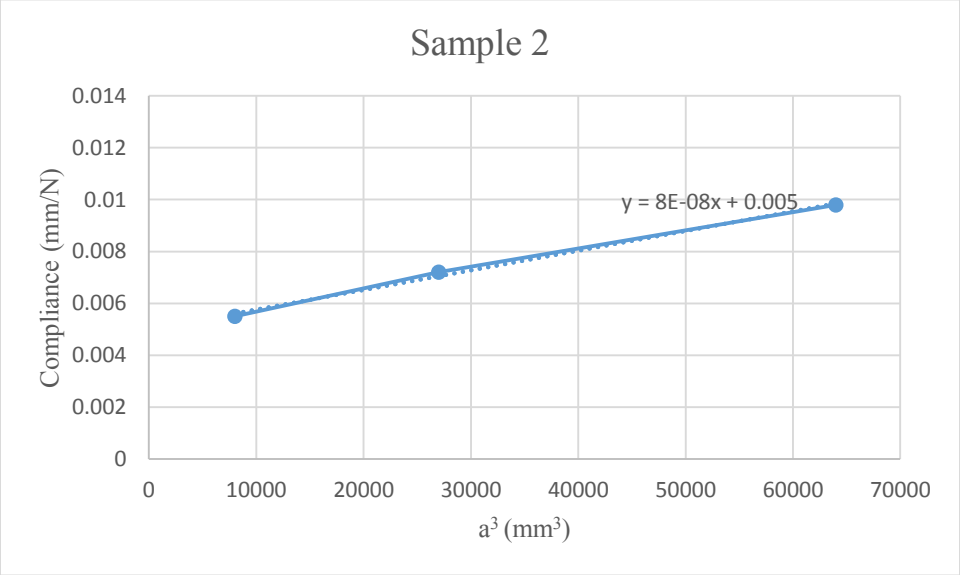
Sample 2
y = 8E-08x + 0.005
Compliance (mm/N)
0.014
0.012
0.01
0.008
0.006
0.004
0.002
0
0
10000
20000
30000
40000
50000
60000
70000
a3 (mm3)

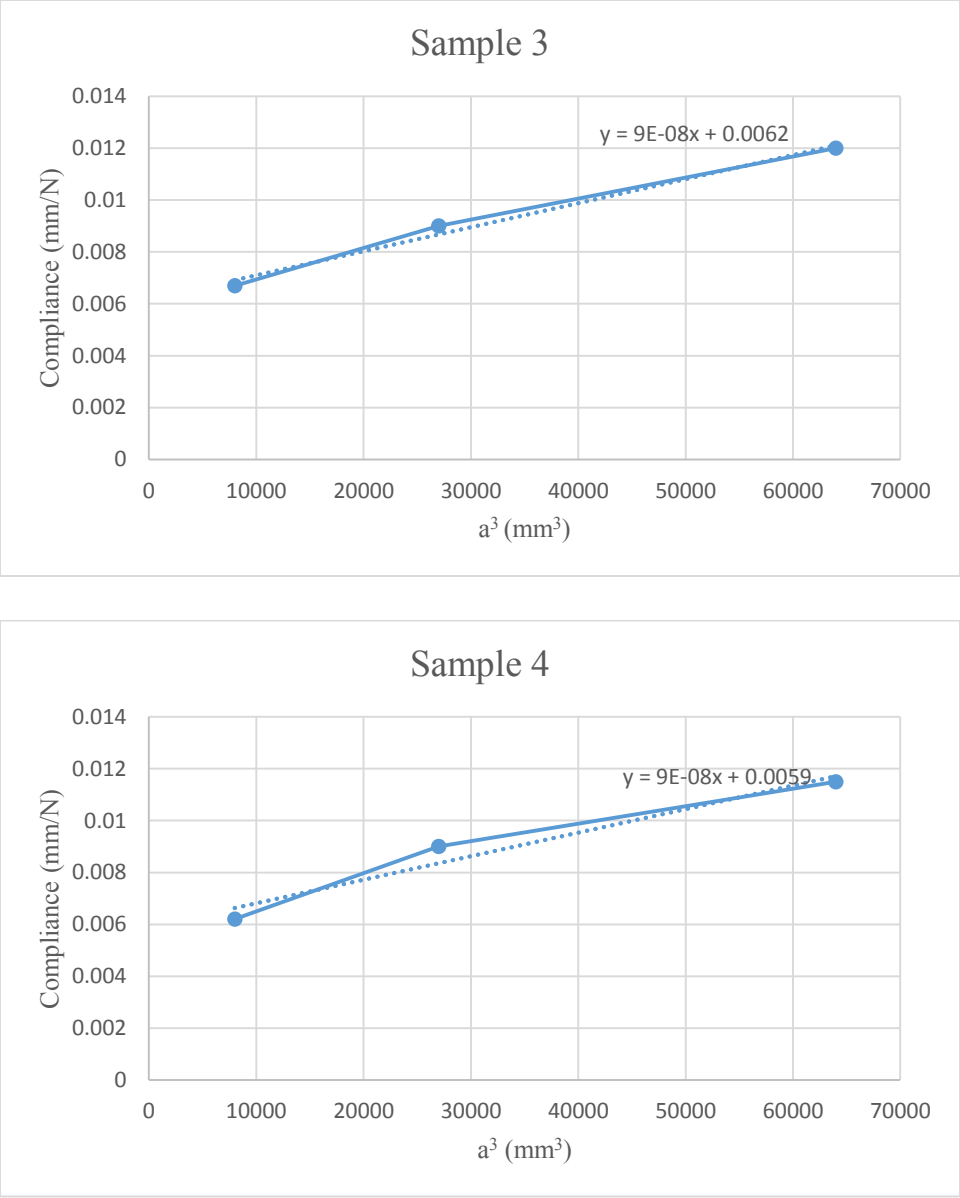

Figure 4.7: Compliance versus crack length cubed of samples without clay for NPC test.

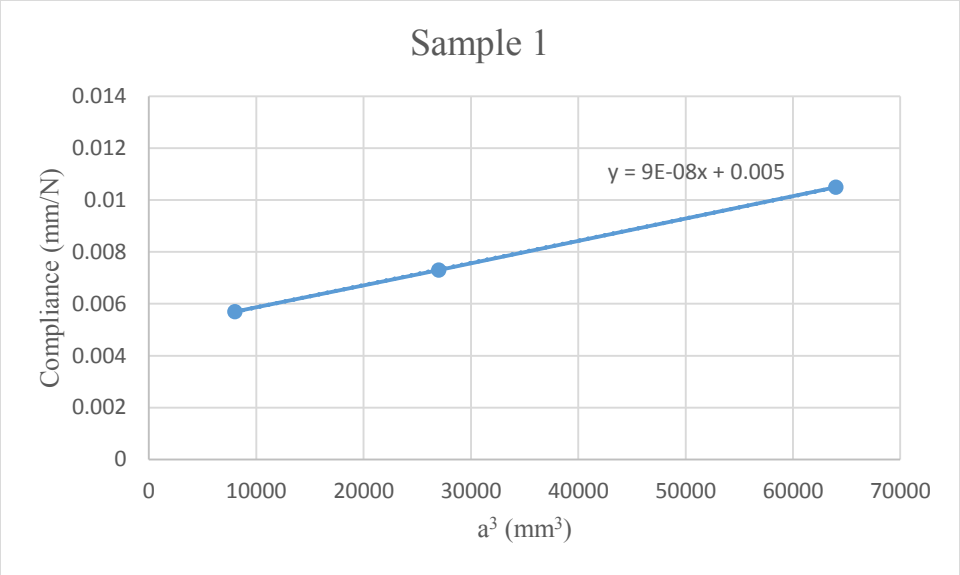
Sample 1
Compliance (mm/N)
0.014
0.012
0.01
0.008
0.006
0.004
0.002
0
y = 9E-08x + 0.005
0
10000
20000
30000
40000
50000
60000
70000
a3 (mm3)

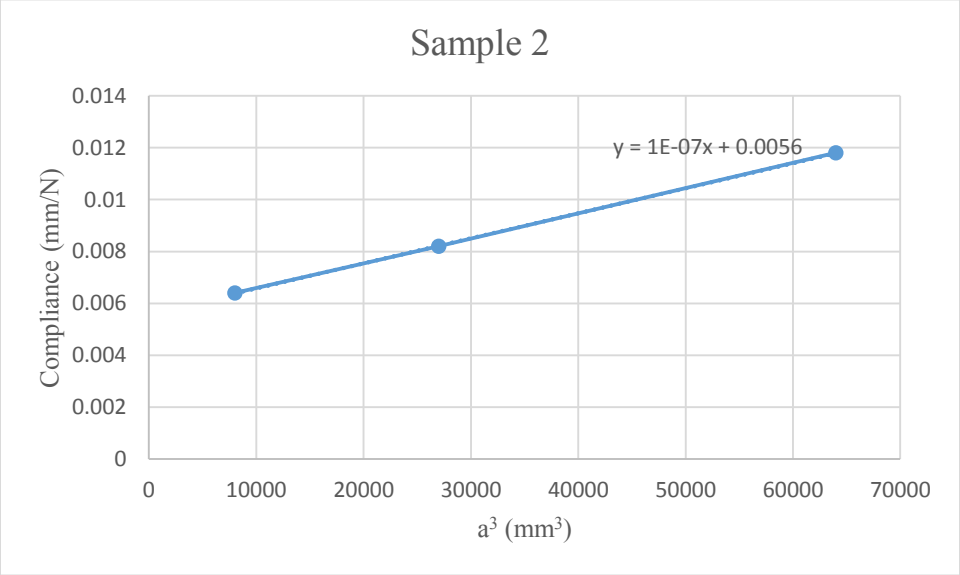
Sample 2
Compliance (mm/N)
0.014
0.012
0.01
0.008
0.006
0.004
0.002
0
y = 1E-07x + 0.0056
0
10000
20000
30000
40000
50000
60000
70000
a3 (mm3)

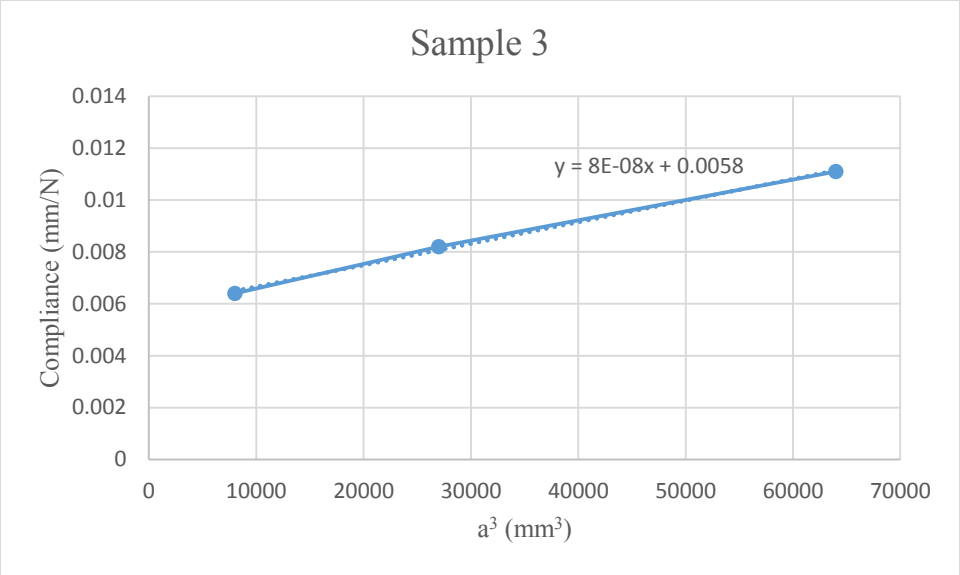

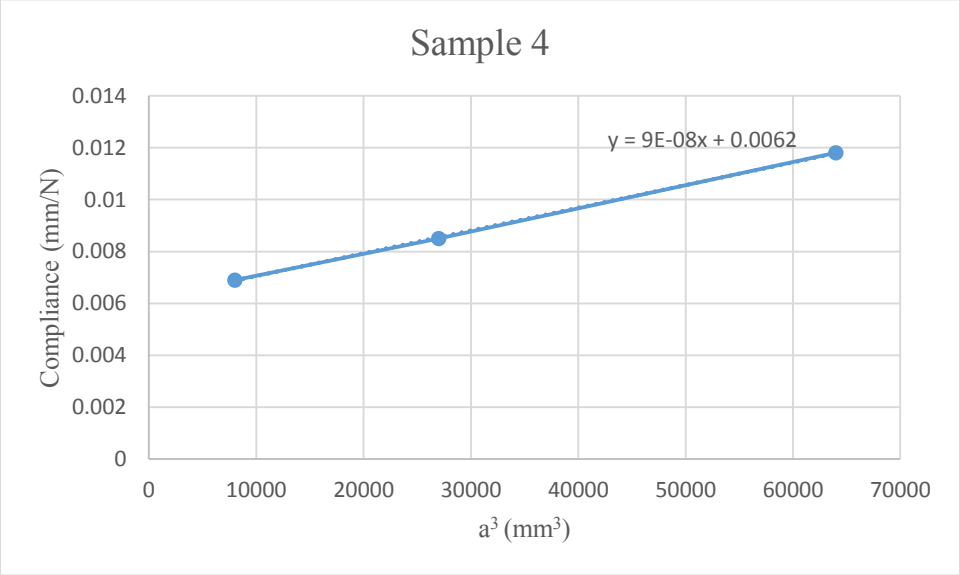

Figure 4.8: Compliance versus crack length cubed of samples with clay for NPC test.

Table 4-8: CC coefficients of specimens without clay for NPC test.

Samples	**A** **(mm/N)**	**m** **1/(Nmm^2)**
1	0.0065	10^{-7}
2	0.0050	$8*10^{-8}$
3	0.0062	$9*10^{-8}$
4	0.0059	$9*10^{-8}$
Average	0.0059 ± 0.0006	$8.67*10^{-8} \pm 5.77*10^{-9}$

Table 4-9: CC coefficients of specimens with clay for NPC test.

Samples	**A** **(mm/N)**	**m** **1/(Nmm^2)**
1	0.0050	$9*10^{-8}$
2	0.0056	10^{-7}
3	0.0058	$8*10^{-8}$
4	0.0062	$9*10^{-8}$
Average	0.00565 ± 0.0005	$8.67*10^{-8} \pm 5.77*10^{-9}$

4.1.6 CC coefficients of PC test

Figure 4.9 and Figure 4.10 show the three compliances versus crack length cubed (a^3). The CC coefficients are indicated in Table 4-10 and Table 4-11.

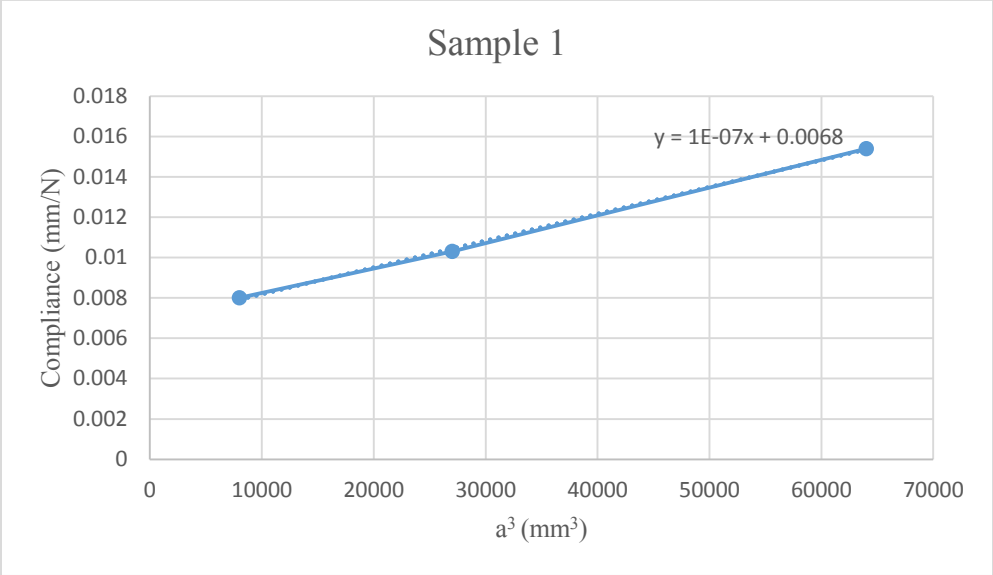
Sample 1
Compliance (mm/N)
0.018
0.016
0.014
0.012
0.01
0.008
0.006
0.004
0.002
0
y = 1E-07x + 0.0068
0
10000
20000
30000
40000
50000
60000
70000
a³ (mm³)

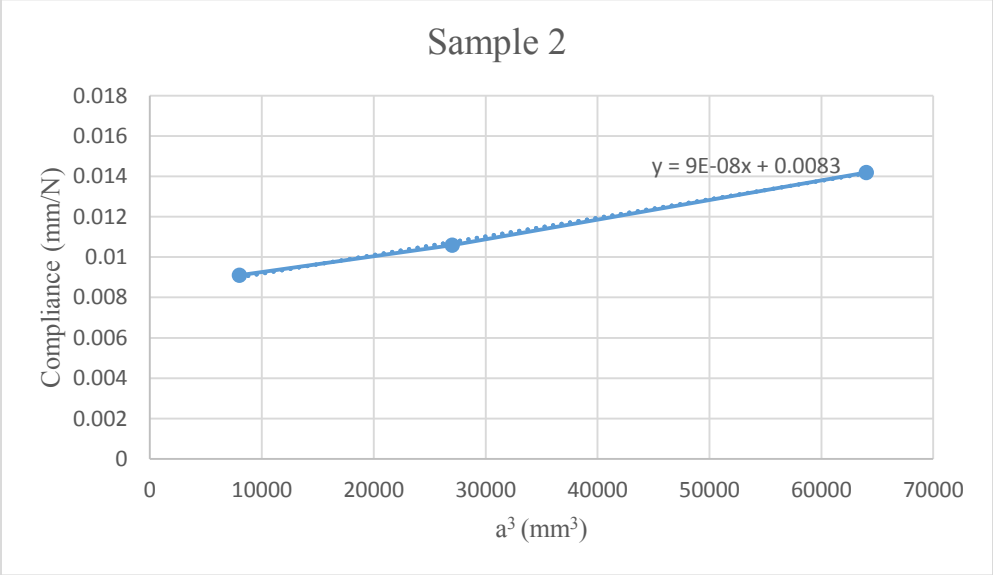
Sample 2
Compliance (mm/N)
0.018
0.016
0.014
0.012
0.01
0.008
0.006
0.004
0.002
0
y = 9E-08x + 0.0083
0
10000
20000
30000
40000
50000
60000
70000
a³ (mm³)

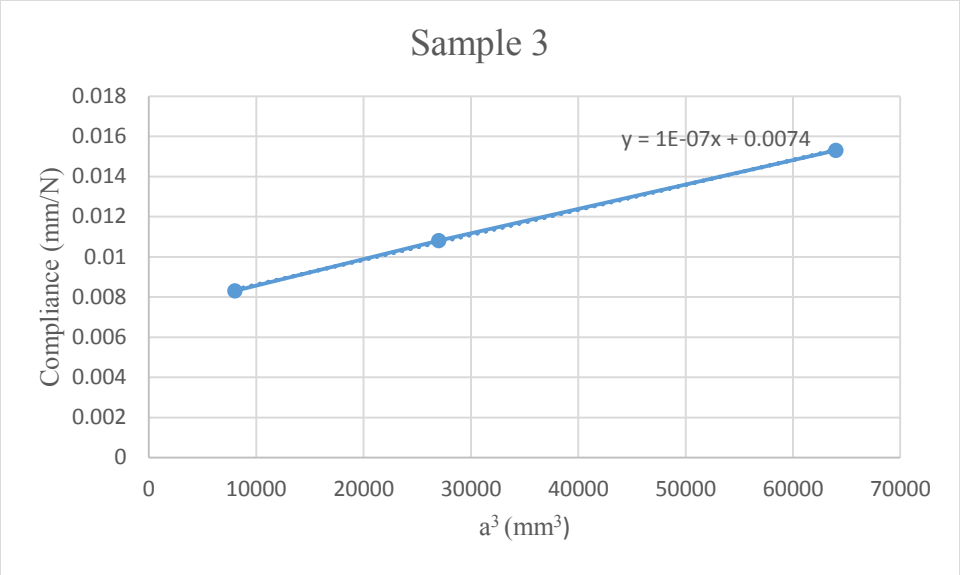

Figure 4.9: Compliance versus crack length cubed of samples without clay for PC test.

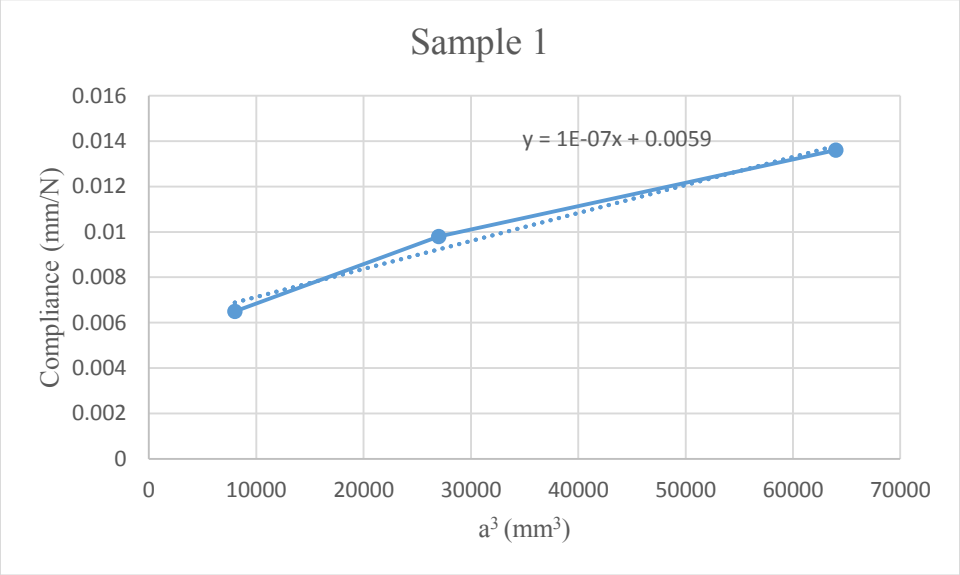

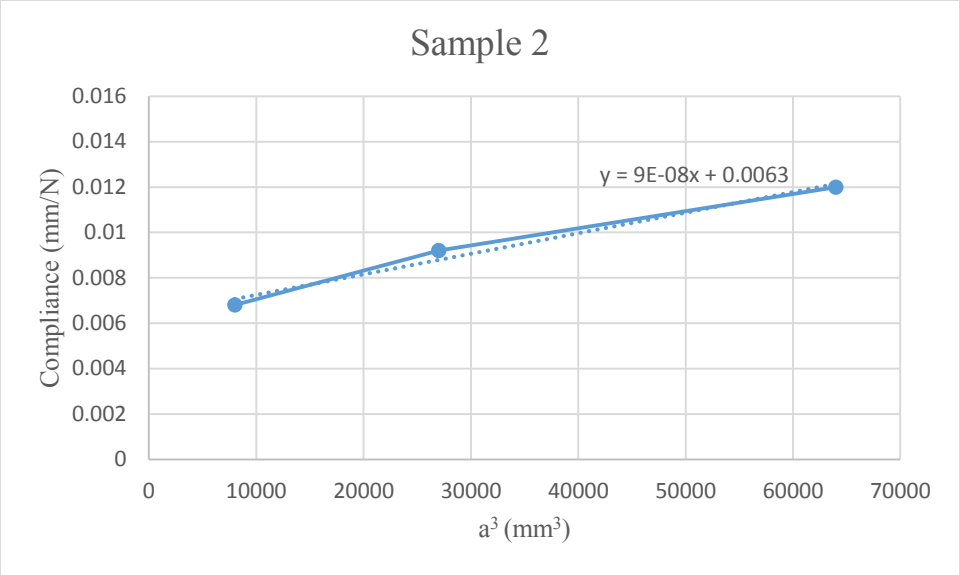

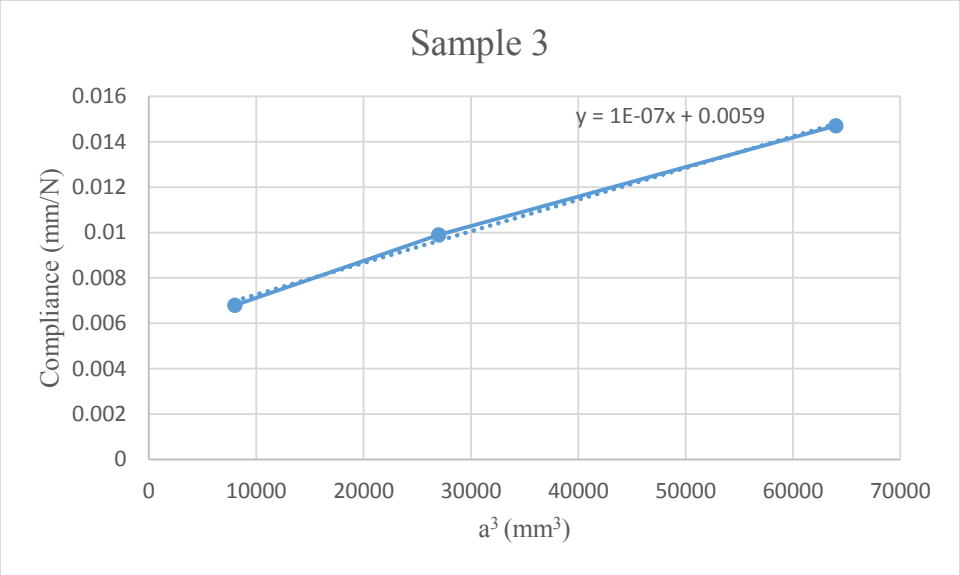

Figure 4.10: Compliance versus crack length cubed of samples with clay for PC test.

Table 4-10: CC coefficients of specimens without clay for PC test.

Samples	**A** **(mm/N)**	**m** **1/(Nmm^2)**
1	0.0068	10^{-7}
2	0.0083	$9*10^{-8}$
3	0.0077	10^{-7}
Average	0.0076 ± 0.0008	$9.5*10^{-8} \pm 5.77*10^{-9}$

Table 4-11: CC coefficients of specimens with clay for PC test.

Samples	**A** **(mm/N)**	**m** **1/(Nmm^2)**
1	0.0059	10^{-7}
2	0.0063	$9*10^{-8}$
3	0.0059	10^{-7}
Average	0.0060 ± 0.0002	$9.5*10^{-8} \pm 5.77*10^{-9}$

4.1.7 Mode II interlaminar fracture toughness of NPC and PC tests

Finally, the candidate toughness is determined by equation (3-6). For all specimens when $\%G_Q$ is acceptable then $G_{IIc} = G_Q$. Table 4-12 and Table 4-13 show the percentage of candidate toughness of both samples for NPC and PC tests respectively. The percentage of G_Q is calculated according to values of forces from Table 4-2 and Table 4-5. Since it is in the range of $15 \leq \%G_Q \leq 35$, then the candidate toughness is acceptable.

Table 4-12: Percentage of candidate toughness (%G_Q) for NPC test.

Samples		**%G_Q (a=a_1)**	**%G_Q (a=a_2)**	**Accepted (Y/N)**
Without clay	1	31	34	Y
	2	31	34	Y
	3	34	25	Y
	4	31	34	Y
	Average	32	34	Y
With clay	1	29	28	Y
	2	34	34	Y
	3	32	31	Y
	4	33	35	Y
	Average	32	32	Y

Table 4-13: Percentage of candidate toughness (%G_Q) for PC test.

Samples		%G_Q (a=a_1)	%G_Q (a=a_2)	Accepted (Y/N)
Without clay	1	18	19	Y
	2	17	21	Y
	3	19	20	Y
	Average	18	20	Y
With clay	1	24	27	Y
	2	21	30	Y
	3	23	23	Y
	Average	23	27	Y

Table 4-14 illustrates the Mode II strain energy release rate (G_{IIc}) of both samples for NPC and PC tests.

Table 4-14: Calculated G_{IIc} of samples without clay and with clay for NPC and PC tests.

Samples		**NPC G_{IIc} (KJ/m^2)**
Without nanoclay	1	1.14
	2	1.13
	3	1.12
	4	1.12
	Average	1.13 ± 0.01
With 2wt% nanoclay	1	1.55
	2	1.45
	3	1.26
	4	1.34
	Average	1.40 ± 0.13
Samples		**PC G_{IIc} (KJ/m^2)**
Without nanoclay	1	0.92
	2	0.91
	3	0.90
	Average	0.91 ± 0.01
With 2wt% nanoclay	1	1.13
	2	1.13
	3	1.12
	Average	1.12 ± 0.006

According to ASTM D7905, NPC G_{IIc} and PC G_{IIc} for S2/5216 (regular samples) which consists of S-2 glass fibers/epoxy were determined to be 1.17 KJ/m^2 (6.68 lbf/in^2) and 0.93 KJ/m^2 (5.31 lbf/in^2) respectively. The experimental results show the average of G_{IIc} is 1.13 KJ/m^2 with standard deviation of 0.01 for NPC test and 0.91 KJ/m^2 with standard deviation of 0.01 for PC test. As compared to 1.17 KJ/m^2 and 0.93 KJ/m^2 from ASTM these values are acceptable.

From Table 4-14, it can be clearly seen that nanoclay has a significant effect on Mode II strain energy release rate G_{IIc}. The average of NPC G_{IIc} is 1.40 KJ/m^2 with standard deviation of 0.13. In other words, at 2wt% nanoclay, the NPC G_{IIc} improvement is 24%. Therefore, the incorporation of clay nanofiller into the epoxy resin demonstrates higher resistance of composites to fracture. The average of PC G_{IIc} is 1.12 KJ/m^2 by standard deviation of 0.006 which shows 23% improvement.

The difference between the response of non-precracked (NPC) and precracked (PC) samples are due to the crack tip condition. In PC test, the crack tip is sharp so crack propagation can occur by lower amount of force. As a result, the PC fracture toughness of laminates is 19% and 20% lower than the NPC toughness for samples without clay and with clay respectively.

4.1.8 Flexural modulus of NPC and PC tests

Flexural modulus can be calculated by equation (3-5) for both types of specimens. According to that equation, the flexural modulus depends on the thickness. But due to the different thickness of regular and modified samples, the values of $E_{1f}h^3$ were calculated to remove the effect of thickness. Table 4-15 and Table 4-16 show the values of $E_{1f}h^3$ for NPC test.

Table 4-15: $E_{1f}\,h^3$ of samples without clay for NPC test.

Samples	$E_{1f}\,h^3$ (Nmm)	A (mm/N)	Thickness (mm)
1	240385	0.0065	3.66
2	312500	0.0050	4
3	252016	0.0062	3.66
4	264831	0.0059	3.85
Average	267433 ± 31661	0.0059 ± 0.0006	3.79 ± 0.16

Table 4-16: $E_{1f}\,h^3$ of samples with clay for NPC test.

Samples	$E_{1f}\,h^3$ (Nmm)	A (mm/N)	Thickness (mm)
1	312500	0.0050	4.7
2	279018	0.0056	3.9
3	269397	0.0058	3.9
4	252016	0.0062	3.82
Average	278233 ± 25431	0.00565 ± 0.0005	4.08 ± 0.42

The average values of $E_{1f}\,h^3$ obtained from NPC test for neat and nanoclay samples, are 267433 Nmm and 278233 Nmm respectively.

The $E_{1f}h^3$ from PC test for samples without clay and with clay are shown in Table 4-17 and Table 4-18. The average values of $E_{1f}\,h^3$ obtained from PC test for regular and modified samples, are 206984 Nmm and 259226 Nmm respectively. The results show the higher stiffness for modified samples than the regular ones.

Table 4-17: $E_{1f}\,h^3$ of samples without clay for PC test.

Samples	$E_{1f}\,h^3$ (Nmm)	A (mm/N)	Thickness (mm)
1	229779	0.0068	3.66
2	188253	0.0083	4
3	202922	0.0077	3.66
Average	206984 ± 21059	0.0076 ± 0.0008	3.77 ± 0.20

Table 4-18: $E_{1f}\,h^3$ of samples with clay for PC test.

Samples	$E_{1f}\,h^3$ (Nmm)	A (mm/N)	Thickness (mm)
1	264831	0.0059	4.7
2	248016	0.0063	3.9
3	259226	0.0059	3.9
Average	259226 ± 9708	0.0060 ± 0.0002	4.17 ± 0.46

4.2 SEM after interlaminar fracture toughness test

SEM images of cross-section of laminates for both types of samples were considered at crack propagation region as shown in Figure 4.11. The a_0 is the artificial crack length.

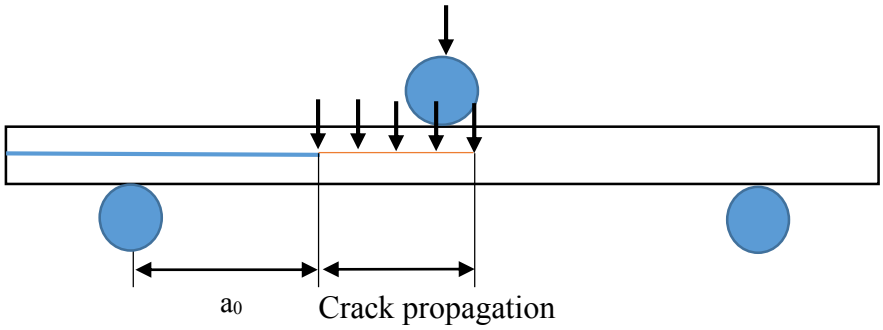

Figure 4.11: Schematic illustration of the location of the cross-section for SEM.

Figure 4.12 shows the SEM images after interlaminar fracture toughness test for both types of samples; regular and modified one. The pristine sample has a smooth surface, indicating a brittle fracture surface. Therefore, the crack initiation of regular sample occurred earlier than the modified samples. In contrast, the composite containing of 2wt% nanoclay has rougher fracture surface than the sample without nanoclay which shows the better fracture toughness.

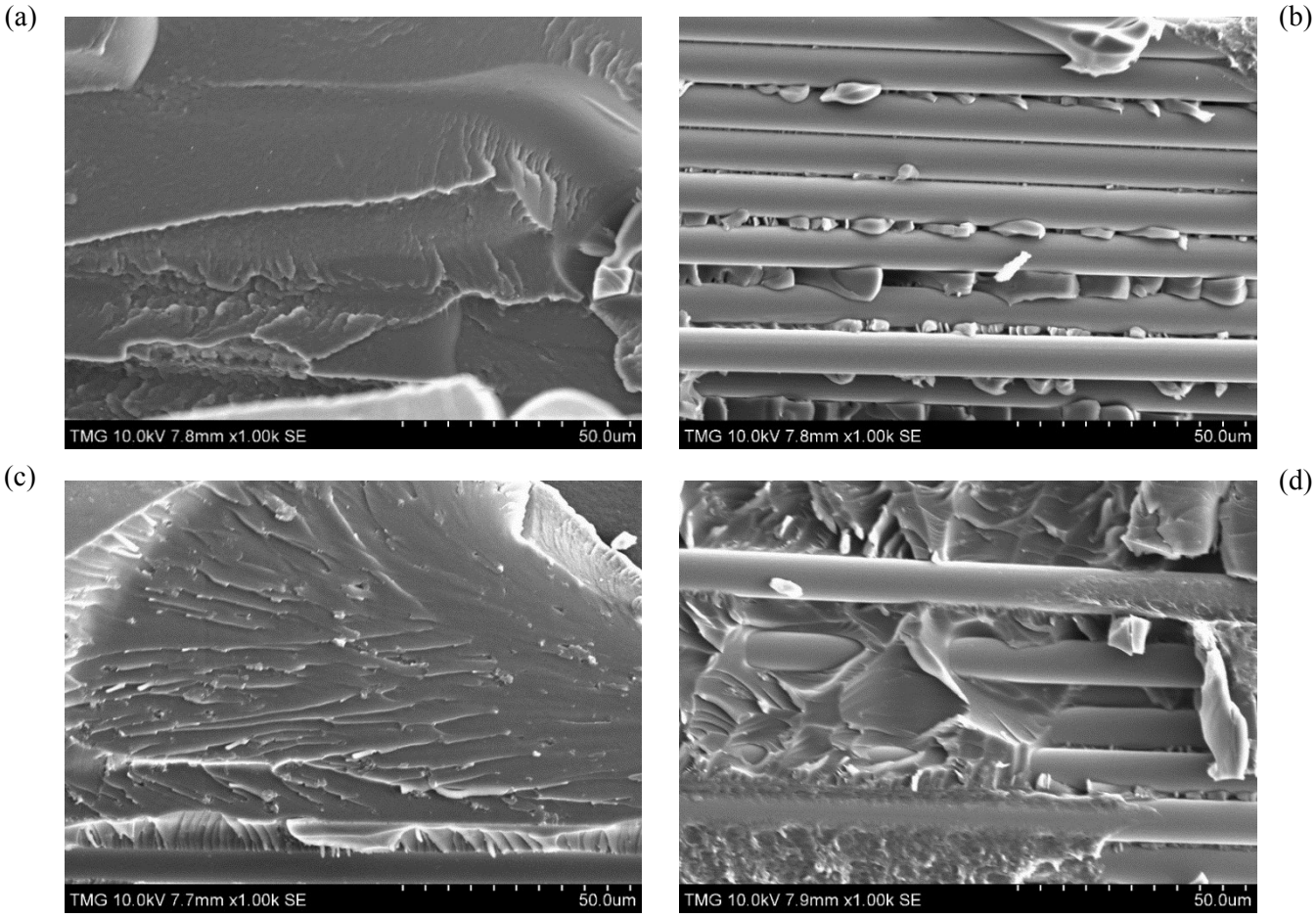

Figure 4.12: SEM images of fracture surface of glass fiber/epoxy system: (a) and (b) samples without nanoclay (c) and (d) samples with 2wt% nanoclay.

4.3 Flexural fatigue test

As mentioned in chapter 3, the fatigue test was carried out under displacement control with frequency of 4 Hz and displacement ratio of R=0.1. Three samples without clay and with clay were tested.

In the flexural fatigue test, failure is defined when number of cycles increases while delamination length is constant. A photograph of a tested laminate at maximum displacement (δ_{max}) level of $0.8\delta_{ult}$= 3.25 mm and minimum displacement (δ_{min}) level of $0.08\delta_{ult}$= 0.325 mm is illustrated in Figure 4.13.

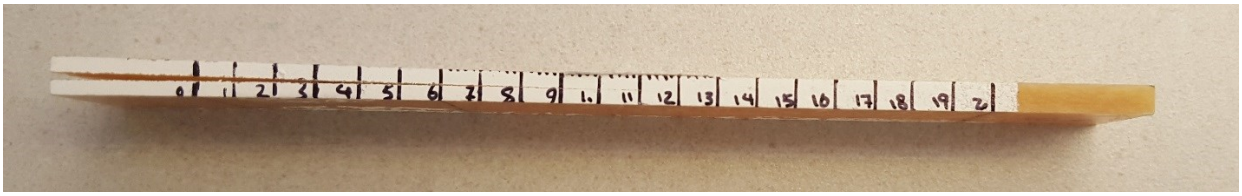

Figure 4.13: Crack propagation under fatigue test.

4.3.1 Fatigue behavior

Figure 4.14 compares the crack propagation lengths versus the number of cycles from flexural fatigue test for both types of samples; with 2wt% nanoclay and neat one.

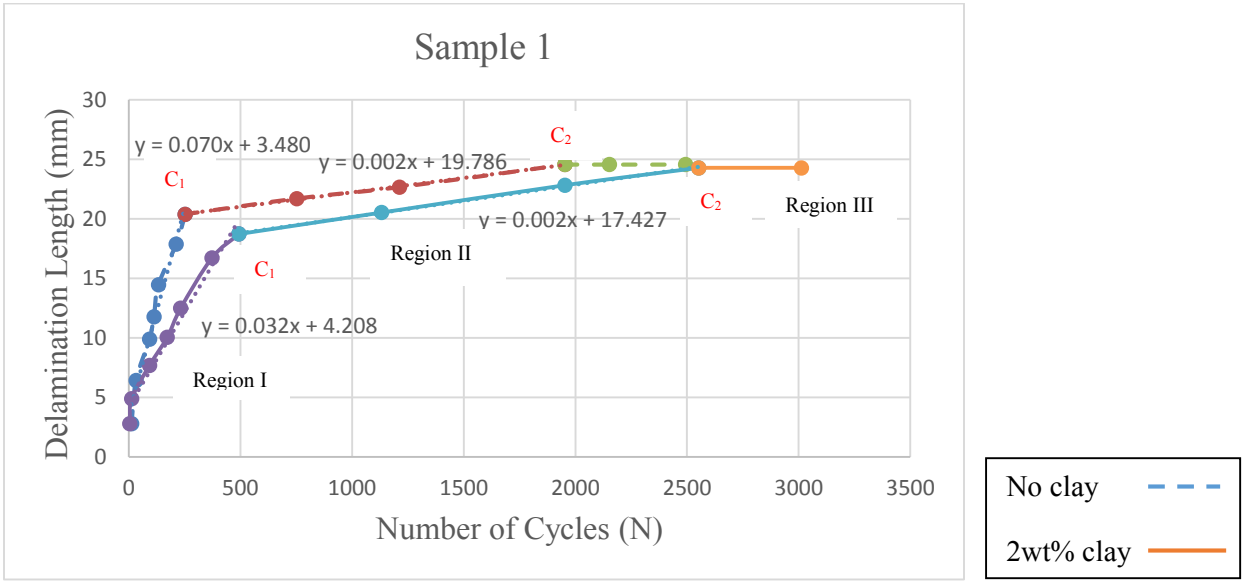

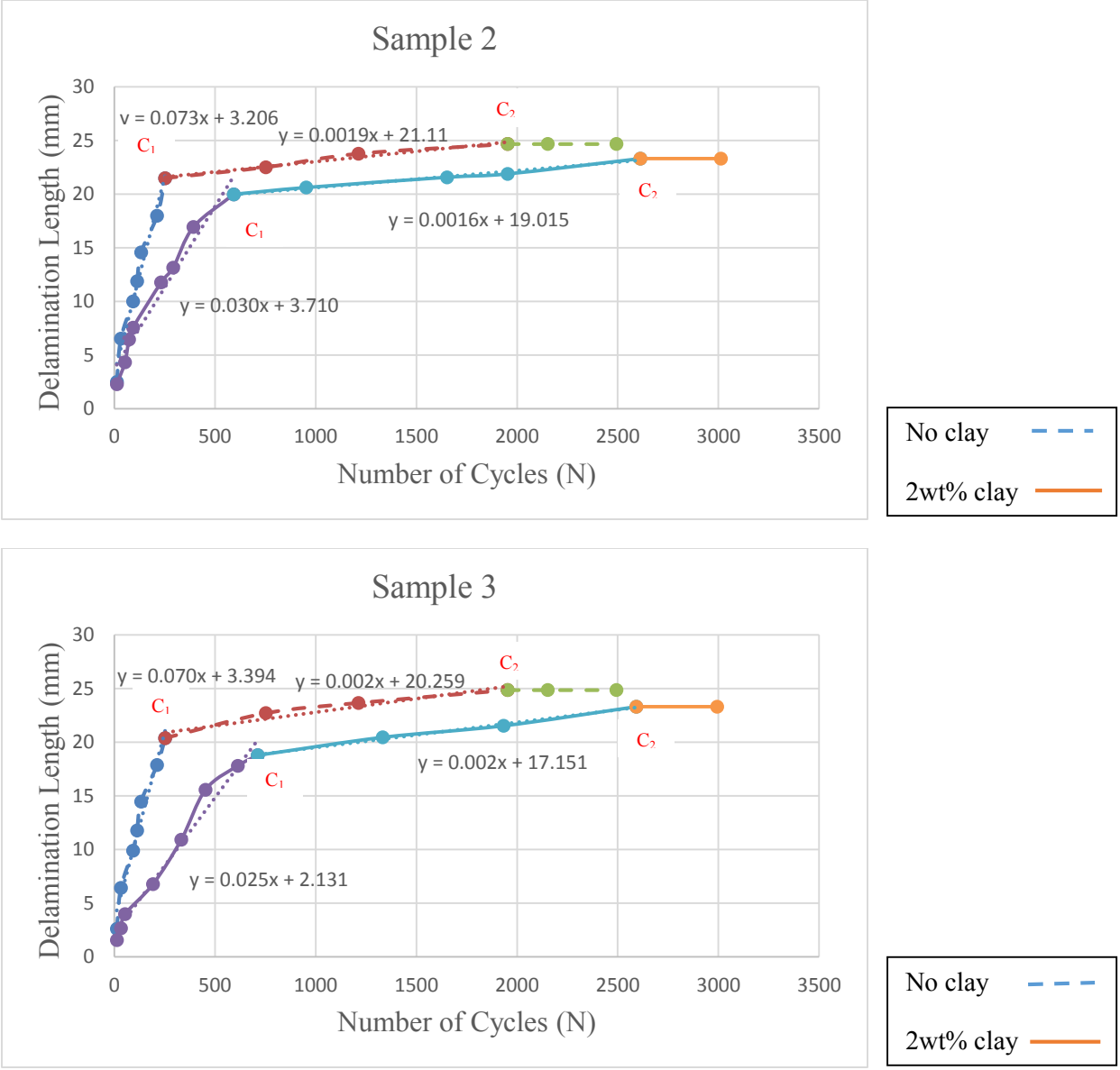

Figure 4.14: Flexural fatigue test results of unidirectional laminates.

The results show that the crack of filled composite laminate grows more slowly than the neat ones. Failure takes place earlier in unfilled laminates than the nanoclay ones. The fatigue life of filled samples is longer than the unfilled ones. Rate of crack propagation at region I and II are summarized in Table 4-19.

Table 4-19: Rate of crack propagation.

Samples		Rate of crack propagation at region I (mm/cycle)	Rate of crack propagation at region II (mm/cycle)
Without clay	1	0.070	0.002
	2	0.073	0.0019
	3	0.070	0.002
	Average	0.071 ± 0.002	$0.0019 \pm 6*10^{-5}$
With clay	1	0.032	0.002
	2	0.030	0.0016
	3	0.025	0.002
	Average	0.029 ± 0.004	0.0018 ± 0.0002

According to the curves, the behavior of laminates without clay and with clay until about of 33 cycles are the same. Then, there are three regions as follows:

- Region I: First there is a sharp increase in the delamination length. Because when the fatigue starts within the laminate, the composite will lose its stiffness. The amount of the load for crack propagation at the first phase is high. The maximum delamination length at this step for regular samples is 20.78 mm with an average of 253 fatigue cycles. On the other hand, the 2wt% nanoclay laminate has 19.16 mm crack length and 600 fatigue cycles at this specific point (C_1). The number of cycles for unidirectional laminate with 2wt% nanoclay was increased 137% compared to the neat laminate. The crack propagation rate of modified samples is reduced by 59% compared to regular ones. The maximum loads at region I (C_1) for unfilled and filled samples are equal to 241.87 (N) and 267.11 (N) respectively. It indicates that the filled laminate needs higher force in order to propagate the crack.
- Region II: The crack propagation rates were reduced 97% and 94% in comparison to region I for regular and modified specimens respectively. The delamination lengths at point C_2

are 24.69 mm and 23.63 mm with 1953 and 2586 fatigue cycles for neat and nanoclay specimens. The number of cycles was improved 32% by adding nanoclay into the epoxy resin at this point (C_2). The crack propagation rate of modified samples is decreased by 5% than regular ones. The maximum loads at region II (C_2) for the unfilled and filled laminates are 203.26 N and 221.24 N respectively. After initiation of crack lower load is required until complete failure happens. The reason is the stiffness of laminate decreased and the sample became weak.

- Region III: When the failure happened, crack did not grow more with increasing the number of cycles and curves show stable condition. The slopes of the curves are constant at this step.

Table 4-20 represents the average values of delamination length, number of cycles, load and time at these two specific points (C_1 and C_2).

Table 4-20: Average values of delamination length, number of cycles, load and time at two specific points.

Samples	**Delamination length (mm) at C_1**	**Number of cycles at C_1**	**P_1 (N) at C_1**	**T_1 (s) at C_1**	**Delamination length (mm) at C_2**	**Number of cycles at C_2**	**P_2 (N) at C_2**	**T_2 (s) at C_2**
Glass/epoxy	20.78	253	241.87	75	24.69	1953	203.26	500
Nanoclay/glass/epoxy	19.16	600	267.11	162	23.63	2586	221.24	658

4.3.2 Load behavior of flexural fatigue test

Figure 4.15 and Figure 4.17 show load versus time for both samples without clay and with clay. The result indicates that samples with nanoclay needs longer time than the regular specimen to propagate the crack. In addition, it is obvious that the load reduces with time.

In order to see the oscillation of force clearly, three different small areas were selected and the graphs of load versus time were plotted as shown in Figure 4.16 and Figure 4.18. The red dotted curve in these figures indicates the average of the load between the maximum and minimum force values.

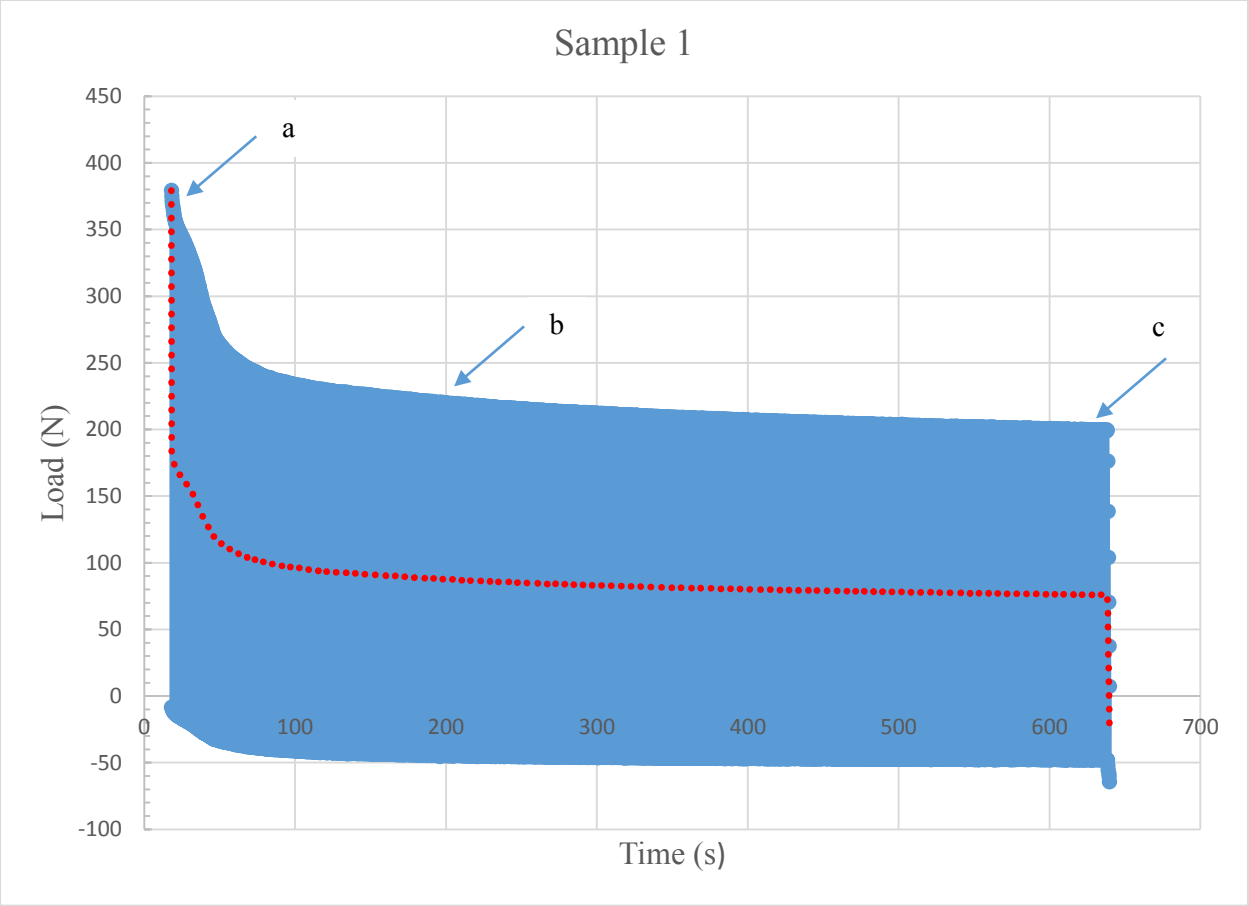

Figure 4.15: Load versus time of sample without clay.

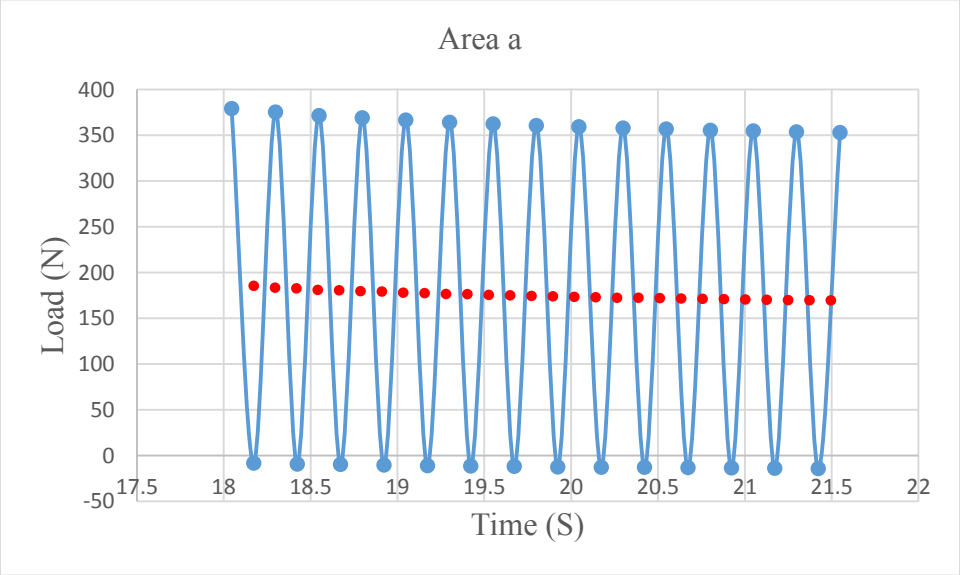

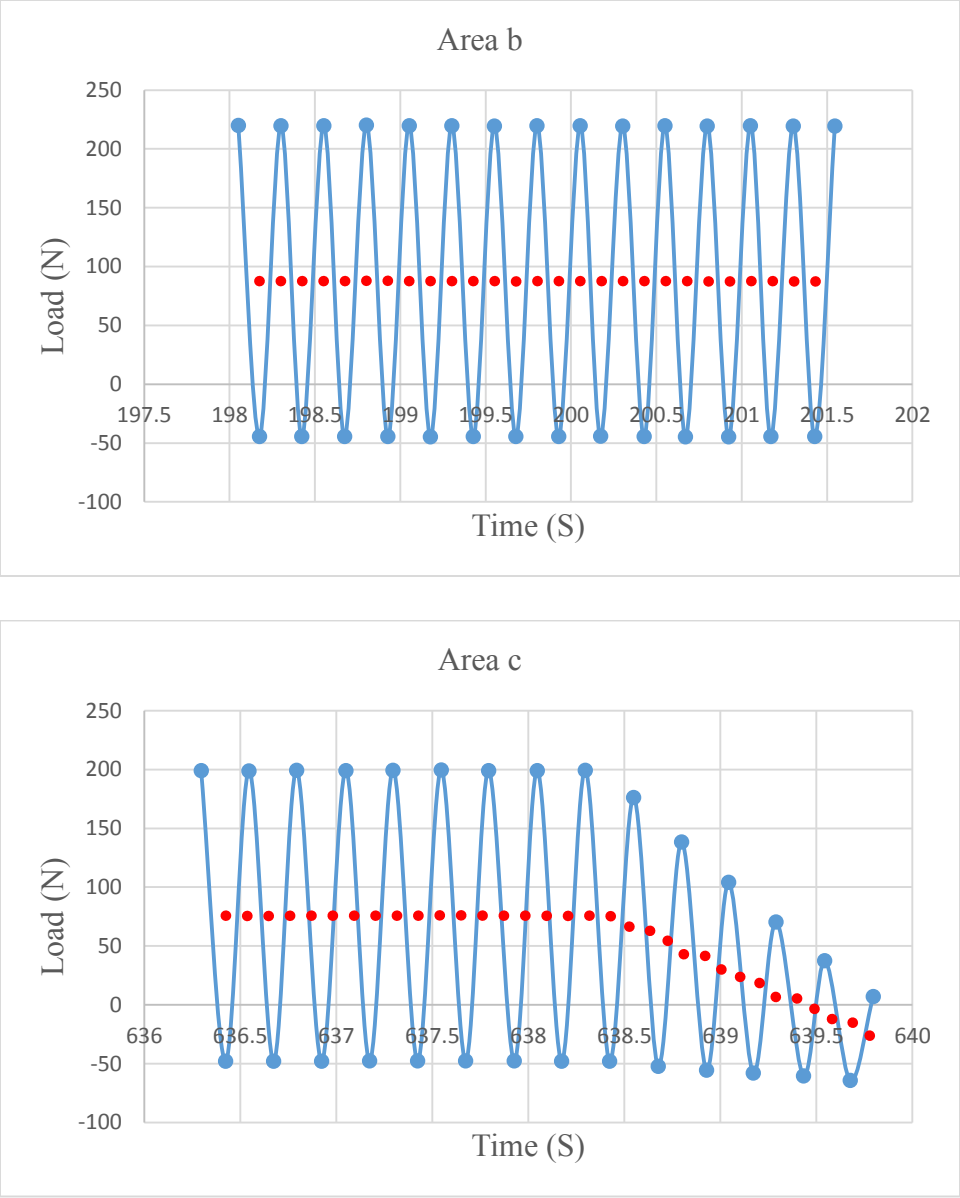

Figure 4.16: Load versus time of sample without clay at three different area a, b and c.

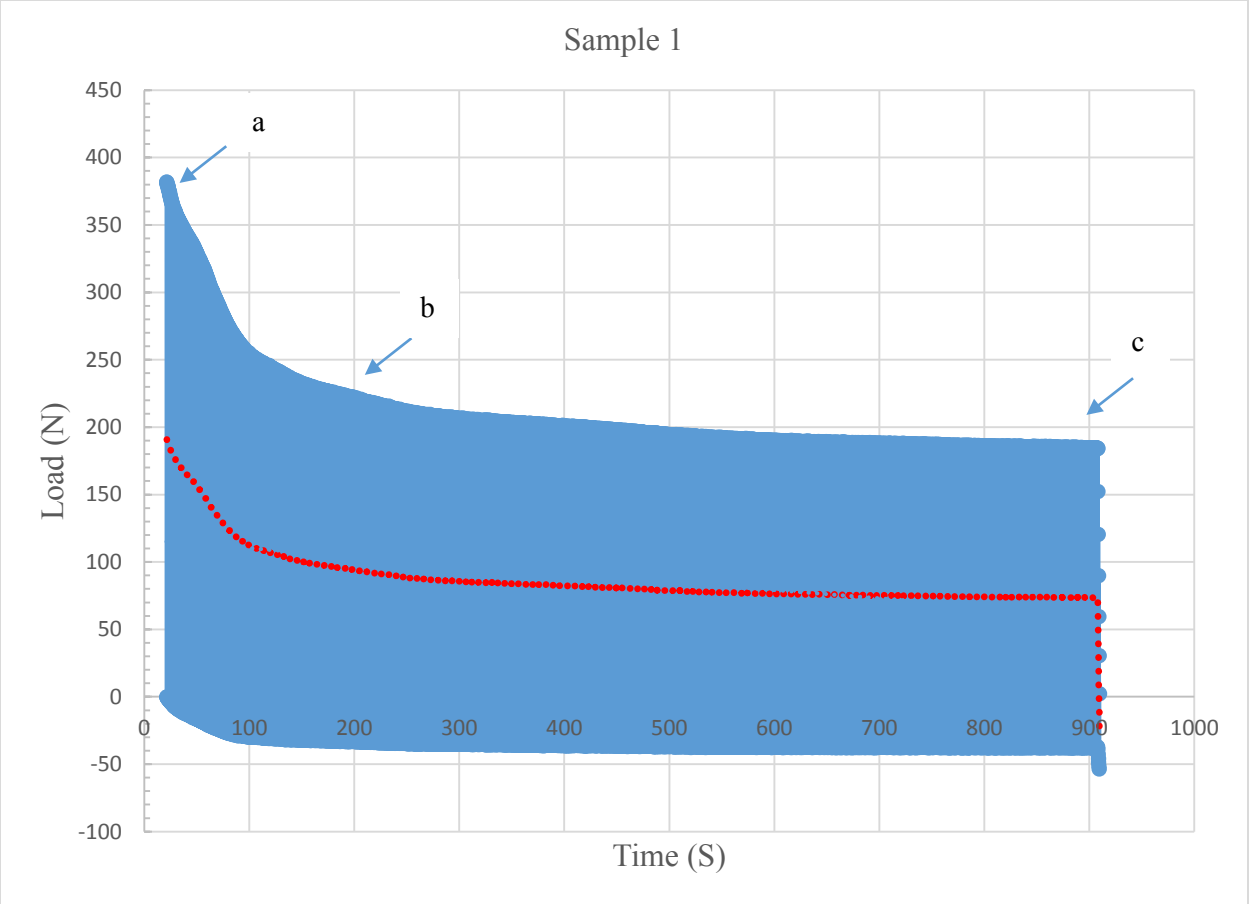

Figure 4.17: Load versus time of sample with clay.

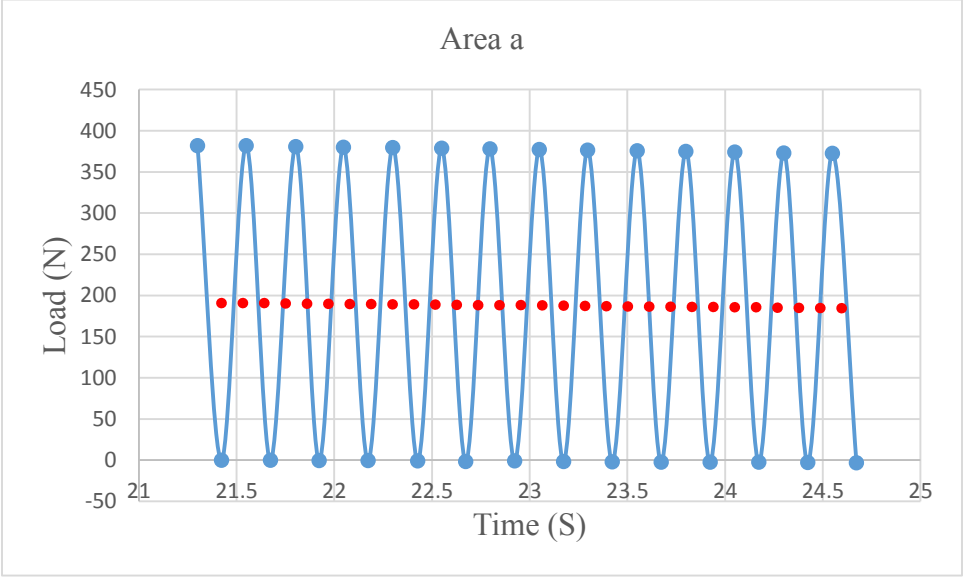

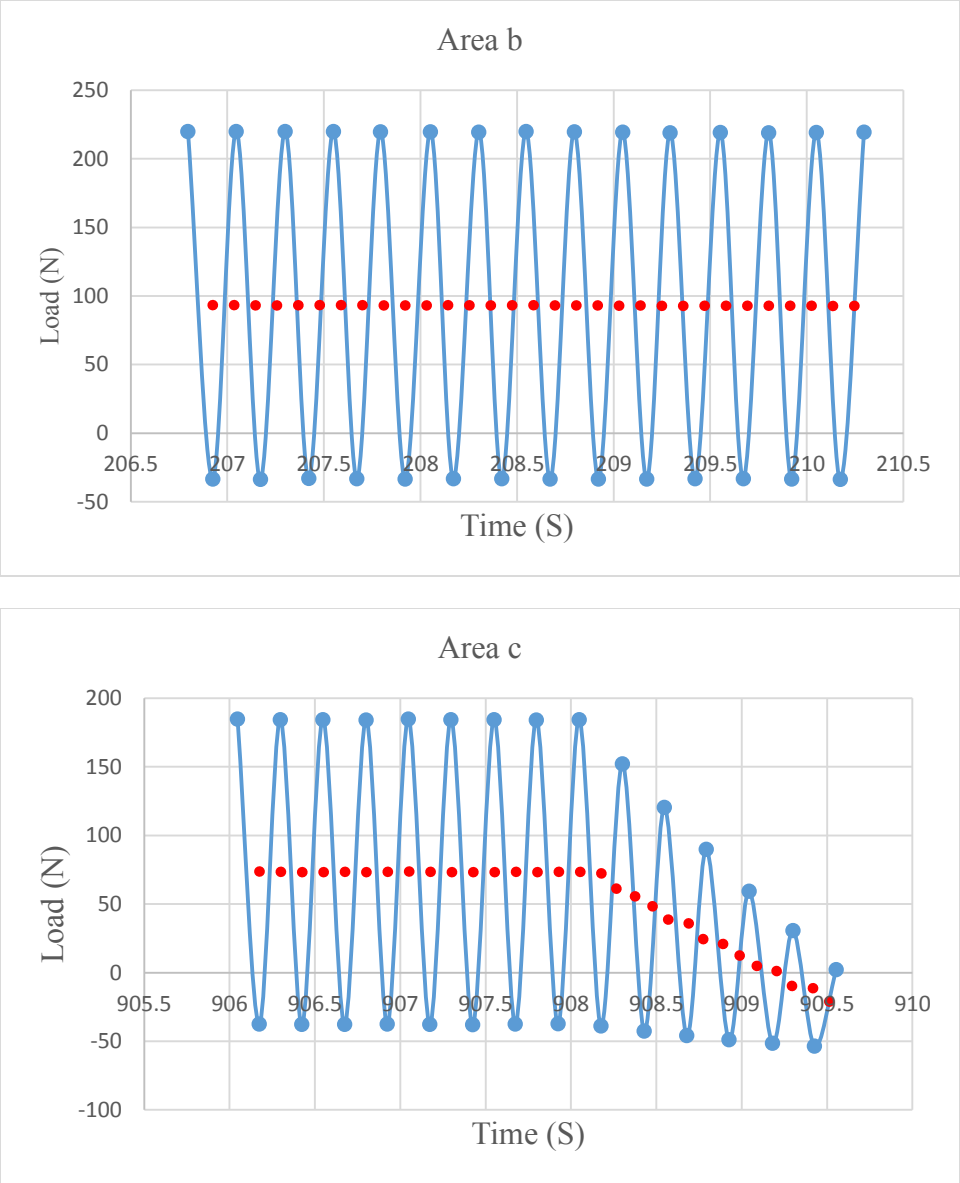

Figure 4.18: Load versus time of sample with clay at three different areas a, b and c.

4.4 Fracture surface after flexural fatigue test

In order to observe the fatigue damage within the laminates, scanning electron microscopy (SEM) was used. Images of cross-sections at different locations of the unidirectional laminates were analyzed after 3000 fatigue cycles. First, the fatigued samples were cut by diamond saw. Then, samples were fixed on sample holder by carbon tape. Since the specimens are not conductive, they need to be coated with Au-Pd (gold-palladium) with a sputtering machine. SEM images of the cross-section of laminates were considered at different locations; Locations A and B (before end of crack front) and location C (after end of crack front). Figure 4.19 shows schematic illustration of the location of the cross-section for SEM.

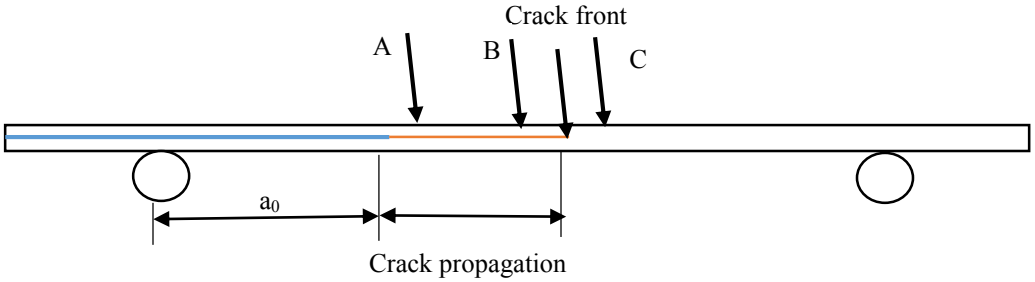

Figure 4.19: Schematic illustration of the location of the cross-section for SEM.

The fracture surfaces from the initiation of crack propagation until after the failure happened were scanned as shown in Figure 4.20.

(a_1)

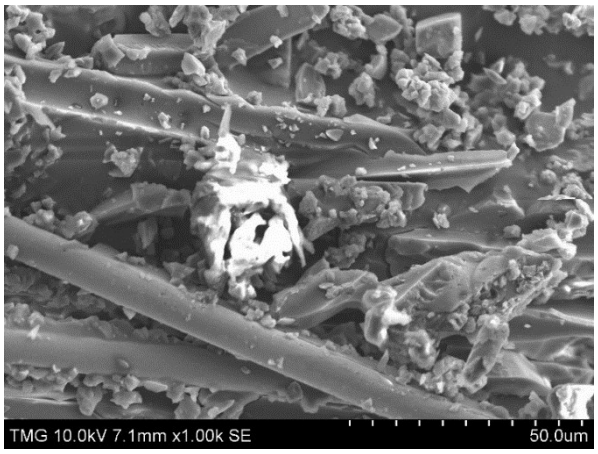

(b_1)

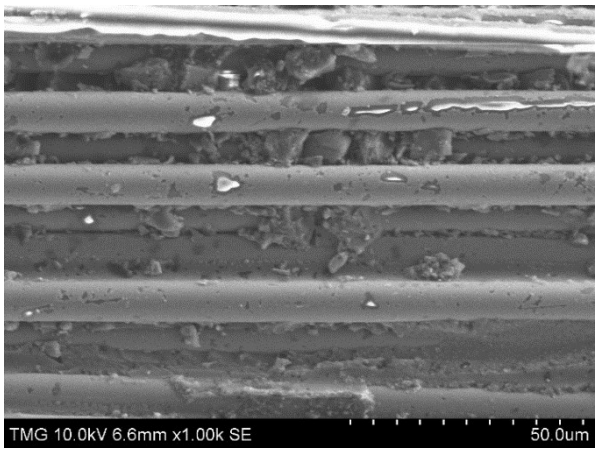

(a_2)

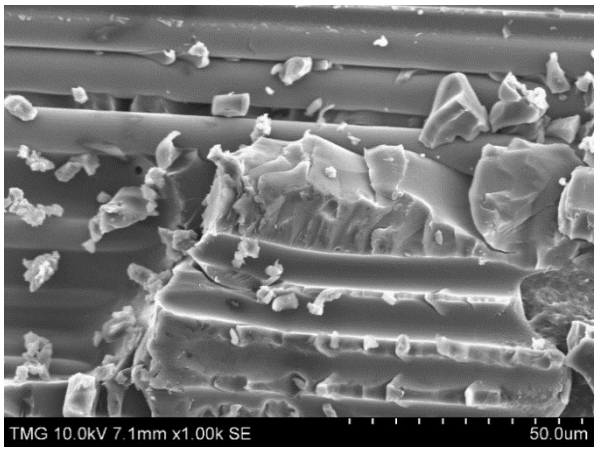

(b_2)

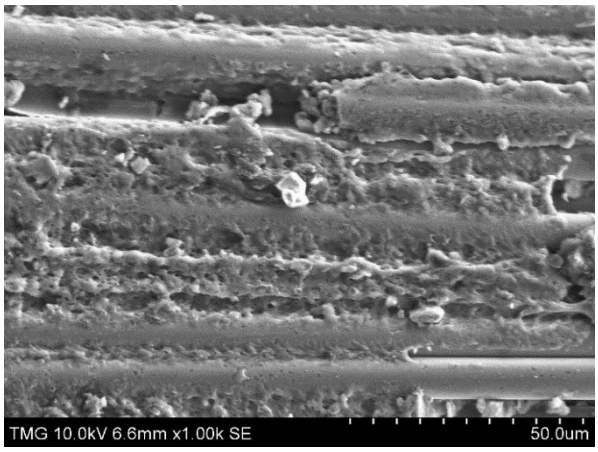

(a_3)

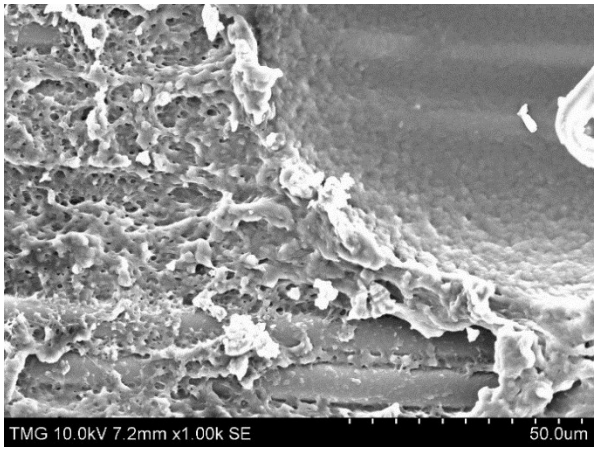

(b_3)

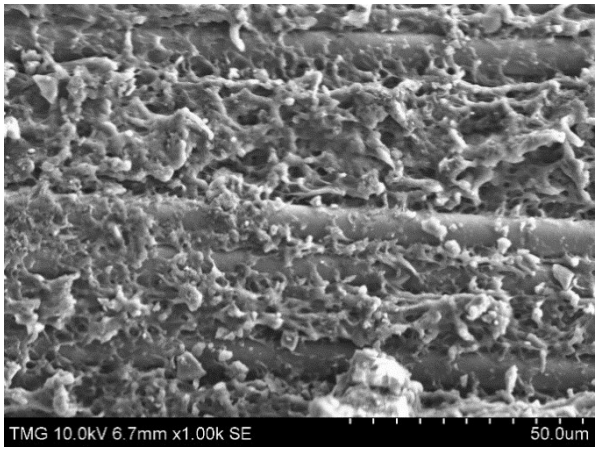

(a_4)

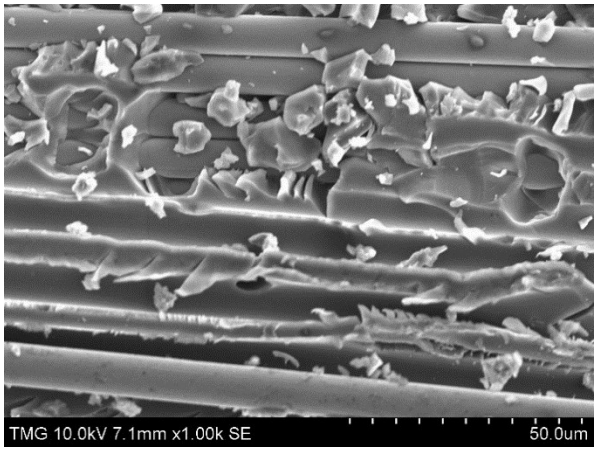

(b_4)

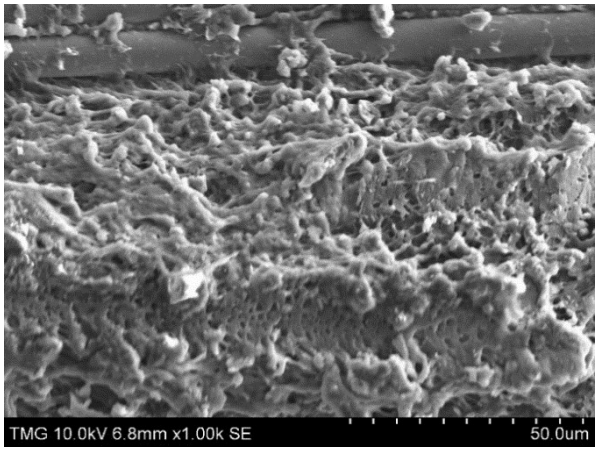

(a_5)

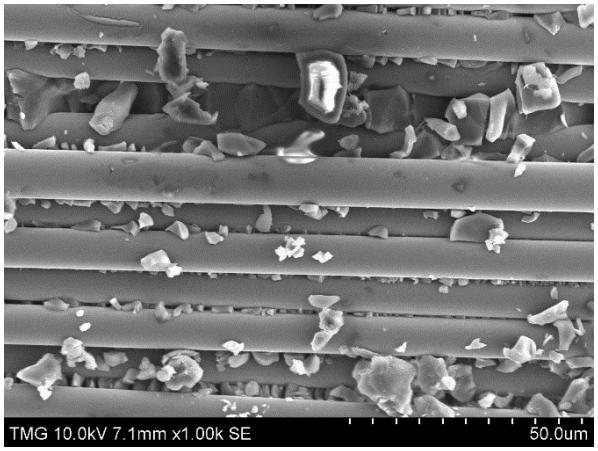

(b_5)

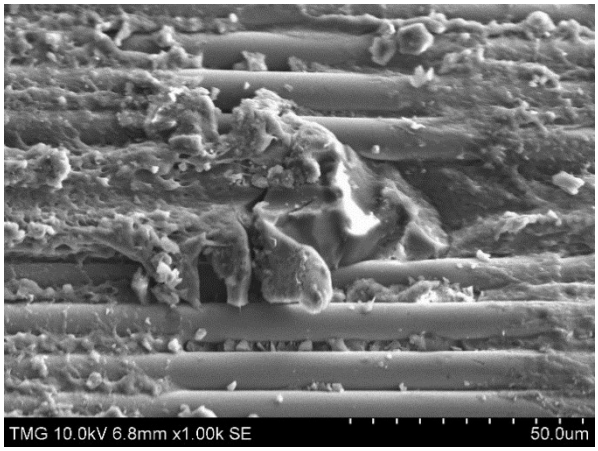

(a_6)

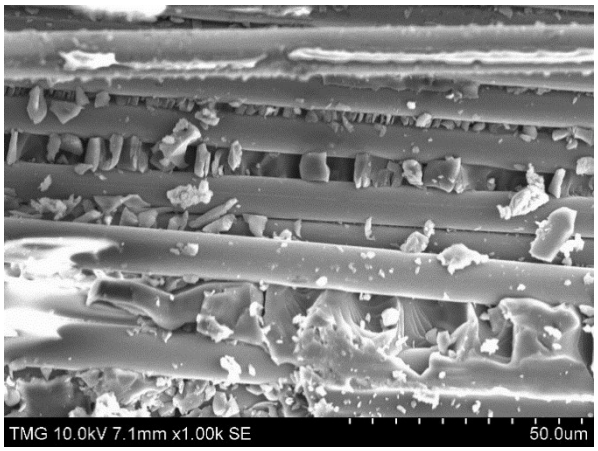

(b_6)

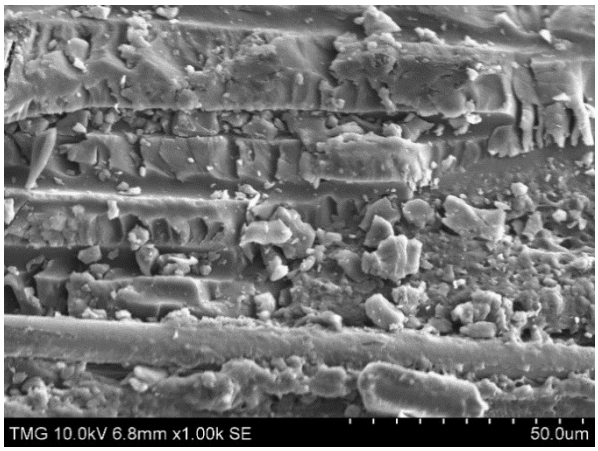

(a_7)

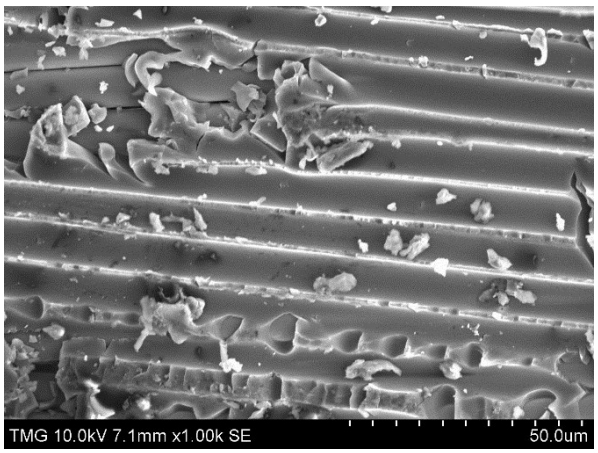

(b_7)

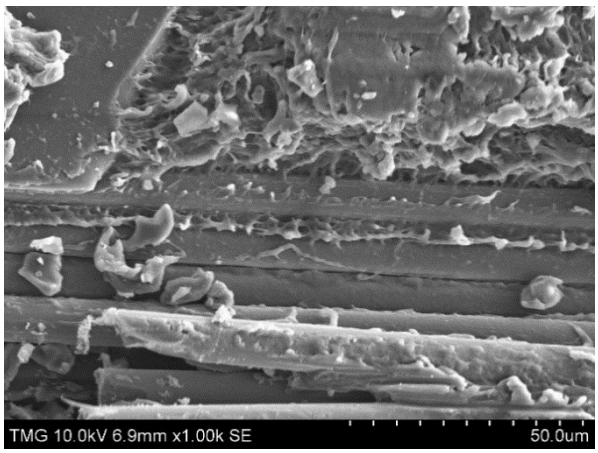

(a_8)

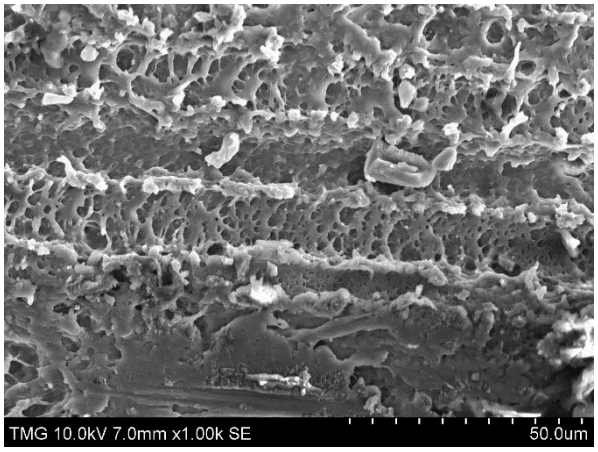

(b_8)

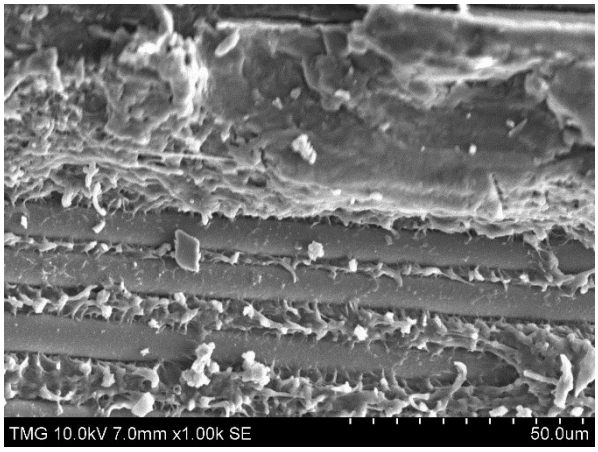

(a_9)

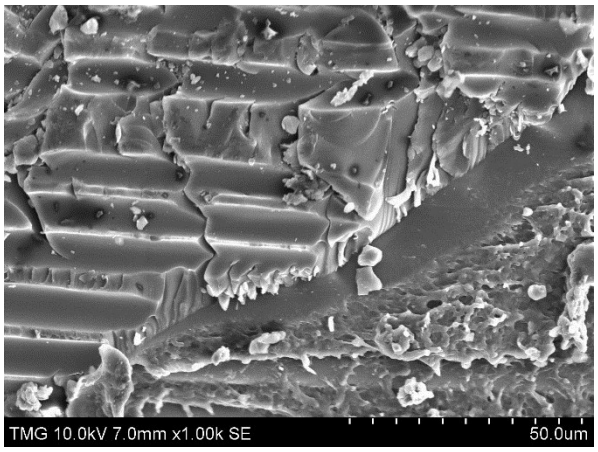

(b_9)

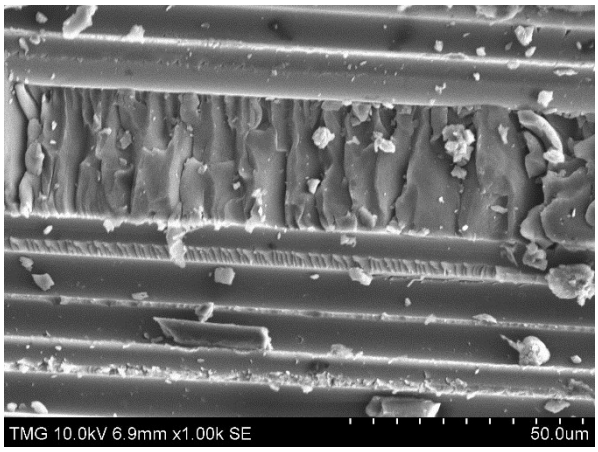

(a_{10})

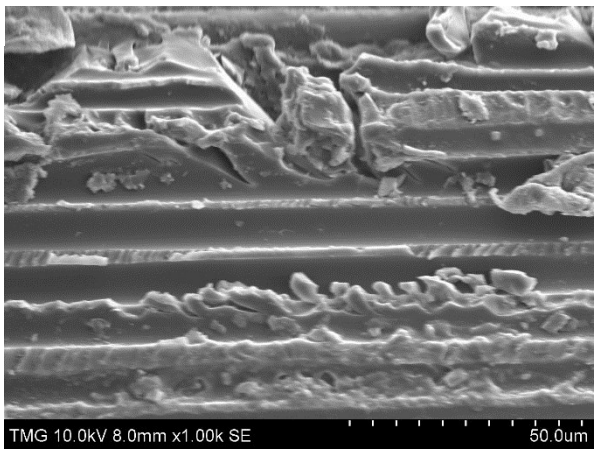

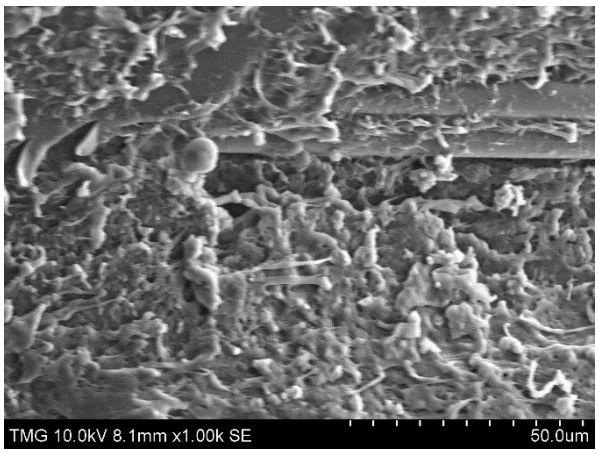

(b_{10})

(a_{11})

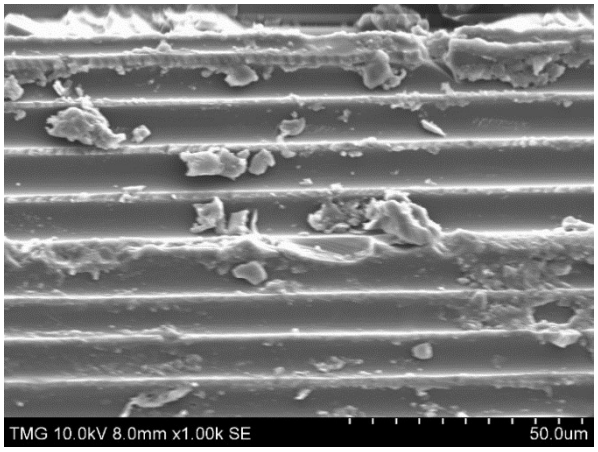

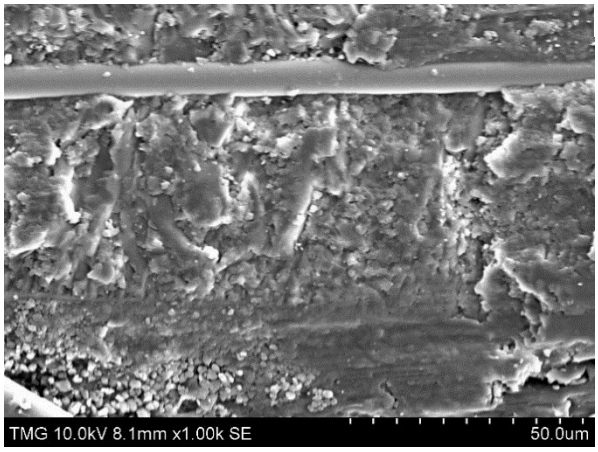

(b_{11})

(a_{12})

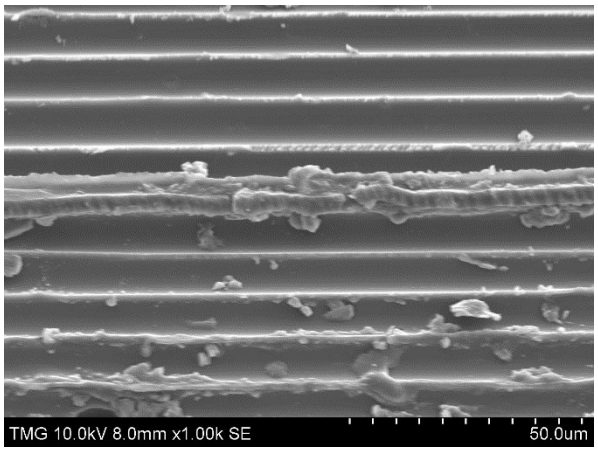

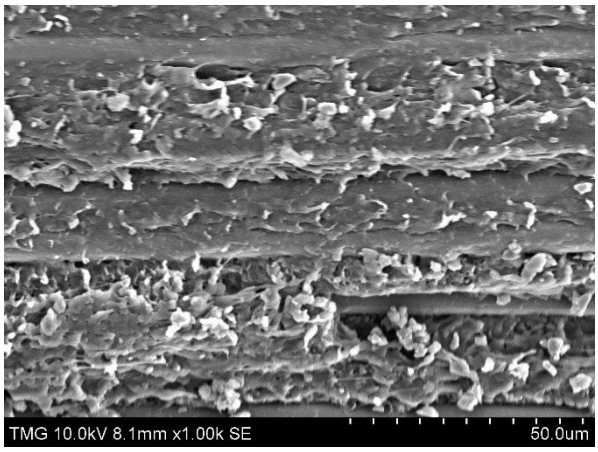

(b_{12})

(a_{13})

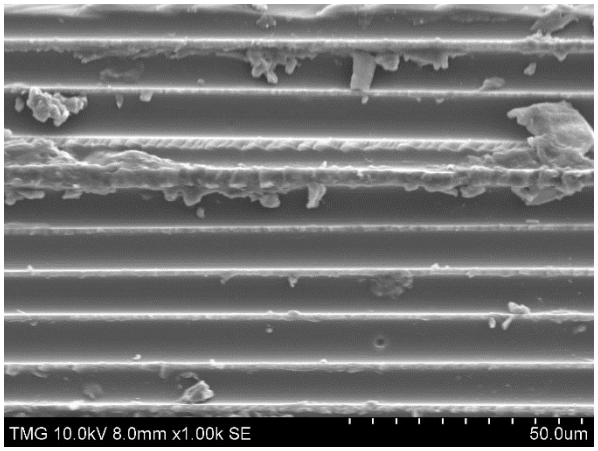

(b_{13})

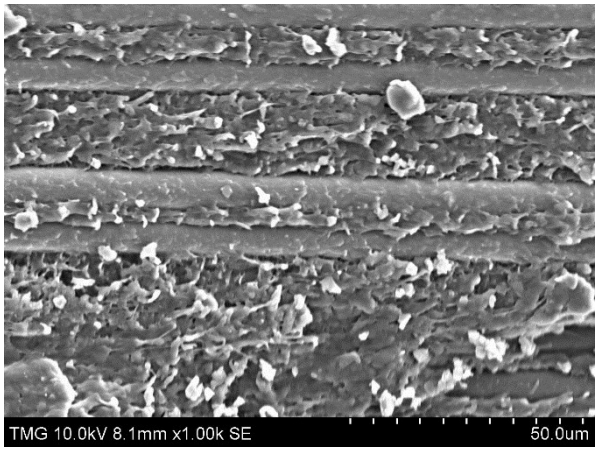

(a_{14})

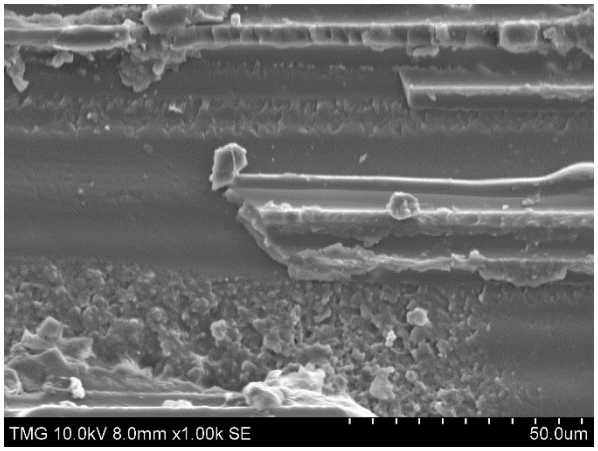

(b_{14})

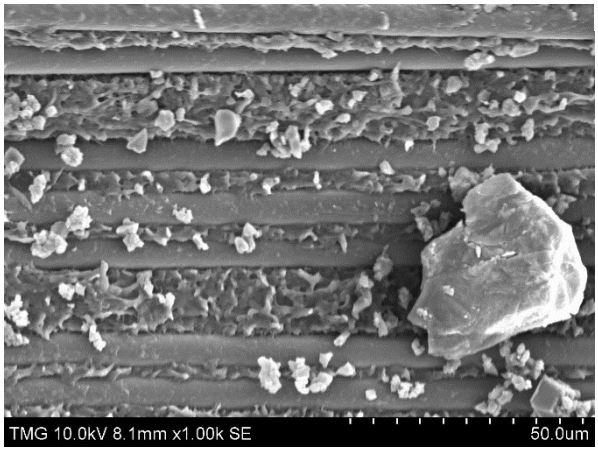

(a_{15})

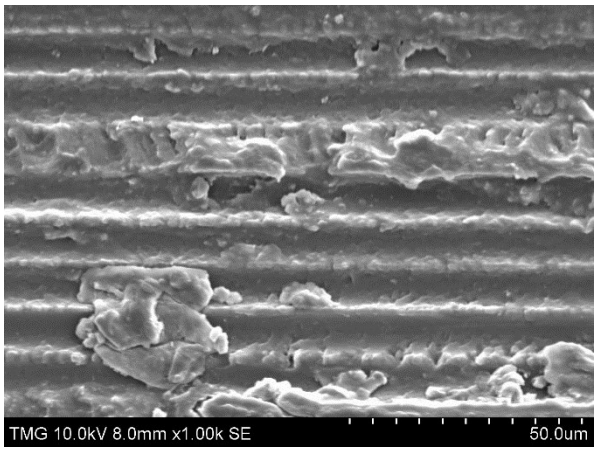

(b_{15})

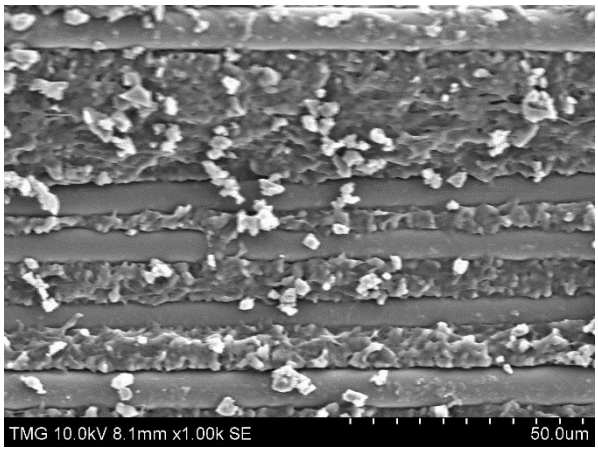

(a_{16})

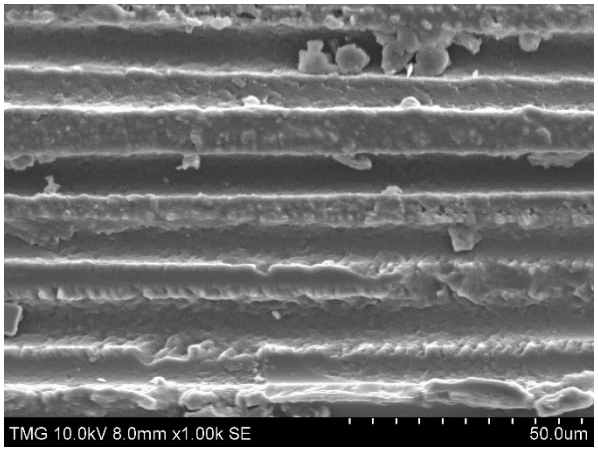

(b_{16})

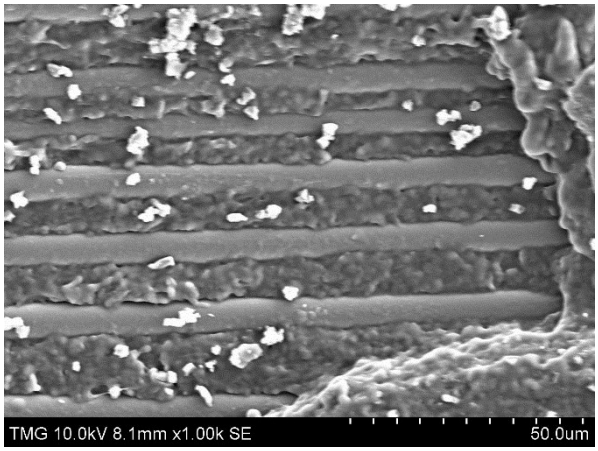

(a_{17})

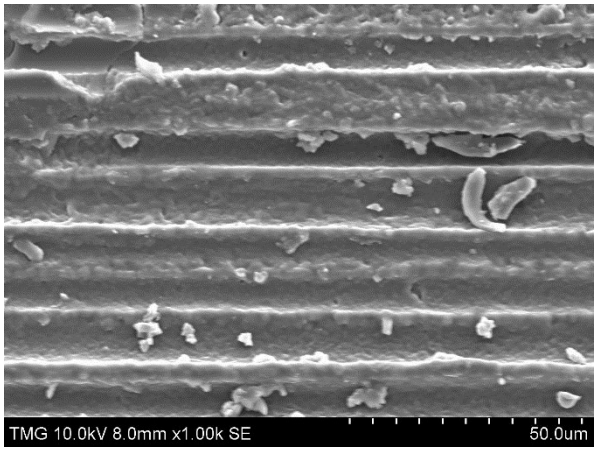

(b_{17})

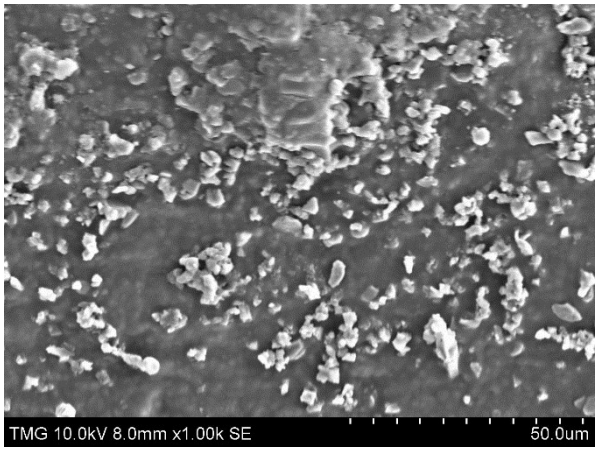

(a_{18})

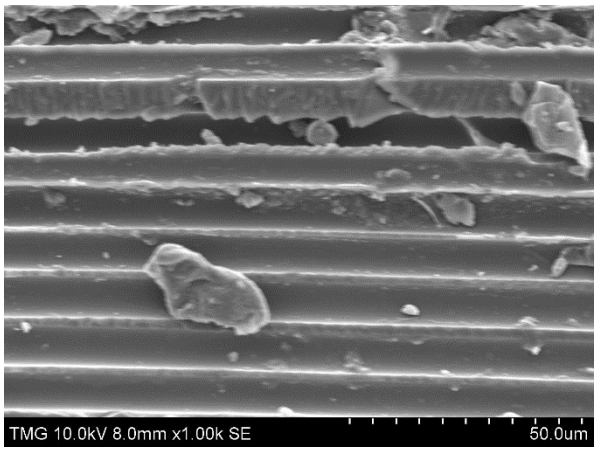

(b_{18})

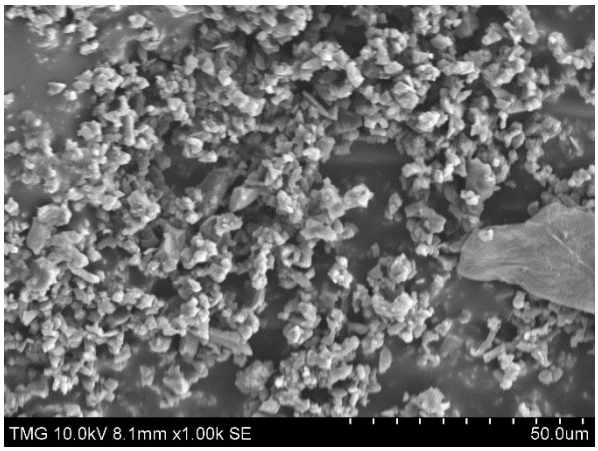

(a_{19})

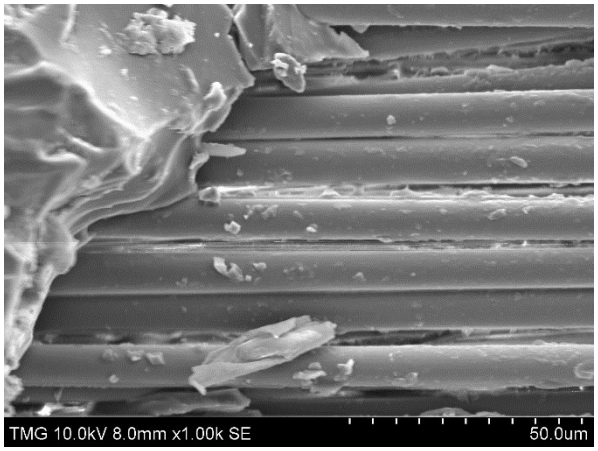

(b_{19})

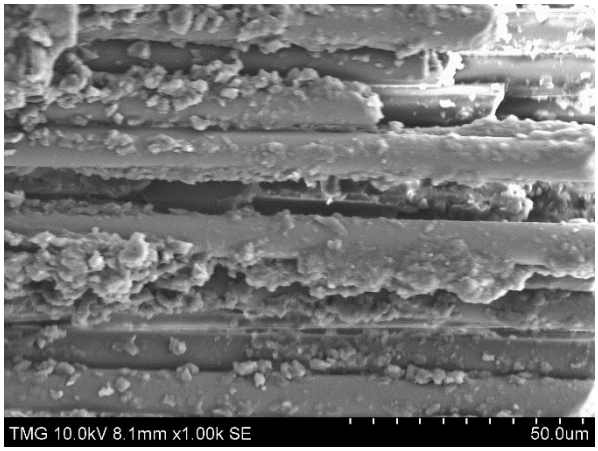

(a_{20})

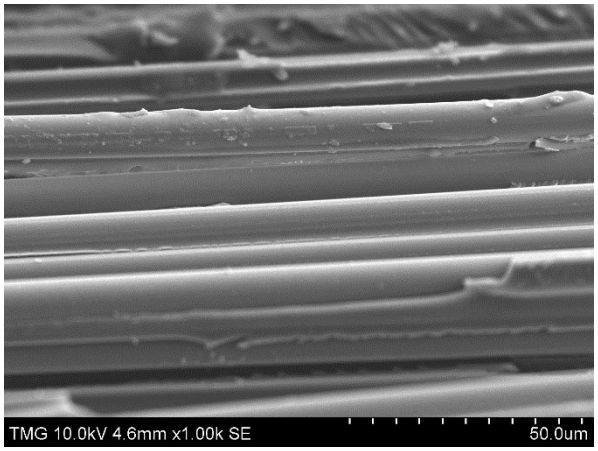

(b_{20})

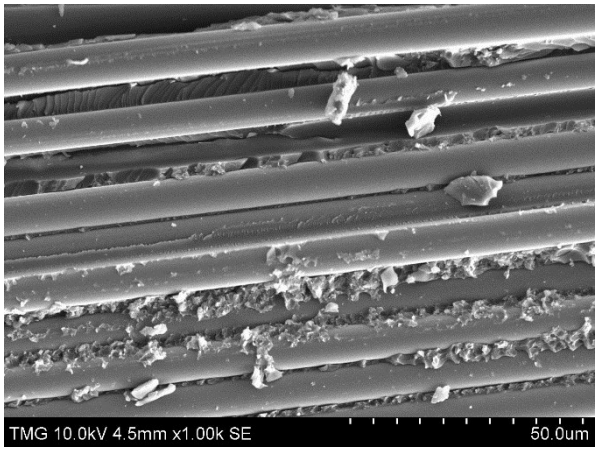

(a_{21})

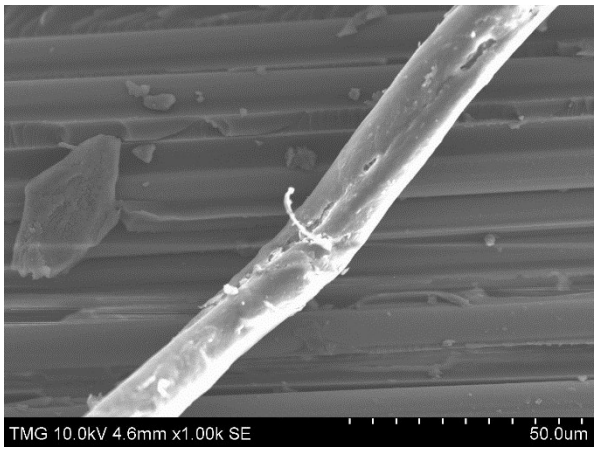

(b_{21})

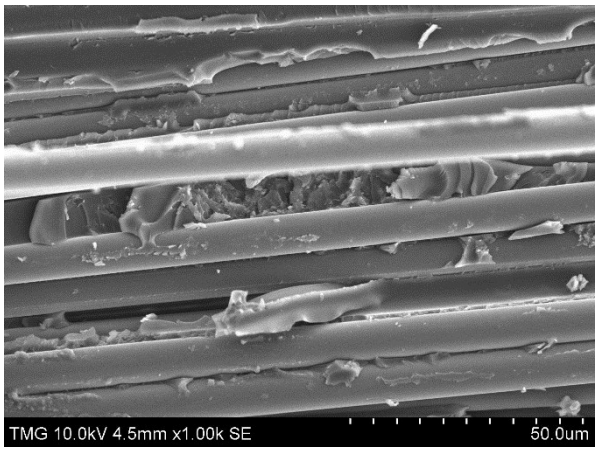

(a_{22}) (b_{22})

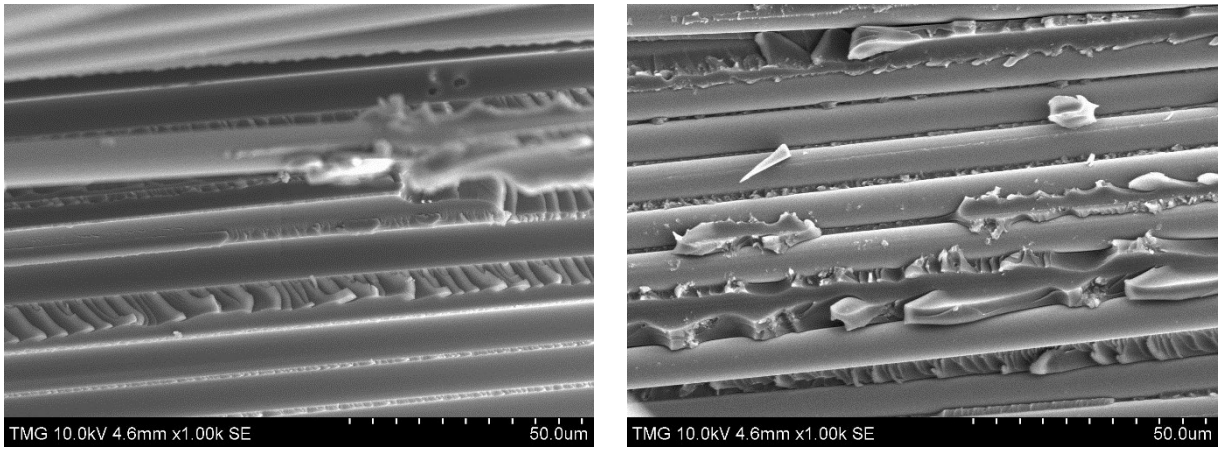

Figure 4.20: Scanning the fracture surface of the laminates after fatigue test for (a) regular sample and (b) modified sample.

Figure 4.20 (a_1-a_9) and (b_1-b_9) illustrate the SEM images of laminates at region I for samples without nanoclay and with nanoclay respectively. Location A is selected as an example at the first region of crack propagation. The SEM image of regular laminate Figure 4.20 (a_2) shows that the fibers are dislodged from the matrix under the cyclic loading. It means that the fracture occurs at interface. Hence, the adhesion between the glass fibers and the matrix is weak. On the contrary, the SEM image of modified sample Figure 4.20 (b_2) indicates that fracture happens within the matrix. So good bonding exists between the fibers and matrix. Consequently, the fracture happens earlier in laminates without clay.

Figure 4.20 (a_{10}-a_{19}) and (b_{10}-b_{19}) shows SEM images of laminates at region II for regular and modified samples respectively. Location B is chosen at the second region of crack propagation. Figure 4.20 (a_{15}) indicates the cleaner appearance than the (b_{15}). Figure 4.20 (b_{15}) shows the better bonding between the fibers and matrix.

SEM images of cross-section of laminates at region III for both samples without clay and with clay were shown in Figure 4.20 (a_{20}-a_{22}) and (b_{20}-b_{22}). Location C is an example at third region of crack propagation. The neat glass/epoxy Figure 4.20 (a_{22}) displays a smooth surface, indicating brittle fracture surface. In contrast, the sample with nanoclay Figure 4.20 (b_{22}) shows rough surface that resisted crack propagation, illustrating good fracture toughness.

Chapter 5

Conclusion, Contributions and Future Work

5.1 Conclusion

In this research, Mode II fracture toughness and flexural fatigue behavior of glass/epoxy/nanoclay composites are studied. High speed mixing method is used to disperse modified nanoclay into epoxy resin. The quality of dispersion is checked by SEM technique.

In order to measure Mode II interlaminar fracture toughness, three point bending tests are carried out. The results indicate that nanoclay incorporation significantly improves the strain energy release rate (G_{IIc}). In other words, the filled laminate dissipates more energy to propagate the crack. Maximum improvements are 24% and 23% at 2wt% nanoclay incorporation in unidirectional laminate for NPC and PC tests. Thus, it can be said that fracture toughness of nanoclay/glass/epoxy is enhanced at 2wt% nanoclay. In addition, The PC fracture toughness is 19% and 20% lower than NPC fracture toughness for without clay and with clay laminates respectively. That is because PC crack tip is sharper than the NPC one. The SEM images after interlaminar fracture test show the brittle surface for regular samples. The rough fracture surface of modified specimen indicates the high resistance of laminate against the crack propagation.

In addition, flexural fatigue test was done on unidirectional laminates in order to see the influence of nanoclay on the fatigue life of composites. A displacement control method was used with maximum displacement of $0.8\delta_{ult}$ and ratio of 0.1 at frequency 4 Hz. The results show that there are three regions for the curve of delamination length versus number of cycles. At region I, the crack propagation rate of 2wt% nanoclay composite laminates is decreased by 59%. The fatigue failure of 2wt% nanoclay occurred more slowly than the unfilled samples. The 5% reduction of crack growth rate for 2wt% nanoclay is achieved at region II. In addition, the rate of crack propagation at region II is decreased 97% and 94% than the region I for regular and modified samples respectively. It happens because the load is reduced due to increase in the crack length. The SEM images of cross-section surface after fatigue test indicate that at first region, the specimen without clay has weak bonding between the fibers and matrix. Fibers are dislodged from the matrix and fracture happens at interface. For samples with nanoclay, fracture occurs within the matrix

which shows the better bonding of the fibers and matrix. At region II, images of samples with nanoclay show better bonding between fibers and matrix. At region III, smoother surface of regular sample than the sample with clay.

5.2 Contributions

The contributions of this study are as follows:

- Demonstrated the effect of adding nanoclay into the glass/epoxy on the improvement of Mode II interlaminar fracture toughness
- Showed the influence of addition of nanoclay on the improvement of fatigue life of glass/epoxy composites

5.3 Future work

The future investigation can be:

- Effect of nanoclay on Mode II interlaminar fracture toughness can be carried out at different temperatures.

References

[1] S. Helmy and S. V. Hoa, "Tensile fatigue behavior of tapered glass fiber reinforced epoxy," Composites Science and Technology, vol. 102, pp. 10-19, 2014.

[2] A. Kabir, "Vibration damping property and flexural fatigue behavior of glass/epoxy/nanoclay composites," Master thesis, Concordia University, Montreal, 2010.

[3] A. K. Heilmy, E. A. Ferreiro and S. G. Bussetti, "Surface area evaluation of montmorillonite," Colloid and Interface Science, vol. 210, pp. 167-171, 1999.

[4] M. Alexandre and P. Dubois, "Polymer-layered silicate nanocomposites: preparation, properties and uses of a new class of materials," Materials Science and Engineering, vol. 28, pp. 1-63, 2000.

[5] S. R. Sinha and M. Okamoto, "Polymer/layered silicate nanocomposites: a review from preparation to processing," Prog. Polym. Sci., vol. 28, pp. 1539-1641, 2003.

[6] T. D. Ngo, "Understanding the effect of adding nanoclays into epoxies," PhD Thesis, Concordia University, Montreal, 2007.

[7] A. Yasmin, J. L. Abot and I. M. Daniel, "Mechanical and thermal behavior of clay/epoxy nanocomposites," Composite Science and Thechnology 66 (2006) 2415 – 2422., pp. 2415-2422, 2006.

[8] T. D. Ngo, M. T. Ton-That, S. V. Hoa and K. C. Cole, "Effect of temperature, duration, and speed of pre-mixing on the dispersion of clay/epoxy nanocomposites," Composites Science and Technology, vol. 69, pp. 1831-1840, 2009.

[9] A. D. Gianni, E. Amerio, O. Monticelli and R. Bongiovanni, "Preparation of polymer/clay mineral nanocomposites via dispersion of silylated montmorillonite in a UV curable epoxy matrix," Applied Clay Science, vol. 42, pp. 116-124, 2008.

[10] X. Kornmann, R. Thomann, R. Mulhaupt, J. Finter and L. A. Berglund, "High performance epoxy-layered silicate nanocomposites," Polymer Engineering and Science, vol. 42, pp. 1815-1826, 2002.

[11] C. D. Munzy, B. D. Butler, H. J. M. Hanley, F. Tsvetkov and D. G. Peiffer, "Clay platelet dispersion in a polymer matrix," Materials Letters, vol. 28, pp. 379-384, 1996.

[12] L. Chun-Ki, L. Kin-Tak, C. Ho-Yan and L. Hang-Yin, "Effect of ultrasound sonication in nanoclay/epoxy composites," Materials Letters, vol. 59, pp. 1369-1372, 2005.

[13] C. Chen and T. B. Tolle, "Fully exfoliated layered silicate epoxy nanocomposites," Polymer Science: Part B, vol. 42, pp. 3981-3986, 2004.

[14] W. P. Liu, S. V. Hoa and M. Pugh, "Organoclay-modified high performance epoxy nanocomposites," Composites Science and Technology, vol. 65, pp. 307-316, 2005.

[15] W. P. Liu, S. V. Hoa and M. Pugh, "Fracture toughness and water uptake of high performance epoxy/nanoclay nanocomposites," Composites Science and Technology, vol. 65, pp. 2364-2373, 2005.

[16] P. B. Messersmith and E. P. Giannelis, "Synthesis and barrier properties of poly(e-capro1actone)-layered silicate nanocomposites," Polymer Science: Part A: Polymer Chemistry, vol. 33, pp. 1047-1057, 1995.

[17] Y. Ke, C. Long and Z. Qi, "Crystallization, properties, and crystal and nanoscale morphology of PET–clay nanocomposites," Applied Polymer Science, vol. 71, pp. 1139-1146, 1999.

[18] J. Ma, Z. QI and Y. Hu, "Synthesis and characterization of polypropylene/clay nanocomposites," Applied Polymer Science, vol. 82, pp. 3611-3617, 2001.

[19] M. Yoonessi, H. Toghiani, T. L. Daulton, J. S. Lin and C. U. Pittman Jr., "Clay delamination in clay/ poly(dicyclopentadiene) nanocomposites quantified by small angle neutron scattering and high resolution transmission electron microscopy," Macromolecules, vol. 38, pp. 818-831, 2005.

[20] H. G. Jeon, H. T. Jung, S. W. Lee and S. D. Hudson, "Preparation and characterization of PMMA-clay hybrid," Polymer Bulletin, vol. 41, pp. 107-113, 1996.

[21] M. Kawasumi, N. Hasegawa, A. Usuki and A. Okada, "Nematic liquid crystal/clay mineral composites," Materials Science & Engineering, pp. 135-143, 1998.

[22] K. Yano, A. Usuki, A. Okada, T. Kurauchi and O. Kamigaito, "Synthesis and properties of polyimide-clay hybrid," Polymer science: Part A: Polymer Chemistry, vol. 31, pp. 2493-2498, 1993.

[23] R. A. Vaia, B. B. Sauer, O. K. Tse and E. P. Giannelis, "Relaxations of confined chains in polymer nanocomposites: glass transition properties of poly (ethylene oxide) intercalated in montmorillonite," Polymer Sceince: Part B: Polymer Physics, vol. 35, pp. 59-67, 1997.

[24] J. L. W. Lee D. C., "Preparation and characterization of PMMA-clay hybrid composite by emulsion polymerization," Applied Polymer Science, vol. 61, pp. 1117-1122, 1996.

[25] R. A. Vaia, K. D. Jandt, E. J. Kramer and E. P. Giannelis, "Microstructural evolution of melt intercalated polymer-organically modified layered silicates nanocomposites," Chem. Mater, vol. 8, pp. 2628-2635, 1996.

[26] R. A. Vaia, H. Ishii and E. P. Giannelis, "Synthesis and properties of two-dimensional nanostructures by direct intercalation of polymer melts in layered silicates," Chem. Mater, vol. 5, pp. 1694-1696, 1993.

[27] L. Liu, Z. Qi and X. Zhu, "Studies on nylon 6/clay nanocomposites by melt-intercalation process," Applied Polymer Science, vol. 71, pp. 1133-1138, 1999.

[28] J. H. Park and S. C. Jana, "The relationship between nano- and micro-structures and mechanical properties in PMMA–epoxy–nanoclay composites," Polymer, vol. 44, pp. 2091-2100, 2003.

[29] X. Kornmann, "Synthesis and characterisation of thermoset-clay nanocomposites," PHD Thesis, Lula University of Thechnology, Sweden, 1998.

[30] M. D. Isaac and I. Ori, Engineering mechanics of composites materials, Oxford University press, 1994.

[31] M. V. Gordic, I. M. Djordjevic, D. R. Sekulic, Z. S. Petrovic and M. M. Stevanovic, "Delamination strain energy release rate in carbon fiber / epoxy resin composites," Materials Science Forum, vol. 555, pp. 515-519, 2007.

[32] A. H. Mahmood, R. H. Gong and I. Porat, "Improvement in the fracture toughness (Mode I) of laminated glass fabric composites through air-jet texturing," Fibers and Polymers, vol. 14, pp. 591-596, 2013.

[33] M. F. S. F. Moura, R. D. S. G. Campilho, A. M. Amaro and P. N. B. Reis, "Interlaminar and intralaminar fracture characterization of composites under Mode I loading," Composite Structure, vol. 92, pp. 144-149, 2010.

[34] N. A. Siddiqui, R. S. C. Woo, J. K. Kim, C. C. K. Leung and A. Munir, "Mode I interlaminar fracture behavior and mechanical properties of CFRPs with nanoclay-filled epoxy matrix," Composites Part A: applied science and manufacturing, vol. 38, pp. 449-460, 2007.

[35] K. Ramsaroop, K. Kanny and T. P. Mohan, "Fracture toughness studies of polypropylene-clay nanocomposites and glass fibre reinfoerced polypropylene composites," Materials Science and Applications, vol. 1, pp. 301-309, 2010.

[36] T. A. Mushtaq, F. Y. Belal and K. Harry, "Fracture toughness and toughening mechanisms of unsaturated polyester-based," in 13th International Conference on Fracture, Beijing, 2013.

[37] Y. Xu and S. V. Hoa, "Mechanical properties of carbon fiber reinforced epoxy/clay nanocomposites," Composites Science and Technology, vol. 68, pp. 854-861, 2008.

[38] P. Davies, F. Pomies and L. A. Carlisson, "Influence of water and accelerated aging on the shear fracture properties of glass/epoxy composite," Applied Composite Materials, vol. 3, pp. 71-78, 1996.

[39] F. Gao, G. Jiao, Z. Lu and R. Ning, "Mode II delamination and damage resistance of carbon/epoxy composite laminates interleaved with thermoplastic particle," Journal of Composite Materials, vol. 41, 2007.

[40] A. B. Pereira, A. Morais, A. T. Marques and P. T. Castro, "Mode II interlaminar fracture of glass/epoxy multidirectional laminates," Composites Part A: applied science and manufacturing, pp. 265-272, 2004.

[41] J. J. Lee, J. O. Lim and J. S. Huh, "Mode II interlaminar fracture behavior of carbon bead-filled epoxy/glass fiber hybrid composite," Polymer Composites, vol. 21, 2000.

[42] A. T. Seyhan, M. Tanogly and K. Schulte, "Mode I and Mode II fracture toughness of E-glass non-crimp fabric/carbon nanotube (CNT) modified polymer based composites," Engineering Fracture Mechanics, vol. 75, pp. 5151-5162, 2008.

[43] X. Li, L. A. Carlsson and P. Davies, "Influence of fiber volume fraction on Mode III interlaminar fracture toughness of glass/epoxy composites," Composites Science and Technology, vol. 64, pp. 1279-1286, 2004.

[44] W. C. Liao and C. T. Sun, "The determination of Mode III fracture toughness in thick composite laminates," Composites Science and Technology, vol. 56, pp. 489-499, 1996.

[45] M. J. Mathews and R. S. Swanson, "Characterization of the interlaminar fracture toughness of a laminated carbon/epoxy composite," Composite Science and Technology, vol. 67, pp. 1489-1498, 2007.

[46] M. Miura, Y. Shindo, T. Takeda and F. Narita, "Cryogenic interlaminar fracture properties of woven glass/epoxy composite laminates under mixed-Mode I/III loading conditions," Appl Compos Master, vol. 20, pp. 587-599, 2013.

[47] T. Rys, L. Chen and B. Sankar, "Mixed mode fracture toughness of laminated stitched composites," Department of Mechanical and Aerospace Engineering, University of Florida, Gainesville, Florida, 2004.

[48] M. Zappalorto, M. Salviato and M. Quaresimin, "Mixed Mode (I+II) fracture toughness of polymer nanoclay nanocomposites," Enginnering Fracture Mechanics, vol. 111, pp. 50-64, 2013.

[49] M. R. Ayatollahi, E. Alishahi and S. Shadlou, "Mechanical behavior of nanodiamond /epoxy nanocomposites," Springer Science, vol. 170, pp. 95-100, 2011.

[50] M. Shokrieh, M. Esmkhani, F. Taheri-Behrooz and A. Haghghatkhah, "Displacement-controlled flexural bending fatigue behavior of graphene/epoxy nanocomposites," Composite Materials, vol. 48, pp. 2935-2944, 2014.

[51] P. N. B. Reis, J. A. M. Ferreira, J. D. M. Costa, S. S. Sauceda and M. O. W. Richardson, "Assessment of the mechanical properties on nanoclayed polymer based composites," 2014.

[52] M. Song and K. J. yao, "X-ray diffraction detection of compliance in polyurethane – organoclay nanocomposites," in Minerals and Mining, London, 2004.

[53] B. Wetzel, P. Rosso, F. Haupert and K. Friedrich, "Epoxy nanocomposites – fracture and toughening mechanisms," Engineering Fracture Mechanics, vol. 73, pp. 2375-2398, 2006.

[54] B. R. K. Blackman, A. J. Kinloch, J. S. Lee, A. C. Taylor, R. Agarwal, G. Schueneman and S. Sprenger, "The fracture and fatigue behaviour of nano-modified epoxy," Springer Science, vol. 2007, pp. 7049-7051, 2007.

[55] N. Chisholm, H. Mahfuz, V. K. Rangari, A. Ashfaq and S. Jeelani, "Fabrication and mechanical characterization of carbon/SiC-epoxy," Composite Structures, vol. 67, pp. 115-124, 2005.

[56] C. S. Grimmer and C. K. H. Dharan, "High-cycle fatigue of hybrid carbon nanotube/glass fiber/polymer," Material Science, vol. 43, pp. 4487-4492, 2008.

[57] "http:// www.agy.com," [Online].

[58] "http:// www.nanocor.com," [Online].

[59] "http:// www.hexion.com," [Online].

[60] "http:// www.ika.net," [Online].

[61] "Standard test method for determination of the Mode II interlaminar fracture toughness of unidirectional fiber-reinforced polymer matrix composites," ASTM D7905, 2014.